Structure – Property Relationships in Polyolefins

Von der Fakultät für Mathematik, Informatik und Naturwissenschaften der Rheinisch-Westfälischen Technischen Hochschule Aachen zur Erlangung des akademischen Grades eines Doktors der Naturwissenschaften genehmigte Dissertation

vorgelegt von

M. Sc. Cristian Eugen Hedesiu

aus Iclod, Romania

Berichter: Universitätsprofessor Dr. Dr. h.c. Bernhard Blümich

Universitätsprofessor Dr. -Ing. Edmund Haberstroh

Tag der mündlichen Prüfung: 12 December 2007

Diese Dissertation ist auf den Internetseiten der Hochschulbibliothek online verfügbar.

Contents

Abbreviations and Symbols

NMR	nuclear magnetic resonance
AFM	atomic force microscopy
a, b, c	dimensions of unit cell
c_p	heat capacity
C_1, C_2	WLF coefficients
CLTE	coefficient of linear thermal expansion
d_a	thickness of the amorphous fraction
d_i	thickness of the intermediate fraction
d_r, d_c	thickness of the rigid fraction
DSC	differential scanning calorimetry
D_a	diffusion coefficient amorphous fraction
D_i	diffusion coefficient intermediate fraction
D_r	diffusion coefficient rigid fraction
DQ	double quantum
FID	free induction decay
GS	Goldman – Shen filter
H	enthalpy
HDPE	high density polyethylene
HEPS	Hahn echo pulse sequence
LDPE	low density polyethylene
I	scattering intensity
ICP	impact copolymer
IR	infrared spectroscopy
L_p	long period
LLDPE	linear low density polyethylene
M_2	second van Vleck moment
M_n	number averaged molar mass
M_w	weight averaged molar mass
PE	polyethylene
PP	isotactic polypropylene
q	scattering vector

SAXS	small angle X-ray scattering
SEM	scanning electron microscopy
SEPS	solid echo pulse sequence
SPE	single pulse excitation
t_a	aging time
t_d	mixing time
T_1	longitudinal relaxation time
T_2	transverse relaxation time
T_g	glass transition temperature
T_m^0	equilibrium melting point
TEM	transmission electron microscopy
XRD	X-ray diffraction
W	crystallinity by DSC
WAXD	wide angle X-ray diffraction
WAXS	wide angle X-ray scattering
WLF	William – Landel – Ferry equation
wt%	weight percent
$\Delta\nu_{1/2}$	full line width at half height
ρ	proton density
γ	correlation function
λ	draw ratio

Chapter 1

Introduction and Motivation

The extensive and still increasing usage of polymeric materials stems from their unique physical and mechanical properties. Combined with economic advantages in terms of price and market availability polymeric materials became a logical choice for a wide range of applications. For many purposes, their performance is much better than that of conventional materials such as metals, ceramics or wood. Among the polymeric materials, polyolefins hold an important role, becoming more and more an indispensable part of our daily life. We can identify so many products around us ranging from our basic necessities such as tooth brushes, clothing, storage bottles, and carry bags to special applications like gas and water pipelines, automotive applications, and biomedical implants all made from polyolefins.

The macroscopic properties of polyolefin materials are not only determined by the size and construction of the application but to a great extend also to the morphology of the polyolefin used. Polyolefins show a very complex morphology in which various levels of hierarchy are distinguished. Four levels of morphology can be identified: chain characteristic (primary level), crystal unit-cell (secondary level), lamellae structure (tertiary level), and crystal aggregates or super-molecular structure (quaternary level).

A wide range of material properties are achieved depending on the chain characteristics, type of polyolefin monomers, e.g. homo- or co-polymer, their architecture, e.g. linear, branched, microstructure, e.g. tacticity, amount and distribution of region- and/or stereo defects and molecular weight and molecular weight distribution. By incorporation of α-olefin comonomers macroscopic properties such as toughness and environmental crack resistance can be influenced.

The morphology of the polyolefin on the tertiary and quaternary levels not only is influenced by the chain characteristics but to a large extend also by the processing conditions, storage conditions, and influence of additives. Due to this variety of possibilities in morphology and with that in the properties, the study of the structure - properties relationships in polyolefins has become an exciting field of research in recent decades.

Different NMR methods applied to polyolefins can provide structural and dynamical information about their morphology that subsequently can be correlated with the macroscopic properties. The potential and the wide range of applicability of ^{1}H solid - state NMR is emphasized in this work, which focuses on the applications of NMR in polyolefins

characterization. Classical and advanced solid-state NMR methods were successfully applied for the investigation of a broad range of systems such as, high-density polyethylene (HDPE), isotactic polypropylene (iPP) and PP impact modified copolymers (ICP). A good understanding of their microscopic structure and dynamics as well as morphology is necessary in order to manufacture materials with improved macroscopic properties.

The primary aim of this work is to investigate the changes in the morphology, e.g. phase composition, chain mobility, and domain sizes of polyethylene and polypropylene samples as a function of composition, (comonomer incorporation, chain structure etc.), storage time, temperature at storage, speed of cooling down from the melt, and behaviour under loading conditions. Another aim relates to investigations of the structure – property relationship in polyethylenes and polypropylenes. For these purposes, several experimental methods and methods of data analysis were used, as detailed in Chapter 3 wherein a comprehensive description of the ^{1}H solid – state NMR methods utilized in this work is given.

The changes in the morphology, phase content, chain mobility, and domain sizes of HDPE samples as a function of annealing temperatures and storage time are presented in Chapter 4. In this chapter, we established the temperature range for which the largest differences are observed in molecular mobility in rigid, semi-rigid, and soft fractions allowing accurate determination of the phase composition and the thickness of these domains. The domain thickness, which was determined by NMR, is in good agreement with those measured by small-angle X-ray scattering (SAXS) and transmission electron microscopy (TEM). It is shown that annealing is accompanied by structural reorganizations in the amorphous layer adjacent to the lamella surface causing a continuous shift of the interface towards the inner part of the amorphous regions and thus reducing the thickness of the amorphous layer. The temperature dependence of the spin diffusivities is reported for the three phases of HDPE. The spin-diffusion experiments performed by time-domain low-field NMR and frequency-domain high-field NMR are compared.

Chapter 5 focuses on the combination of different experimental techniques, e.g. DSC, SAXS, WAXD, ^{1}H time-domain, and frequency domain NMR measurements, for determination of the amount of rigid / crystalline, semi-rigid, and soft fractions of isotactic polypropylene (iPP). Changes in the rigid, semi-rigid, and soft fractions of iPP were investigated as a function of annealing time and annealing temperature. The most probable iPP morphology was established by TEM in combination with results from ^{1}H spin-diffusion data compared to data from multidimensional solutions of the spin-diffusion equations. The

temperature dependence of spin diffusivities was taken into account, and a semiquantitative theory is presented for this dependence in the case of the amorphous domains. A combination of ^{1}H spin-diffusion, NMR and SAXS was used to estimate the lamellar thicknesses for non-annealed and annealed iPP samples. Annealing at temperatures above 110° C causes increases in the lamellar thickness and the crystallinity, and a decrease in the chain mobility of the rigid and semi-rigid fractions. The quantities of the different phases and the chain dynamics are reported for three annealing temperatures 134° C, 143° C, and 153° C, and annealing times in the range from 15 minutes to 30 hours.

Chapter 6 focuses on the changes in the phase composition and chain mobility in injection moulded, melt-crystallized and quenched homopolymeric iPP samples, associated with aging at temperatures well above T_g for 150 and 1000 hours. Those changes are studied with high sensitivity using low field ^{1}H solid-state NMR and X-ray diffraction (XRD). By NMR the aging effect at 28° C was monitored each hour during 1000 hours for all iPP samples. Aging in the temperature range from 70° C to 130° C was studied each hour during 150 hours for melt-crystallized homopolymer iPP samples. The aging effects of the morphology of the homopolymer iPP are rationalized in terms of increased restrictions of the chain mobility in the semi-rigid and soft fractions. All sample exhibit physical aging when raised to elevated temperatures, and the physical aging kinetics was observed to depend on the morphology of the homopolymeric iPP and aging temperatures. A significant increase in the tensile modulus with time was observed for injection molded homopolymeric iPP samples. The observed property changes induced by aging are attributed to micro − structural changes within the semi-rigid and amorphous phases. This is consistent with a reduction in chain mobility of the semi-rigid and soft fractions.

In chapter 7 changes in the amount of the rigid, semi-rigid, and soft fractions, molecular mobility, and domain thickness of uniaxially stretched isotactic polypropylene (iPP) were investigated as a function of temperature, draw ratio, drawing temperature, and drawing rate, using ^{1}H solid - state NMR at low field. The amount of the rigid fraction determined by NMR, is in good agreement with crystallinity measured by IR. The study largely focuses on strain-induced changes in the soft phase that have not been analyzed previously in detail. The effect of drawing temperature on the studied molecular parameters shows an important effect of the rate of molecular motions on the strain - induced transformation of the spherulitic morphology of iPP to the fibrillar one.

Chapter 8 presents the influence of the rubber content and nucleating agents on the morphology, phase content, chain mobility, and mechanical properties of impact

copolymeric PP samples. Changes in the morphology, phase content, and chain mobility were studied using a combination of different techniques like NMR, X-Ray, TEM, SEM, AFM, and DSC. Structure-property relationships for impact modified copolymeric PP's are also presented in this chapter.

Chapter 2

Polyethylene and Polypropylene Morphology

2.1 Polyethylene

2.1.1 History

In 1953 Karl Ziegler discovered heterogeneous catalyst based on titanium halides ($TiCl_3 \cdot 1/3$ $AlCl_3$) that produced HDPE upon activation with an organoaluminium cocatalysit such as $Al(C_2H_5)_2Cl$ by coordination polymerization at low temperature and pressure [Nat1955]. Later, Natta independently produced stereoregular polymers such as propylene, butane - 1 and styrene by the same principle [Nat1955]. The subsequent discovery of a $MgCl_2$ supported $TiCl_4$ catalyst system resulted in a two fold increase in the activity [Nat1955, Nat1956, Nat1964].

2.1.2 Properties and economic relevance

Polyethylene is now one of the most common plastics in the word. It is used to make grocery bags, bottles, children's toys, and a host of other everyday items. Polyethylene is of great industrial importance, and is produced in millions of tones each year. Its versatility combined with the physical and chemical properties makes it an attractive commodity to produce. Polyethylene is prepared either via free radical polymerization or via coordination polymerization using a catalyst. The type of polymerization, reaction conditions such as temperature, pressure, type of catalyst, cocatalyst, and comonomer can considerably influence the composition, molecular weight and degree of branching in the polymer and hence the final architecture.

2.1.3 Morphology of polyethylene

Molecular characteristics

Based on the polymer architecture and the resulting density of packing, polyethylene's are classified into high density polyethylene (HDPE; few short or no chain branches), linear low density polyethylene (LLDPE; many equal short branches) and low density polyethylene (LDPE; various branches).
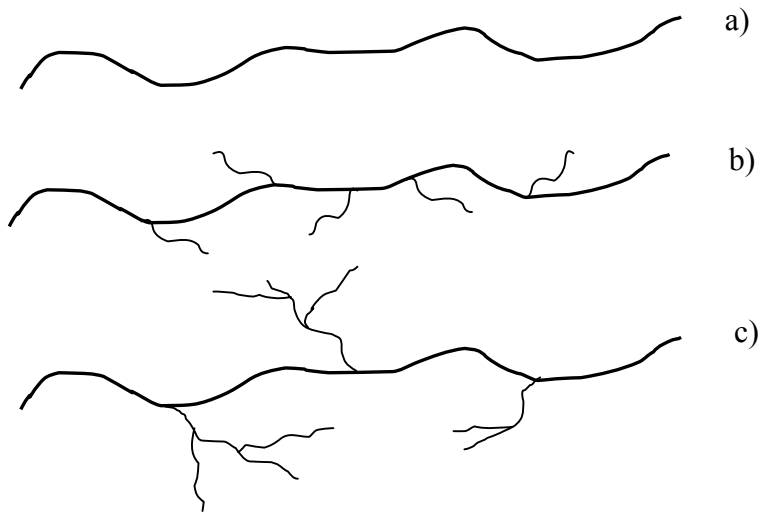
Figure 2.1 Chemical structures of various kinds of polyethylene (a) HDPE (linear) (b) LLDPE (many equal short branches) (c) LDPE (various branches on branches)

Crystal phases of polyethylene

The orthorhombic phase of polyethylene

The crystal structure of polyethylene was first determined by Bunn [Bun1939]. The orthorhombic unit cell is the most stable crystal structure. The zigzag planes of the chain of the orthorhombic cell have different orientations (Fig. 2.2). The dimensions at 23° C of the orthorhombic cell of linear polyethylene are according to Busing [Bus1990] a = 7.4069Å, b = 4.9491Å and c = 2.5511Å (chain axis) which give a crystal density of 996.2 kg m^3. The angle between the zigzag planes of two chains and the b axis on the unit cell was first determined by Bunn [Bunn1939] to be 41°. A later study by Chantani et al. [Cha1977] on linear polyethylene gave a somewhat larger value, 45°.
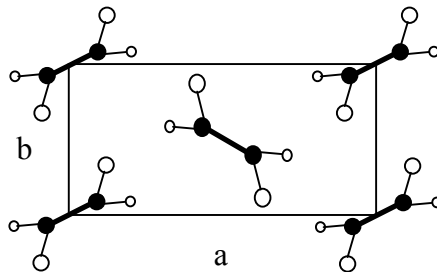
Figure 2.2 Crystal structure of polyethylene showing a view along the chain axis: orthorhombic unit cell.

The monoclinic phase of polyethylene

The monoclinic cell was first discovered by Teare and Holmes [Tea1957]. The monoclinic cell is less stable than the orthorhombic cell and is found in samples subjected to mechanical

stress (Fig. 2.3). The dimension at 23° C of the monoclinic cell of linear polyethylene with 4 CH_2 groups are according to Seto et al. [Set1968]; a = 8.09Å, b = 2.53Å (chain axis), and c = 4.79Å, which gives a crystal density of 997 kg m^3. The zigzag planes of the chains of the monoclinic cell have a uniform orientation (Fig. 2.3).
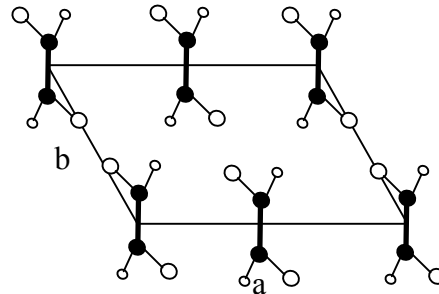
Figure 2.3 Crystal structure of polyethylene showing a view along the chain axis: monoclinic unit cell.

The hexagonal phase of polyethylene

The high - pressure hexagonal phase was discovered by Basset et al. [Bas1974]. The hexagonal phase has very special properties: a regular hexagonal packing of conformational disordered chains with extreme translational chain mobility that allows rapid crystal thickening.

2.2 Polypropylene

2.2.1 History

Polypropylene (PP) was discovered in the early 1950s. In 1953 Ziegler discovered that polyethylene could be prepared with a mixture of metal salts and transition metal salts [Bus2001, Cip2001]. Giulio Natta succeeded in preparing polypropylene using the Ziegler catalyst and was able to obtain and characterize isotactic PP by fractionation [Sal1996]. In 1957 polypropylene was taken into commercial production [Kar1995]. The polymer yield of the catalyst (so-called Ziegler - Natta catalysts) had increased enormously from 0.8 Kg/(gram catalyst) to more than 100 Kg/(gram catalyst) along with a significant increase in isotacticity. In normal practice the term polypropylene means isotactic polypropylene obtained from Ziegler - Natta catalysis.

2.2.2 Properties and economic relevance

Polypropylene has grown to a commodity polymer with numerous grades for specific end and uses. At present, the physical properties of PP can be tailored to the requirements with respect to processing and structure. To achieve the desired properties several modifications of PP could be obtained during polymerization.

The catalyst involved during the polymer synthesis is a complex system. A better understanding of the mechanism involved has lead to the development of flexible, economical, and environmentally friendly polymers and their products. The flexibility of the material can be noticed in the processibility (molding and extrusion) where the polymer chains can easily be oriented into high modulus thin films and fibers. Another major advantage of using polypropylene is the recyclability of the polymer which is becoming and important issue.

2.2.3 Morphology of isotactic polypropylene

Molecular characteristics

The chain characteristics follow directly from the chemistry of the particular polymerization reactions. Stereo regular polypropylene can be obtained by using various catalysts that promote regular insertion of the monomers in the growing chain. Thus, the type of catalyst used, together with the support of the catalyst [Pau1993] has a important influence on the primary chain architecture.

The main chain – characteristics of linear PP are the molar mass (MM), molar mass distribution (MMD), and chain regularity. Gel permeation chromatography (GPC) is typically used to measure the MM and MMD.

Polypropylene is a stereoregular polymer. The stereoregular nature is determined by the position of the methyl side - groups along the main chain as illustrated in Fig. 2.4a. This means that the neighburing methyl groups in polypropylene chain have two stereo - isomeric positions with respect with each other.

a.

$$-\left[CH_2-CH\right]_n$$
$$|$$
$$CH_3$$

b.

c.

d.
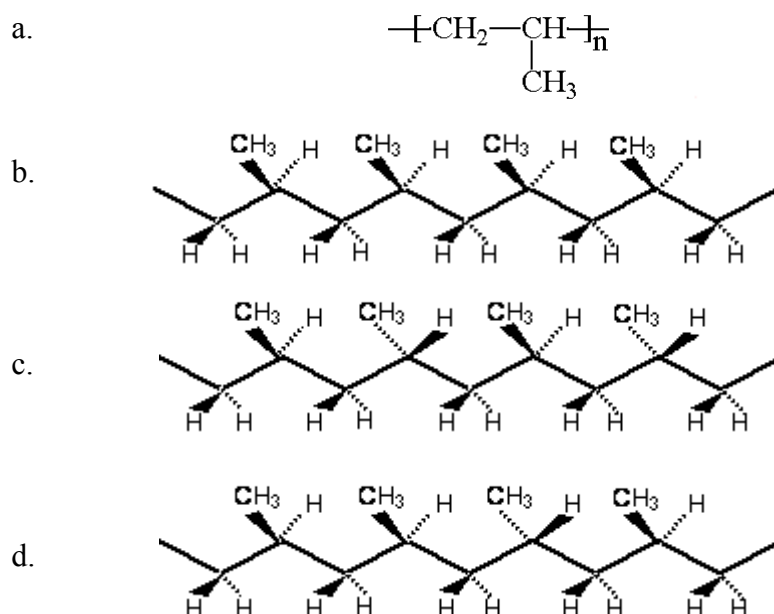
Figure 2.4 Isomerism in polypropylene. a) Chemical structure of polypropylene. b) Isotactic polypropylene. c) Syndiotactic polypropylene. d) Atactic polypropylene, as illustrated by Karger – Kocsis [Kar1995]

The three physical stereo - configurations that can be distinguished in polypropylene are: isotactic, syndiotactic and atactic (as presented in Fig. 2.4b, c, d, respectively). From ^{13}C – NMR it is possible to extract the information about the degree of regularity within the polymer.

Crystal phases of iPP

Isotactic polypropylene is a polymer with a number of crystal modifications [Var1992]. In all of the crystal structures the chain is packed in the lattice as a left or right handed (or both) $2*3_1$ – helix conformation with either and 'up' or 'down' positions of the methyl groups.

The α-phase of polypropylene

The α-phase of iPP is described by an alternation in the b – axis direction of layers parallel to the ac – plane and composed of only left-handed (L) or right - handed (R) helices, indicated in Fig. 2.5 by white and black triangles, respectively. The position of the methyl group in both the left and right - handed helices can be positioned 'up' or 'down' (up or dw). Due to the possibility of the chains to be situated 'up' or 'down' two limiting α - phases (α_1: disordered, α_2: ordered) can be recognized (see Fig. 2.5). The ordered α_2 phase (Figure 2.5 right) can be obtained by re - crystallization or annealing [Ros2002]. The monoclinic unit cell has the following parameters a = 6.65 Å, b = 20.96Å, c = 6.5Å [Lot1996, Awa1988], and β = 99.62°. The overall density at room temperature is 0.946 g/mol [Awa1988].
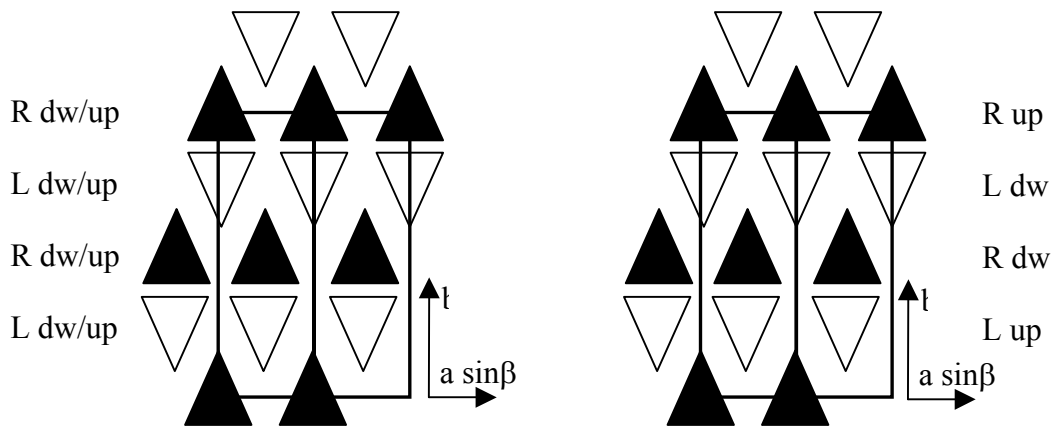
Figure 2.5 Two limiting forms of the α - phase. Left: α_1; Right α_2. The horizontal arrows indicate the projection of the a – axis, the vertical arrow indicates the b – axis. The c – axis is perpendicular to the plane of view [Aur2000].

One of the characteristic morphological features of the α - phase is the so – called cross – hatching, also known as lamellar branching. This feature is recognized by the initial lamella (mother – lamella) showing branches (daughter – lamellae) that are attached to mother – lamellae with angles of $\approx 80°$ or $\approx 100°$. The molecular background of crosshatching is described by Lotz and Wittmann [Lot1996].

The β - phase of polypropylene

Under proper crystallization conditions (shear, large temperature gradient, or use of a β - nucleating agent), polypropylene samples with a high content of β - phase can be made [Vle1997, Tri1998, Per1999].
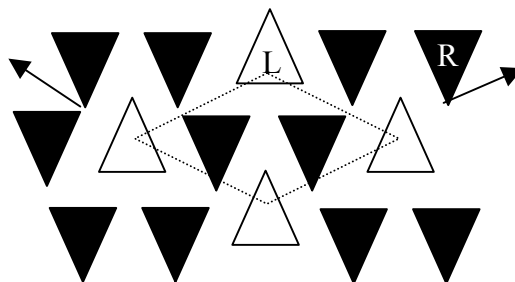
Figure 2.6 Schematic representation of the arrangement of iPP – helices in the β - phase. The arrows indicates the b – axis, the c – axis is perpendicular to the plane of view.

The β - phase has a trigonal unit – cell with lattice parameters a = b =11Å, c = 6.5Å, β = 120°. The β - phase is metastabile relative to the α - phase.

The γ – phase of polypropylene

The γ – phase is usually associated with the α – phase, although individual single crystals of the γ – phase has also been observed. The γ – modification may be formed in degraded, low molecular weight isotactic polypropylene and in the samples crystallized under high pressures [Mez1997, Cam 1993]. Also, considerable amounts of the γ – modification were obtained under atmospheric pressure, both in systems with low tacticity or made by homogeneous metallocene catalysts [Per1999, Mez1998].

The crystalline structure of the γ – modification was first denoted as triclinic [Per1999, Lov1983]. However, it has been shown that the structure is orthorhombic with parameters a = 8.54Å, b = 9.93 Å, and c = 42.41 Å [Cam1993]. The structure is composed of sheets of parallel chains in which the molecular orientations in adjacent sheets are inclined at an angle of 80° [Tho1996]. In this unit cell the c – axis is not parallel to the chain axis direction.
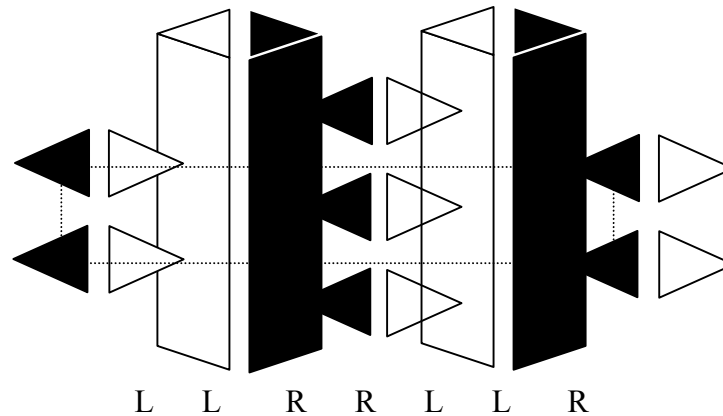
Figure 2.7 Schematic representation of the arrangement of iPP helices in the γ – phase [Cam1993, Lot1991].

Chapter 3

Experimental Methods

3.1 Introduction

In this thesis PE and PP samples are investigated using transmission electron microscopy (TEM), atomic force microscopy (AFM), scanning electron microscopy (SEM), differential scanning calorimetry (DSC), X-Ray diffraction (XRD) and nuclear magnetic resonance (NMR). All these experimental methods and the associated experimental issues are described in brief in this chapter.

3.2 Transmission electron microscopy (TEM)

TEM has been utilized to probe the morphology and structure properties including lamella thickness and the nature of crosshatching. Transmission electron microscopy (TEM) has been performed using Philips CM200 equipment at an acceleration voltage of 120 kV. The polyethylene and polypropylene samples were trimmed at temperature of -120° C and stained for 24 hours in a RuO_4 solution. Sections of 70 nm thick were obtained by slicing the sample with an ultramicrotrome at -120° C.

3.3 Scanning electron microscopy (SEM)

In order to obtain information about the microstructure of impact modified copolymeric PP, scanning electron microscopy was performed. The Scanning Electron Microscope (SEM) is an electron microscope capable of producing high-resolution images of a sample surface. Due to the manner in which the image is created, SEM images have a characteristic three-dimensional appearance and are useful for judging the surface structure of the sample. The SEM has a large field of depth, which allows a large amount of the sample to be in focus at one time. Preparation of the samples is relatively easy since most SEMs only require the sample to be conductive. The combination of higher magnification, larger depth of focus, greater resolution, and ease of sample observation makes the SEM one of the most popular research instruments today.

3.4   Atomic force microscopy (AFM)

AFM experiments were performed to investigate the morphology of impact modified copolymeric PP. The atomic force microscope (AFM) is a high-resolution type of scanning probe microscope, with demonstrated resolution in the range of fractions of a nanometer, i.e. more than 1000 times better than the optical diffraction limit.

The AFM can be operated in a number of modes, depending on the application. In general, possible imaging modes are dived into static (also called contact) mode and a variety of dynamic modes. AFM provides a three-dimensional surface profile and does not require any special sample treatments that would irreversibly change or damage the sample [Mag1996].

3.5   Differential scanning calorimetry (DSC)

DSC experiments were performed using a Perkin Elmer DSC-7 at a heating rate of 10° C/min. In these experiments, a negative heat flow is defined as an exothermal process and positive heat flow as an endothermal one. Small amounts of polymer (typically 2 – 3 mg) were put into pans. After a first quick melting and recrystallization of the sample, specific treatments were applied. The melting- and crystallization temperatures were determined from the maximum of the melting endotherm and the minimum of the crystallization exotherm, respectively.

Various cooling rates were applied from the melt while recording the heat flow during cooling (crystallization) and heating (melting). For most samples, heating experiments were performed immediately after crystallization by controlled cooling.

3.6   Small-angle X-ray scattering (SAXS)

The small angle X-ray scattering (SAXS) experiments were performed with a modified Kratky setup in order to study the structure of polyethylene and polypropylene samples in terms of average lamellae sizes. The method is accurate, non-destructive and requires only a minimum of sample preparation. Conceptually, SAXS experiment is simple: the sample is exposed to X-rays and a detector registers the scattering radiation. The analysis of the X-ray scattering curve (intensity versus scattering angle) provides estimates of the thickness of the rigid domains and long period in polyethylene and polypropylene.

3.7   Wide angle X-ray diffraction (WAXD)

Wide angle X-ray diffraction (WAXD) is an X-ray diffraction technique that is used to determinate the crystalline structures of polyethylene and polypropylene. Moreover, with WAXS it is possible to obtain information about the unit cell orientation in the material.

In a X-ray experiment the monochromatic X-ray beam (with a wavelength λ) is scattered (diffracted) by the material at a specific angle θ [Ale1969], due to the presence of regular (crystal) planes in the material separated a distance (d). The scattering angle (2θ) is related to the inter-planar distance (d) by the Bragg equation,

$$2d = \frac{n\lambda}{\sin\theta},$$

where n is an integer. The equation indicates a reciprocal relationship between the characteristic length d and $\sin\theta$.

3.8   Infrared spectroscopy (IR)

Infrared measurements are suitable for the determination of the orientation of individual components or phases (crystalline or amorphous domains in semi-crystalline polymers or an average of the two domains). The method is based on the principle of selective absorption of polarized IR radiation parallel and perpendicular to a certain reference direction.

IR experiments were performed on a Perkin Elmer AutoImage FTIR microscope. IR spectra (4000-6000 cm^{-1}) were acquired at a spectral resolution of 4 cm^{-1}, using 200 accumulations. Three spectra were acquired for every spectrum, namely without polarisation, with IR light polarised parallel to the stretching direction of the polymer, and with the IR light polarised perpendicular to the stretching direction of the polymer. Dichroic analyses were carried out using a wire grid polariser. The sample was rotated rather than the polariser, as it is known that the exciting beam of the spectrometer used is partly polarised. The data processing procedure follows the method provided by Kissin [Kis1983]. The method is used as provided, i.e. without renewed validation, and the results should be considered indicative rather than a fully validated.

3.9 Mechanical tests

Impact testing method: A single point Izod test was used to measures the resistance of the investigated material to impact. Izod impact strength is defined as the strength at which the specimen breaks when hit with a pointed hammer having a set kinetic energy. The specimen is notched to prevent its deformation upon impact.

The tests were performed with a Zwick Type 5110 testing machine according to ASTM D256 on 65 x 12.7 x 3.2 mm specimens and with a striking speed of the hammer of 3.5 m/s. The given value of the impact strength is an average of five tests.

The impact strength a_{iN}, expressed in kJ/m^2 was calculated from the following equation:

$$a_{iN} = \frac{E_c}{h \cdot b_N} \times 10^3 \, ,$$

where: E_c is the corrected energy, in joules, absorbed by breaking the specimen

   h is the thickness of the specimen in mm

   b_N is the width at the notch in mm

Two hammers were used having a kinetic energy of 2.75 J and 5.5 J, respectively. If after carrying out the test with the lighter hammer, the specimen did not fully brake, the specimen was discarded without recording the impact strength and the heavier hammer was used.

Flexural testing method: The principle of this test is to bend or flex the specimen in the middle at a constant bending rate until the specimen fractures or until the deformation reaches some predetermined value. During the test the force applied to the specimen is measured. Flexural modulus was computed and used as an indication of the material's stiffness when flexed.

   The tests were carried out with a Zwick tensile machine according to ASTM D790. The dimensions of the specimen were 65 x 12 x 3.2 mm. The values of flexural modulus are an average values of five tests.

Tensile testing method: Is used to investigate the tensile behaviour of the specimens and for determining the tensile strength and tensile modulus. The tests were carried out with a Zwick Z050 tensile machine according to ISO 37-II. The tests were performed at 25° C with a deformation rate of 50 mm/min.

   The aim of the tensile tests were to determine the effect of the rubber content and the addition of the nucleating agents on the yield point of the specimens under investigation.

3.10 Nuclear magnetic resonance (NMR)

Different solid-state ^{1}H NMR methods, namely wide-line NMR spectroscopy, transverse magnetization relaxation (T_2 relaxation), and spin-diffusion experiments were used to study the phase composition, molecular mobility, and the domain thickness in polyethylene and polypropylene. The experiments were performed at low magnetic field using a Bruker Minispec MQ20 spectrometer (Fig. 3.1a) operating at a proton resonance frequency of 19.6 MHz, and at high magnetic field using a Bruker DSX-500 MHz spectrometer (Fig. 3.1b) operating at a proton resonance frequency of 500.45 MHz. The data were collected for static samples at temperatures between 25$^°$ C and 140$^°$ C. The measurements, as a function of increasing temperature, were conducted following a 10 minute stabilization time at each temperature.

a)

b)
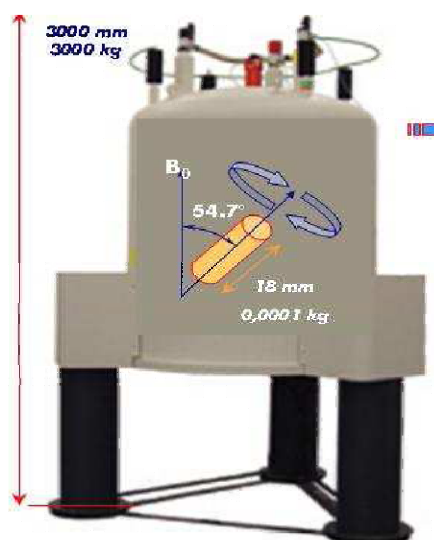
Figure 3.1. (a) Low field and (b) high field NMR spectrometers [Web1, Web2]

3.10.1 Proton wide-line NMR spectroscopy

Proton wide-line NMR spectra were acquired to study the phase composition and chain mobility in polyethylene and polypropylene. The NMR spectra measured in high magnetic field were deconvoluted using the Bruker WinFit program (Fig. 3.2). The line shape of the rigid component was taken as Gaussian, those of the semi-rigid, and soft components were taken as Lorentzians. At high magnetic field, the duration of a 90$^°$ pulses was 3 µs, the dwell time was 0.75 µs, and the recycle delay was 5 s for all the experiments.
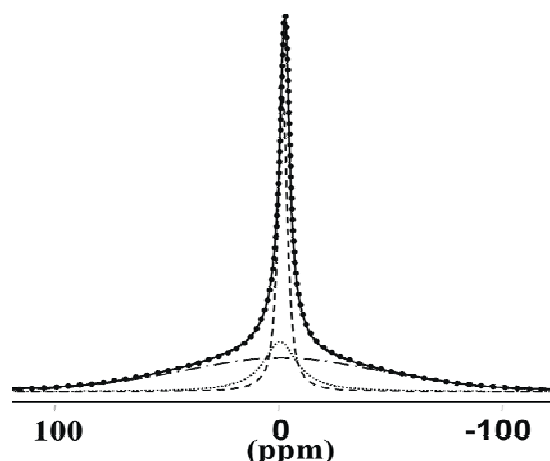
Figure 3.2. Proton wide-line NMR spectra (solid line) of iPP measured at 70° C with a 500 MHz NMR spectrometer. The dashed lines show the spectral components that are assigned to the rigid, semi-rigid, and soft fractions of iPP corresponding to broad, intermediate, and narrow line widths, respectively.

3.10.2 Proton transverse magnetization relaxation

Proton transverse magnetization decays were recorded to study the changes in the phase composition and chain mobility in polyethylene and polypropylene. At low magnetic field, the duration of a 90° pulse was 2.7-2.8 µs and the dwell time was 0.5 µs. A BVT-3000 temperature controller was used for temperature regulation with a temperature stability better than 1° C. In order to measure the decay of the ^{1}H transverse magnetization (T_2 decay) of polyethylene and polypropylene three different NMR pulse sequences were used. In the first experiment, the free induction decay (FID) was recorded after a 90°-pulse excitation (SPE – **s**ingle **p**ulse **e**xcitation), i.e. 90°_x – dead time – acquisition of the amplitude $A(t)$ of the transverse magnetization as a function of time t. The second experiment was the **s**olid **e**cho **p**ulse **s**equence (SEPS), i.e. $90^\circ_x - t_{se} - 90^\circ_y - t_{se}$ – acquisition of the amplitude of the transverse magnetization $A(t)$, with t_{se}=10 µs. The third one was the Hahn-echo pulse sequence (HEPS), i.e. $90^\circ_x - t_{He} - 180^\circ_y - t_{He}$ – acquisition of the amplitude of the echo maximum for a variable value of $2t_{He}$.
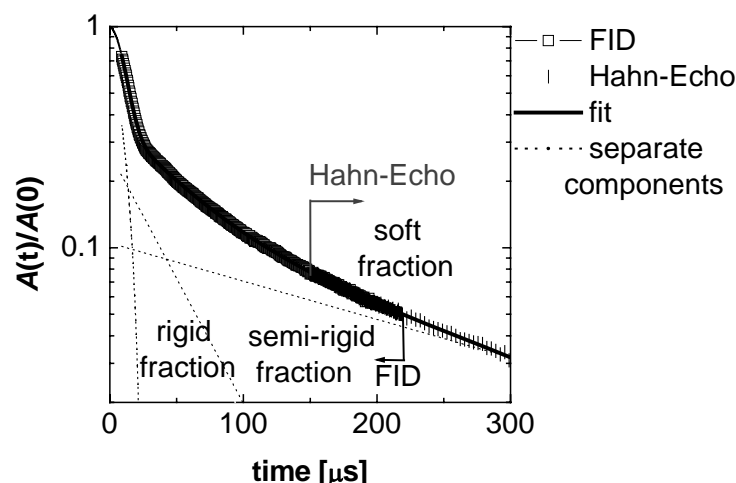
Figure 3.3. The decay of the transverse magnetization relaxation (points) for iPP at 70° C. The decay (FID) was measured at 20 MHz NMR spectrometer using the SPE (□) and the HEPS (ı) methods. The solid line represents the result of a least-squares fit of the decay with a linear combination of the Abragam function and two exponential functions. Dotted lines show the separate components that are assigned to rigid, semi-rigid, and soft iPP fractions.

The Hahn-echo pulse sequence was used to avoid the effect of the inhomogeneity of the magnetic field on the decay of the transverse magnetization of the soft fraction of iPP, and to obtain reliable information about the molecular mobility and amount of the soft fraction. The 90° pulse excitation (SPE) and HEPS were finally used to record the FID for quantitative analysis of the phase composition (Fig. 3.3). Repeated experiments for the same sample indicated that the relative error of the extracted relaxation parameters was about 1 %.

3.10.3 Spin-diffusion NMR experiments with dipolar filters

An accurate analysis of domain sizes of PE and PP by ^{1}H NMR spin-diffusion experiments requires (1) highest selectivity to different phases by optimization of dipolar filters, (2) knowledge of the spin-diffusion coefficients for modeling the experimental data and (3) proper choice of a model that fits the morphology of the material studied.

Double Quantum (DQ) filter. Spin-diffusion experiments with a double-quantum (DQ) dipolar filter were performed to determine the thickness of the rigid and amorphous domains in both PE and PP samples. Proton double-quantum build-up curves and spin-diffusion data were recorded at high- and low-magnetic fields using the pulse sequence $90^0_x - \tau - 90^0_{-x} - t_{DQ} - 90^0_y - \tau - 90^0_{-y} - t_d - 90^0_x - FID$ with the excitation time τ and the spin-

diffusion time t_d. The evolution time of the DQ coherences is t_{DQ} which was taken as 5 μs in all experiments.
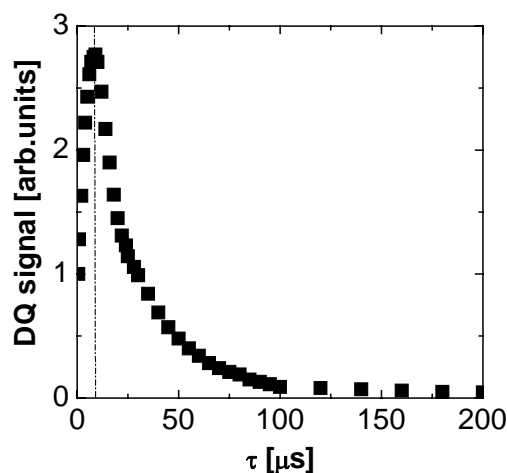
Figure 3.4. Proton DQ build-up curve for iPP at room temperature showing the dependence of the integral signal on the excitation time τ. The DQ build-up curve was measured with high-field NMR spectrometer. The maximum of the curve is observed at 10 μs that is marked by a dashed line.

The dipolar filter excites double-quantum coherences and selects mainly the magnetization of the rigid fraction at a short excitation time τ [Bud2003, Hed2007]. The optimum τ value in the DQ filter for selection the rigid fraction [Sch1999] was obtained from the DQ build-up curve. It shows one maximum for iPP (Fig. 3.4) at short excitation times τ of approximately 10 μs. The efficiency of the filter is judged from ^{1}H wide-line NMR spectra recorded at different excitation/reconversion times τ (Fig. 3.5). These spectra allow us to choose the optimum filter time for selecting the magnetization of the rigid fraction. For short excitation/reconversion time τ, the DQ filtered spectra are doublets (Figs. 3.5a and 3.5b) which are related to the spin pairs of the methylene groups having the strongest dipolar couplings. It should further be mentioned that the doublet structure of the DQ-filtered spectra is due to the fact that at short excitation times, only the rigid polymer chains with dipolar tensor orientation around 0 and 90 degrees are preferentially excited, while those orientated around the magic angle are suppressed. An interesting property of the DQ filter is that at long excitation times, only the signal from the most mobile chain fragments in the amorphous phase is selected (Fig. 3.5d).

a)

b)

c)

d)
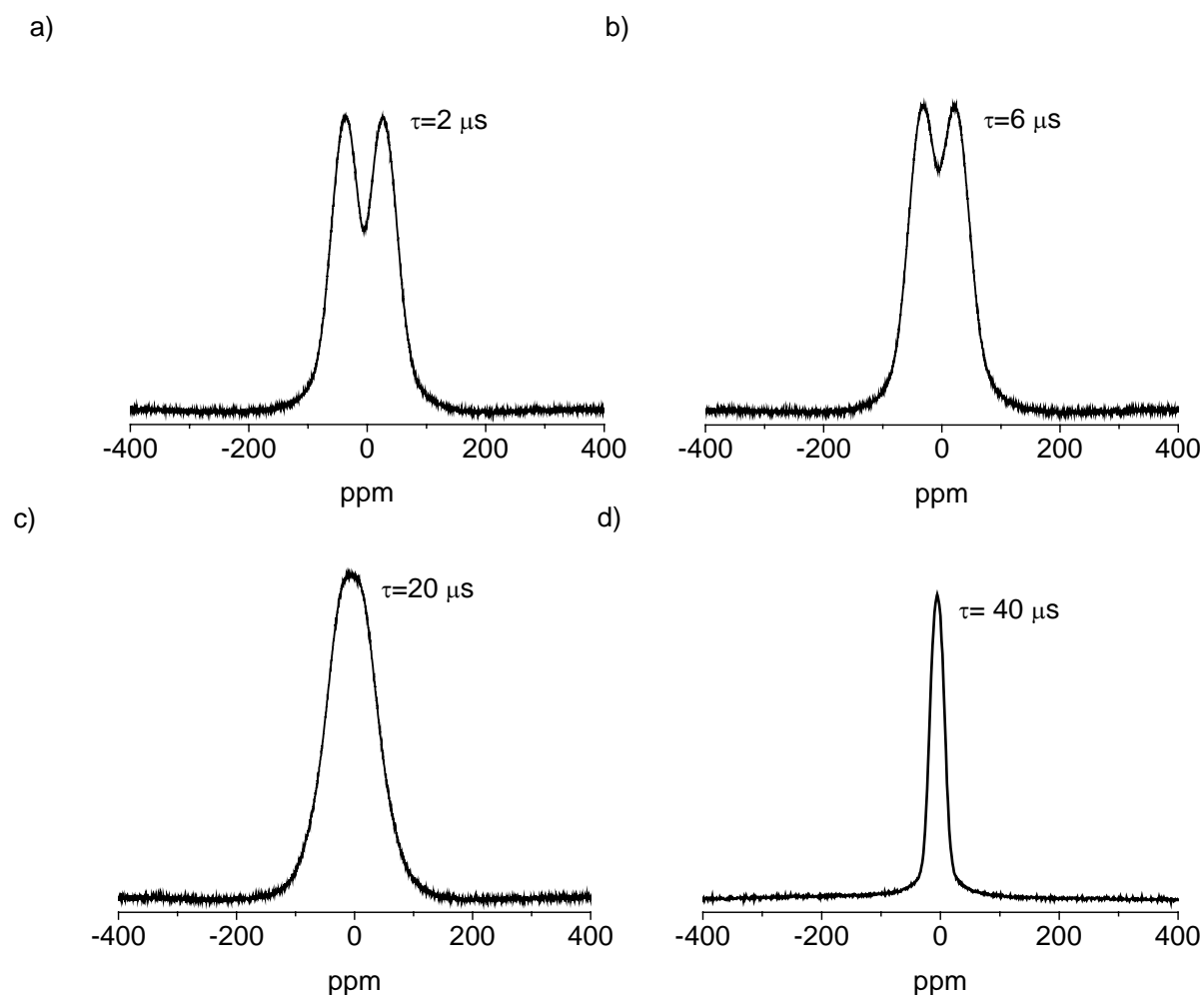
Figure 3.5. High-field proton wide-line NMR spectra of iPP at room temperature recorded after different excitation/reconversion periods of the DQ dipolar filter: τ = 2 μs (a), τ = 6 μs (b), τ = 20 μs (c), and τ = 40 μs (d). The spin-diffusion time t_d was set to 5 μs.

The DQ filter shows high efficiency in selecting the magnetization of particular iPP and PE domains with distinct molecular mobilities. The high selectivity of the DQ filter was also observed in T_2 relaxation experiments at low resonance frequency. For all experiments, the excitation/reconversion time of 10 μs and short spin-diffusion time t_d of 5 μs (Fig. 3.6) were chosen to select the rigid iPP and PE fractions in the spin-diffusion experiment, both at high- and low- proton resonance frequencies. The proton NMR spectra edited for different spin diffusion times are shown in Fig. 3.6.

a)

b)

$t_d = 5\ \mu s$

x0.57

$t_d = 10\ \mu s$

x0.71

-200   -100   0   100   200

ppm

-200   -100   0   100   200

ppm

c)

d)

$t_d = 10\ ms$

x0.90

$t_d = 1\ s$

x1

-200   -100   0   100   200

ppm

-200   -100   0   100   200

ppm
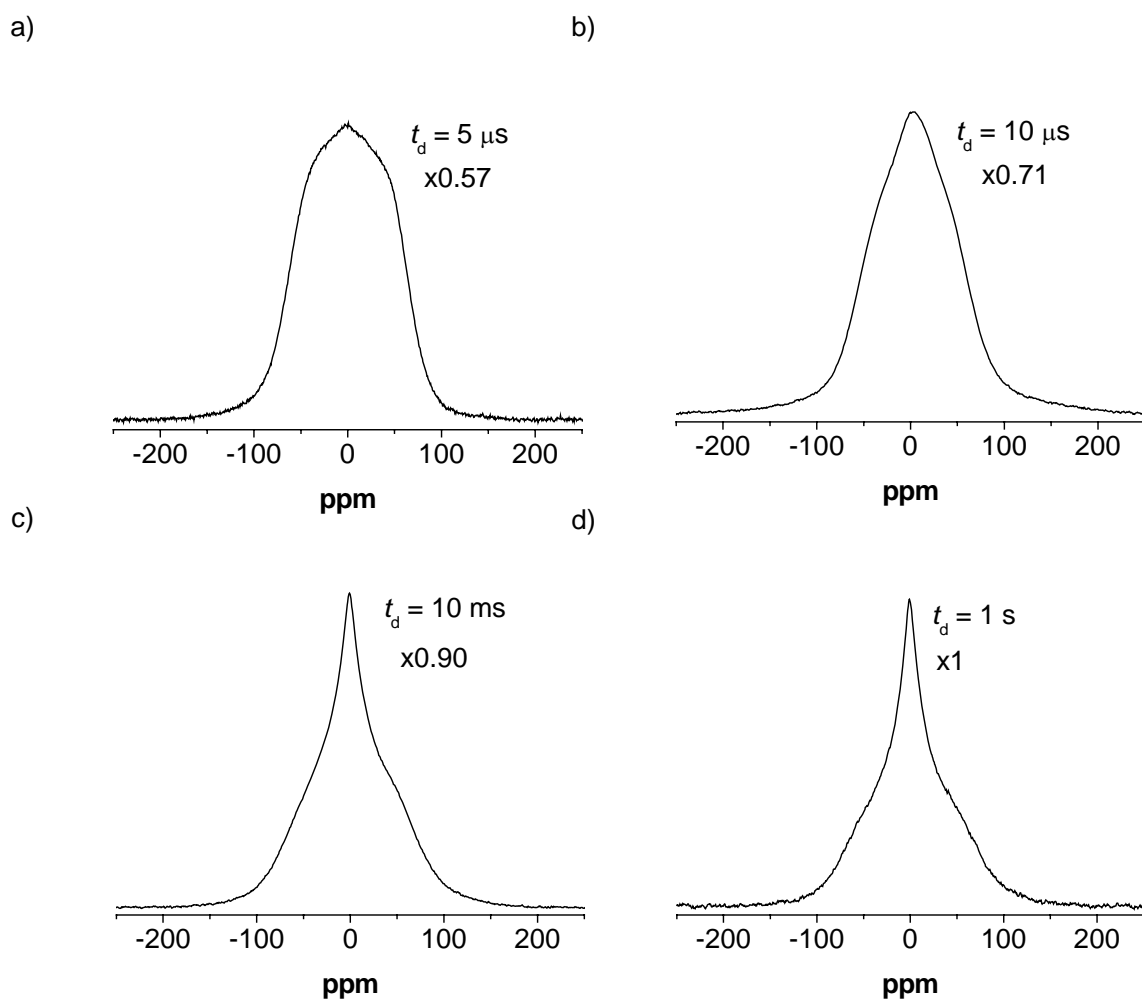
Figure 3.6. Proton wide-line NMR spectra of iPP at room temperature. The spectra were recorded using the spin-diffusion experiment with different spin-diffusion times: a) $t_d = 0.005$ ms, b) $t_d = 0.010$ ms, c) $t_d = 10$ ms and d) $t_d = 1$ s, and $\tau = 10\ \mu s$.

Goldman – Shen filter. Another dipolar filter used in this investigation explores the Goldman-Shen scheme [Gol1961]. The amorphous domains are selected by the pulse sequence $90^0_x - \tau - 90^0_{-x} - t_d - 90^0_x - FID$ with the filter time $\tau = 100\ \mu s$ and t_d being the spin-diffusion time. Both dipolar filters were employed in the present study to gain a higher confidence in determinations of the polyolefins morphology.

Spin-diffusion coefficients. The values of the spin-diffusion coefficients should change with increasing temperature due to an increase in molecular mobility. Therefore, the spin-diffusion coefficients should be determined at different temperatures for accurate analysis of domain sizes in PE and PP as a function of temperature.

The values of the spin-diffusion coefficients D for the rigid and the soft fractions of PE and PP can be determined assuming, to a good approximation, that the NMR line shapes of the rigid and soft fractions are Gaussian and Lorentzian, respectively. The spin-diffusion coefficients can be related to the second van Vleck moment of the NMR absorption lines,

which, in turn, is related to the full line width $\Delta v_{1/2}$ at half height. Hence, the spin diffusivity for the rigid (D_r) and soft (D_a) fractions is as follows [Dem1995]:

$$D_r \approx \frac{1}{12}\sqrt{\frac{\pi}{2\ln 2}}\langle r^2\rangle \Delta v_{1/2}, \tag{3.1}$$

and

$$D_a \approx \frac{1}{6}\langle r^2\rangle[\alpha\Delta v_{1/2}]^{1/2}, \tag{3.2}$$

where $\langle r^2\rangle$ is the mean square distance between the nearest spins, and α is a cut-off parameter for the Lorentzian line shape [Dem1995]. The temperature dependence of $\Delta v_{1/2}$ is determined at each temperature by spectral deconvolution as shown at one temperature in Fig. 3.2. For calculating $\langle r^2\rangle$ the Discover program (version 2004.1) was used. The estimated weighted mean square of these distances $\langle r^2\rangle$ equal approximately 0.0484 nm^2 for PE and 0.08 nm^2 for PP, respectively.

The calculated spin-diffusion coefficients are plotted as a function of temperature in Fig. 3.7. The temperature dependence of the spin diffusivity in different fractions of iPP is difficult to predict quantitatively, due to the complex origin of the chain motion and multi-spin interactions. Nevertheless, a semi-quantitative approach can be presented based on the arguments provided in Ref. [Abr1961]. In the presence of motions of the spins, the theory of the NMR line width predicts that $\Delta v_{1/2} \approx M_{2,rigid}\tau_c$, where $M_{2,rigid}$ is the second van Vleck moment for a rigid polymer, and τ_c is the correlation time of the chain motions.
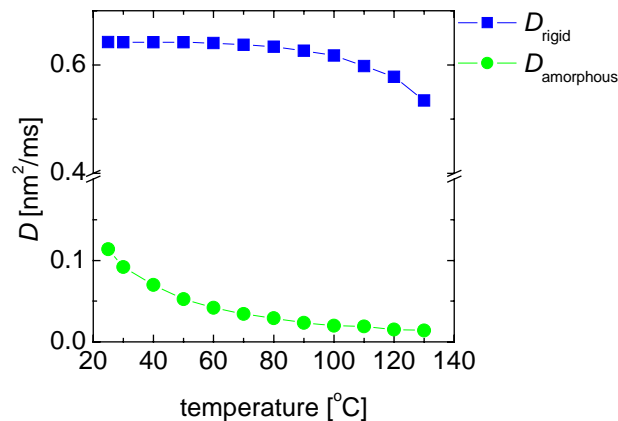
Figure 3.7. The temperature dependence of the spin-diffusion coefficient for the rigid D_r and amorphous D_a fractions of iPP.

From Equation 3.2 and the above relationship, one obtains: $D_a \propto (\tau_c)^{1/2}$. The temperature dependence of the correlation time in amorphous polymers can be approximated by the Williams-Landel-Ferry (WLF) equation (see Ref. [Sch1994]), i.e.,

$$\tau_c(T) = \tau_c(T_g) \exp\left[\frac{-C_1(T - T_g)}{T - (T_g - C_2)}\right],$$
(3.3)

where T_g is the glass transition temperature and C_1 and C_2 are the WLF coefficients.

Using the above equation, the temperature dependence of the spin diffusivity D_a of the amorphous fraction of iPP can be described by the following equation.

$$D_a(T) = D_{ag} \exp\left[\frac{-\left(\dfrac{C_1}{2}\right) \cdot (T - T_g)}{T - (T_g - C_2)}\right],$$
(3.4)

where D_{ag} is the spin-diffusion coefficient at temperature T_g. The spin-diffusion coefficient of the rigid fraction at 25° C is taken as $D_{a0} \approx D_{ag}$ (see Fig. 3.7). A least-squares fit of the dependence in Fig. 3.8 provides the following values of the WLF parameters: $C_1 = 10$, $C_2 = 57K$ and $T_g = 273K$.
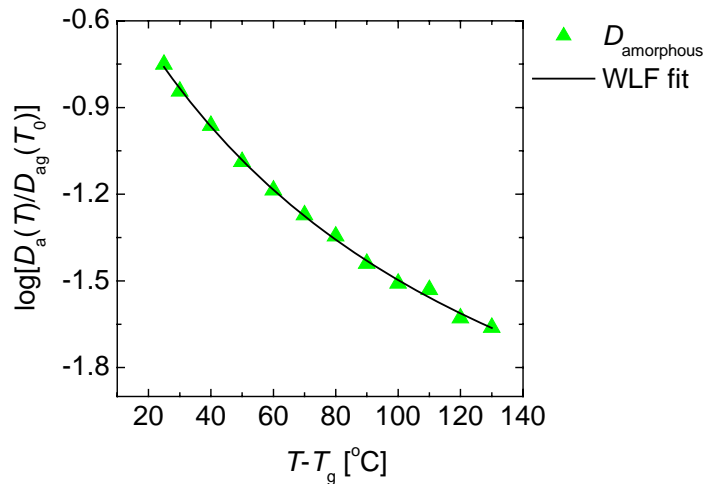
Figure 3.8. The dependence of $log[D_a(T)/D_{ag}(T_0)]$ on temperature. The line shows the fit of the dependence with Eq. (3.4).

These values are in the range of typical WLF coefficients that describe dynamic mechanical and dielectric data for amorphous polymers, namely $C_1 \approx 16$ and $C_2 = 25K - 104K$ [Str1997]. The observed differences could be due to the fact, that the WLF

function has originally been proposed to describe the temperature dependence of the viscosity. An increase in the amplitude and the length scale of the chain motion with increasing temperature could affect the spin-diffusion coefficients and mechanical data in a slightly different way.

Morphology of polyofefins by ^1H spin-diffusion. The ability of NMR spin-diffusion experiments to provide self-consistent information on the dimensionality of the diffusion process was discussed in Ref. [Dem1996]. Proton spectra recorded at 70° C with the DQ filter after different diffusion times for iPP are shown in Fig. 3.6. The flow of longitudinal magnetization from the rigid domains to the amorphous domains is observed with increasing diffusion time, causing an increase in the intensity of the narrow line at the expense of the broad line. The time-dependent integral of the spin-diffusion spectra intensities reach their equilibrium values for iPP samples in about 70 ms. In a good approximation, the spin-diffusion DQ edited ^{1}H NMR spectra can be decomposed into two components. The two-component analysis is used to establish the average thickness of rigid (crystalline) and amorphous domains. It can be shown that the solutions of the spin-diffusion equations for different morphologies exhibit different sensitivities to the dimensionality of the process, as a result of different surface/volume ratio (interface area) for a given source volume. The information about the dimensionality of the spin-diffusion process can be obtained using the following equations [Vod2006]:

$$\frac{r \cdot E}{p} = 1 \text{, 1D case}$$

$$\frac{r \cdot E}{p(2+p)} = 1 \text{, 2D case}$$

$$\frac{r \cdot E}{(1+p)^3 - 1} = 1 \text{, 3D case} \tag{3.5}$$

where $r = \rho_r / \rho_a$ and $E = M_{a,eq} / M_{r,eq}$. The equilibrium magnetizations for the amorphous and rigid domains are denoted as $M_{a,eq}$ and $M_{r,eq}$, respectively. The ratio between the domain thicknesses d_a and d_r is denoted by $p = d_a / d_r$. In the two-phase approximation, the r and E values for non-annealed iPP samples are obtained as 1.11 and 0.25, respectively. These values are established independent of the spin-diffusion process. The spin-diffusion decay and build-up curves shown in Fig. 3.9 are fitted with the solutions of the spin-diffusion equations for 1D morphology [Bud2003,Wan1996]. For each spin-diffusion dimensionality, the values of d_a and d_r are established from the best fit (Table 3.1). These values are used to

estimate the ratio p. The estimated dimensionality ratios (Eqs. (3.5)) are near unity for the 1D lamellae morphology (Table 3.2).
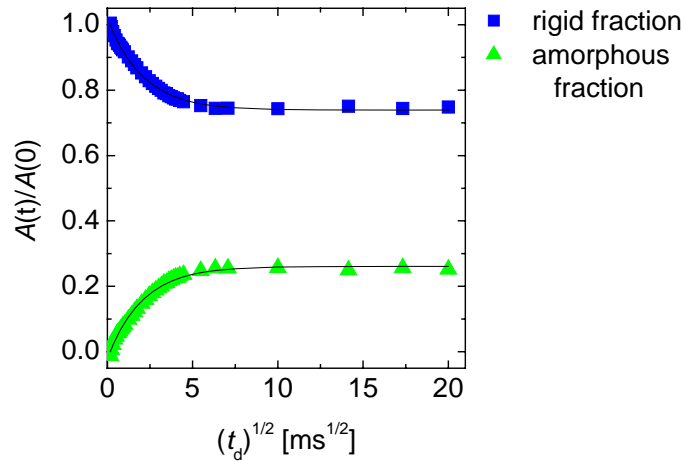
Figure 3.9. Proton spin-diffusion decay and build-up curves for the rigid (■) and amorphous (▲) fractions of iPP recorded using the DQ dipolar filter. These filters select the magnetization of the rigid fractions of iPP. The solid lines represent the best fit for the 1D solutions of the spin-diffusion data for the two-phase morphology.

Table 3.1. Long period (L_p), the thicknesses of rigid (d_c) and amorphous (d_a) domains, at 70° C for iPP samples obtained by NMR spin-diffusion experiments for 1D, 2D and 3D morphology models.

Model	d_r (nm)	d_a (nm)	L_p (nm)
1D	10	2.5	12.5
2D	15.4	3	18.4
3D	21	3.5	24.5

Table 3.2. The spin-diffusion dimensionality, as determined by Equation (6) for iPP.

dimensionality	dimensionality ratio	values of the dimensionality ratio
1D	rE/p	1.2
2D	$rE/[p(2+p)]$	0.68
3D	$rE/[(1+p)^3-1]$	0.52

The values of the proton densities for the different phases of iPP, which are required for the calculation of domain thickness, are determined from the densities of the crystalline and amorphous phases of iPP, i.e., $\rho_c = 0.94$ g/cm^3 and $\rho_a = 0.84$ g/cm^3 [Bra1999]. No correction of the spin-diffusion data due to the longitudinal relaxation effect, has been performed, because the spin-diffusion process is nearly completed at the longest mixing time of $t_d = 70$ ms. This time is significantly shorter than $T_1 = 120$ ms. Moreover, the absolute values of relative fractions instead of the absolute values of the signal intensities, compensate to a large extend for the effect of T_1 relaxation in the present case.

Chapter 4

High Density Polyethylene (HDPE)

4.1 Introduction and motivation

The morphology of semi-crystalline polymers has important effects on the materials properties including the mechanical performance [Pop1987, Man1988]. A quantitative characterization of the phase composition and molecular mobility in semi-crystalline polymers is therefore of great importance to advance our understanding of their properties. In this respect, the phase composition is probably one of the most important morphological parameters, mainly because the amorphous and crystalline phases exhibit vastly different behavior and their relative contributions to the material properties should be accurately known. Traditionally, a two-phase model is used to describe the morphology of undeformed, melt-crystallized polyethylene (PE) and other semi-crystalline polymers [Flo1978, Man1990]. The most common methods for crystallinity determination are X-ray diffraction, density measurement and differential scanning calorimetry. In general, different methods for crystallinity determination do not always yield the same results on exactly the same sample [Isa1999, Hir1990] because of the following reasons: (1) The complex morphology of semi-crystalline polymers requires different sets of assumptions for the analysis of the data recorded by different techniques. (2) The discrimination of the crystalline and amorphous phases is made on the basis of different characteristics, such as the enthalpy of melting (DSC), long range periodicity (WAXD) and the specific volume (density analysis). (3) The two-phase model is a simplified for description of semi-crystalline polymers due to the presence of a crystal-amorphous interface, which can be detected either as crystalline or amorphous fraction depending on the method used [Isa1999]. Various experimental methods, such as neutron scattering, dielectric relaxation, calorimetry and solid-state NMR, show that a thin layer separates crystalline and amorphous phases, and the properties of this layer are intermediate between those for crystalline and amorphous phases [Man1988, Man1990, Iwa2002, His1999]. Therefore, the term "phase composition" is perhaps more appropriate than simply "crystallinity" to emphasize the multi-phase nature of semi-crystalline polymers.

Solid-state NMR is one of the most informative techniques for characterization of molecular mobility and molecular scale heterogeneity in materials [Sch1994]. During the years, different solid-state NMR methods have been used for investigations of morphology

and molecular mobility in PE. At temperatures well above T_g of the amorphous phase, the T_2-relaxation decay and wide-line NMR spectra for PE can usually be decomposed into three components, which originate from a crystalline phase, a semi-rigid crystalline-amorphous interphase, and a soft fraction of the amorphous phase. The intermediate phase has distinct dynamic properties and may not be considered as a true thermodynamic phase. Apparently, the definition of *an interface* or *a semi-rigid fraction of the amorphous phase* is more appropriate for this phase. ^{13}C NMR spectroscopy has provided more detailed information about molecular mobility in the different phases of PE, than ^{1}H NMR because of the high phase selectivity of ^{13}C NMR exploring differences in the chemical shift for crystalline and amorphous phases [Lit2002, Kit1994, Hil1998, Che1994, Sch1991, Kle2002, Kuw2000]. Most of the ^{13}C NMR studies support the three-phase model of semi-crystalline PE. However, other studies suggested four types of structures with distinctly different molecular mobilities [Hil1998, Hu2000]: *two types of crystalline environments,* both with an *all trans* chain conformation - a more perfect one and one with "twist" defects, and *two types of chain fragments in the amorphous phase* - less mobile chain units mainly in the *trans* conformation rotating around the trans chain axis, and more mobile chain fragments whose mobility approaches isotropic tumbling. Detailed information about the nature of the molecular mobility in linear PE has been obtained by two-dimensional (2D) ^{13}C exchange NMR and ^{2}H wide-line NMR [Sch1991, Hen1984].

Despite numerous studies, the morphological origin of PE regions with different molecular mobilities is still a matter of discussion. Therefore, the determination of the thickness of domains with distinctly different molecular mobility is of a substantial interest for a better understanding of the morphology and relaxation properties of PE. Domain sizes in heterogeneous polymers [Bri1993, Pac1984] and polymer fibers [Hu2000, Bud2003, Bud2004, Van1996] have been determined by proton NMR spin-diffusion experiments. Previous ^{1}H NMR spin-diffusion experiments have shown that the lamellae thickness of melt-crystallized PE and PE fibers varies in a wide range depending on the degree of the branching and the thermal history of the sample [Eck1997, Pac1984]. It should be mentioned that *the thickness of the rigid fraction* in semi-crystalline polymers could differ from *the lamellae thickness* since some fraction of the amorphous phase adjacent to the lamellae surface can be largely immobilized and cause an apparent increase in the lamellae thickness. The estimated thickness of the mobile amorphous fraction in PE ranges from 1 nm to 5 nm [Eck1997, Hu2000, Pac1984]. The morphology and phase characteristics of HDPE were also investigated by ^{13}C edited ^{1}H spin-diffusion using a dipolar filter for filtering out the

magnetization from the rigid phase [Van1996]. The dimensions of 6.5 nm, 0.8 - 1.3 nm, and 5 nm were determined for the crystalline, intermediate, and amorphous phases, respectively. ^{13}C solid-state NMR methods offer certain advantages for the analysis of domain sizes in PE due to high phase selectivity [Axe1983, Kit1986].

The high sensitivity of proton NMR makes this method very attractive for characterization of crystallization kinetics [Kri2000], premelting behaviour [Tan1995], and quality control [Bud2003]. The main disadvantage of ^{1}H NMR for a phase analysis in PE is a lack of high selectivity regarding the crystalline and amorphous phases, if the experiments are performed at room temperature. A discrimination of these phases by proton NMR is made on the basis of differences in molecular mobility. Despite numerous ^{1}H NMR studies of PE, it is still not well known how annealing at elevated temperatures affects the phase composition and the thickness of the domains. To the best of our knowledge neither the temperature dependence of the domain thickness was studied by NMR so far, as well as the effect of annealing on the domain thickness.

Based on the above considerations, we aim to establish a reliable method for the analysis of the phase composition and domain sizes in HDPE using high-field proton wide-line NMR and low-field ^{1}H NMR transverse magnetization relaxation methods. By comparing the results of these two methods the performance of low-field NMR measurements for characterization of the domain sizes in semi-crystalline polymers can be validated. Furthermore, the effects of measurement temperature and annealing at elevated temperatures on the polymer morphology are studied in detail, as temperature may play a decisive role in the outcome of the measurements. Knowledge of the temperature effect will help to identity the temperature range for which the largest NMR difference between the different phases can be obtained, while ensuring high accuracy of the method by avoiding annealing. A recently developed NMR spin-diffusion experiment is applied for measuring the domains sizes [Bud2003, Bud2004]. This method explores a double-quantum dipolar filter [Bud2003, Bud2004, Ba1998, Che2005], provides higher differences, and consequently a more accurate analysis is possible. In order to evaluate the reliability of the NMR method, the results are compared to crystallinity and domain sizes determined for the same sample by SAXS and TEM.

4.2 Materials

High-density polyethylene (HDPE) samples were obtained from SABIC Europe BV. The molar mass and molar mass distribution, as determined by size exclusion chromatography in 1,2,4-three chlorobenzene, were characterized by: $M_n = 15 \cdot 10^3$ g/mol, $M_w = 78 \cdot 10^3$ g/mol, and $M_w/M_n = 5.2$. Four millimetre thick compression moulded plates were prepared by melting HDPE in a mould first under atmospheric pressure at 180° C with a subsequent pressure increase to 500 kPa. To create a homogeneous melt, the HDPE sample was kept in the mould for 15 minutes. Afterwards, the mould was cooled with cold water and the HDPE plates were annealed at 100° C in an oven for one hour followed by slow cooling to room temperature. For the annealing study, the sample was further annealed at different temperatures inside the NMR probe for 100 hours.

4.3 Morphology of HDPE by TEM

The transmission electron micrograph of the sample shows in Fig. 4.1 stacked lamellar crystals that are separated by a thin amorphous layer. The estimated thickness of lamellae in the core part of the sample is 16 ± 2 nm. The thickness of the amorphous layer does not exceed 2 - 3 nm. The value of the L_p was measured directly from the TEM image. The real values of the L_p were obtained by converting the actual measured value (mm) using the scale of the TEM image. No more analysis of the TEM image has been performed.
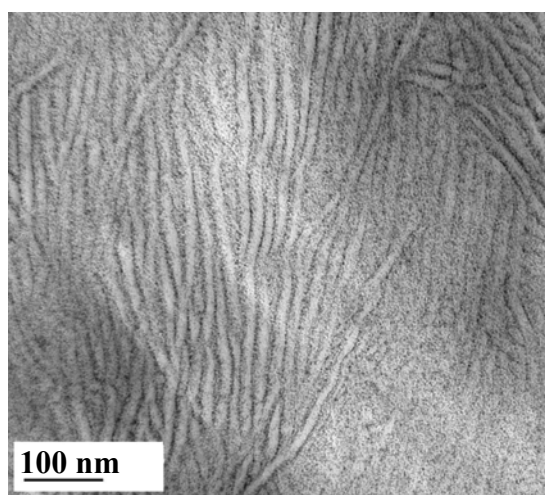
Fig. 4.1 TEM picture of a core part of a compression moulded HDPE plate. The length of 100 nm is shown in the bottom left-down corner of the figure.

4.4 Crystallinity and morphology by SAXS

The SAXS patterns reveal a maximum due to the long period (Fig. 4.2a), which is a typical feature of semi-crystalline polymers. For HDPE, this can be interpreted in terms of a quasi-periodic, lamellar morphology as outlined in more detail above. The analysis of the one-dimensional electron density correlation function assumes the two-phase model, which cannot be strictly valid due to the presence of the interfacial layer, as shown below by NMR experiments.
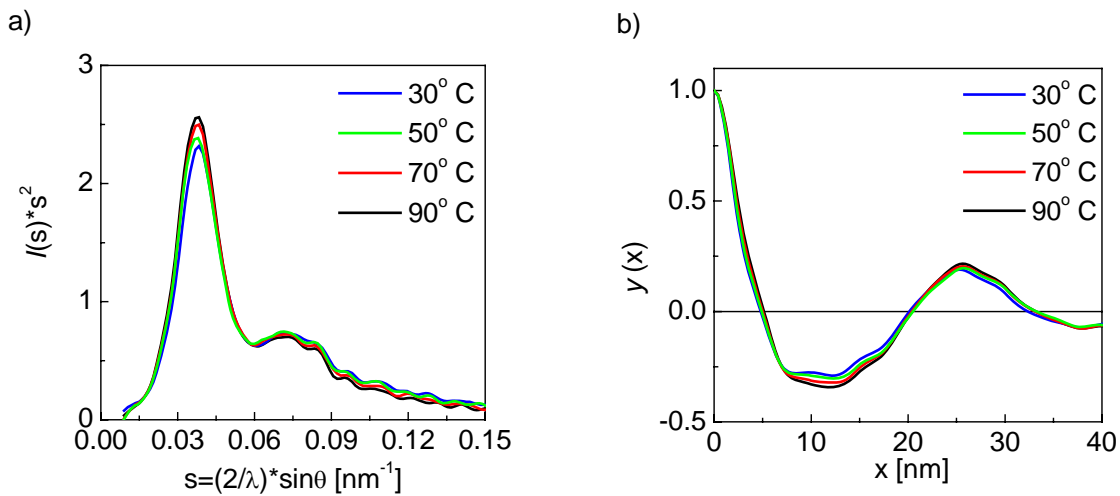
Fig. 4.2 (a) One-dimensional scattering intensities $I_1(s)=I(s)*s^2$ recorded at various temperatures, indicating the maximum of the long period due to periodic stacking of crystalline lamellae. (b) Normalized linear correlation functions $\gamma(x)$ derived from the SAXS.

The long period L_p is estimated from the position of the first interference maximum, at about 0.038 nm^{-1} (Fig. 4.2a), and from the normalized correlation function, which is shown in Fig. 4.2b. According to these data, the long period is close to 25 nm, which is larger than the values obtained by TEM, i.e. (18 - 19) ± 2 nm. It is noted that the L_p value can suffer from systematic errors due to the experimental set-up used.

Based on the analysis of the correlation functions, the thickness of the crystalline domains is estimated to 17 – 18 nm, which is in good agreement with the value measured by TEM and NMR, as shown below. With the values of d and L_p from the correlation functions, the crystallinity is estimated to 68 ± 5 vol%. This value corresponds to a crystallinity in mass per cent of 71 ± 5 wt %, which is calculated with the densities of the crystalline and amorphous phases of 0.99 g/cm^3 and 0.87 g/cm^3, respectively. It is suggested in this

calculation that the density of an interfacial layer is given by the mean value of the densities for the crystalline and amorphous phases. SAXS experiments at different temperatures reveal almost the same long period, lamella thickness, and crystallinity in the temperature range from 30° C to 90° C.

4.5 Temperature dependence of the phase composition and chain mobility of HDPE by NMR

The existence of three fractions with different molecular mobilities is revealed by ^{1}H NMR spectra, and the proton NMR free induction decay (FID) was measured for HDPE at 100° C. The relaxation components are assigned to three fractions with different molecular mobilities, the rigid - T_2^{rigid}, semi-rigid - $T_2^{semi-rigid}$, and soft -T_2^{soft} fractions, respectively [Ber1978, Fed1985, Han1998, Lit2004]. Like the FID, the spectra can be deconvoluted into three components (example Fig.3.3 and Fig. 3.4). Broad, intermediate and narrow lines originate from rigid, semi-rigid and soft fractions of HDPE, respectively. However, the quantitative analysis of FID and wide-line NMR spectra in terms of crystalline phase, crystal-amorphous interface and soft fraction of the amorphous phase can be complicated due to the following reasons: (1) To observe distinct differences in molecular mobility of the crystalline and amorphous phases, and consequently in the T_2 relaxation and the line width, the temperature of the sample should substantially exceed the dynamic glass transition temperature at the time scale of the NMR experiment, i.e. in the range of 10^{-4} - 10^{-5} sec. The T_g of the HDPE sample that was determined by a high performance DSC equals –57° C. The NMR T_g should be observed in the temperature range from –30° C to –10° C. Therefore, a proper choice of the temperature of the NMR experiment is required. (2) Since the T_2-relaxation experiments should be performed at temperatures well above T_g, the sample exposure to elevated temperatures can cause irreversible changes in the phase composition and thus in the molecular mobility. Therefore, the temperature for the experiments should not be too high to prevent annealing of the sample during the NMR experiment. In order to find the optimum temperature for determination of the phase composition by NMR, we recorded the temperature dependence of the T_2 relaxation and the wide-line spectra (Fig. 4.3).

At room temperature, a significant fraction of the amorphous phase is rigid on the time scale of the NMR experiments and this amorphous fraction contributes to the intensity of the broad line of the NMR spectra and the short T_2-relaxation component of the FID, as can be concluded by comparing the amount of the rigid fraction with the crystallinity determined by

SAXS, i.e 71 ± 5 wt%. Upon increasing temperature, the amount of the rigid fraction, which is composed of the crystalline phase and the rigid fraction of the amorphous phase, gradually decreases, whereas the amount of the semi-rigid and soft fractions increases. These changes are caused by an increase in molecular mobility of the less constrained chain fragments in the amorphous phase, and possibly by melting of thin lamellae, which are inserted into the primary stack of crystallites upon cooling of HDPE which was crystallized at elevated temperatures [Mat1994].
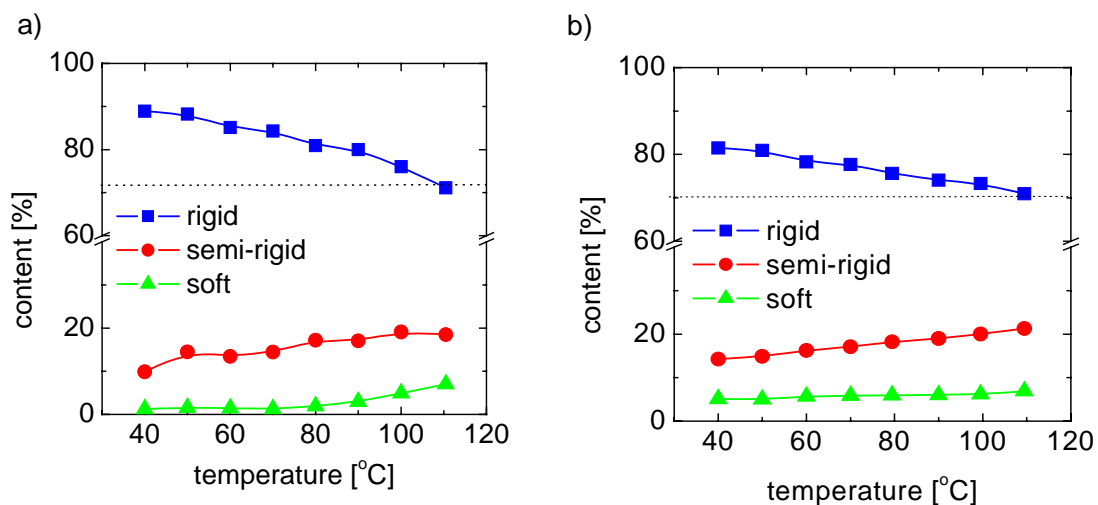
Fig. 4.3. Temperature dependence of the amount of rigid, semi-rigid, and soft fractions of HDPE measured with (a) low-field, and (b) high-field NMR spectrometers. Dotted line shows crystallinity that was determined by SAXS in the temperature range from 30 ^{0}C to 90 ^{0}C.

In the temperature range from approximately 100° C to 120° C, the amount of rigid fraction is close to the crystallinity measured by SAXS. Above 120° C, the amount of the rigid fraction decreases due by melting. The DSC analysis of this sample shows that the extrapolated onset temperature of melting, as determined by a method described elsewhere [Cru2004] is in proximity of 125° C and the peak of melting is observed at 136° C. Thus, the temperature range from 100° C to 110° C is the most suitable for an accurate determination of the phase composition in HDPE, since (1) the largest contrast in molecular mobility in the different fractions of HDPE is observed at these temperatures, (2) no substantial sample annealing occurs as will be shown below, and (3) the amount of the rigid HDPE fraction is close to crystallinity determined by SAXS. It is mentioned in this context that, in general, different methods for determination of crystallinity do not necessarily yield the same crystallinity value for exactly the same sample.
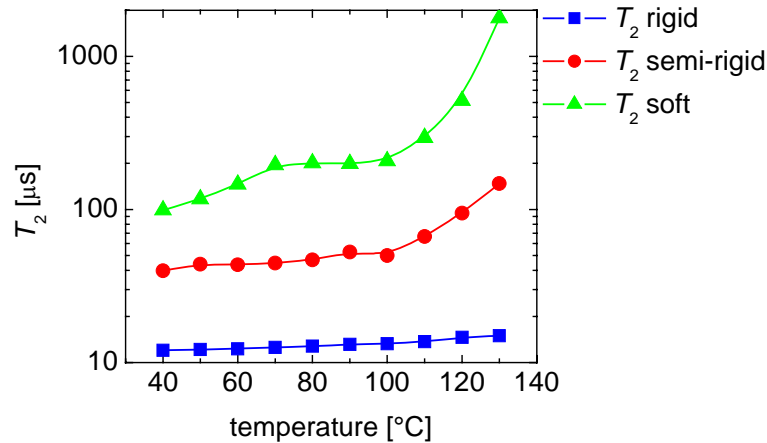
Fig. 4.4. Temperature dependence of ^{1}H T_2 relaxation times for HDPE. The relaxation components with short (T_2^{rigid}) intermediate ($T_2^{semi-rigid}$), and long (T_2^{soft}) decay time (see Figure 4.3) are assigned to the rigid, semi-rigid and soft fractions of HDPE, respectively.

As far as the molecular mobility in HDPE is concerned, the changes in the T_2 relaxation times in the temperature range studied (Fig. 4.4) can be assigned to the following relaxation transitions in HDPE [Boy1985]. A small increase in T_2^{rigid} above 60 – 80° C is related to chain motions in the crystalline phase - the α-relaxation process, which occurs prior to melting. Interpretation of the molecular mobility in the amorphous phase is more cumbersome. Despite numerous studies of relaxation processes in PE by different methods, a molecular interpretation of the relaxation processes in the amorphous phase is under discussions [Woo1993]. The increase in T_2^{soft} with increasing temperature from 40° C to 70° C can be associated with a relaxation process in the soft fraction of the amorphous phase. This temperature range and frequency of this relaxation, as estimated from change in T_2^{soft} ($\approx$ 5 – 10 kHz), are in the range that is characteristic for the β-relaxation in the amorphous phase. It is noted that the β-relaxation in HDPE is very broad and hardly detectable by mechanical and dielectric relaxation methods [Woo1993]. Partial melting of HDPE crystals above 120° C causes a decrease in constraints on chain motions in the amorphous phase and therefore an increase in molecular mobility in the amorphous phase, as reflected by an increase in $T_2^{semi-rigid}$ and T_2^{soft} (Fig 4.4).

4.6 The effect of annealing on molecular mobility and the phase composition by NMR

The experiments above have shown that the analysis of the phase composition should be preferably performed at elevated temperatures where the NMR parameters show enhanced contrast. Since the NMR experiments take approximately 2 hours, sample annealing is indeed an issue. In order to determine a temperature, at which no detectable changes in the relaxation will be observed during NMR experiments, the T_2 relaxation was recorded in real-time at 100° C, 110° C and 121° C. The data were recorded at one-hour intervals. Sample exposure to 100° C and 110° C for 60 hours causes hardly any change in the molecular mobility and the phase composition. Annealing at 121° C for 100 hours showed an increase in the amount of the rigid fraction by 1 wt% at the expanse of semi-rigid and the soft fractions of the amorphous phase (Fig. 4.5a).
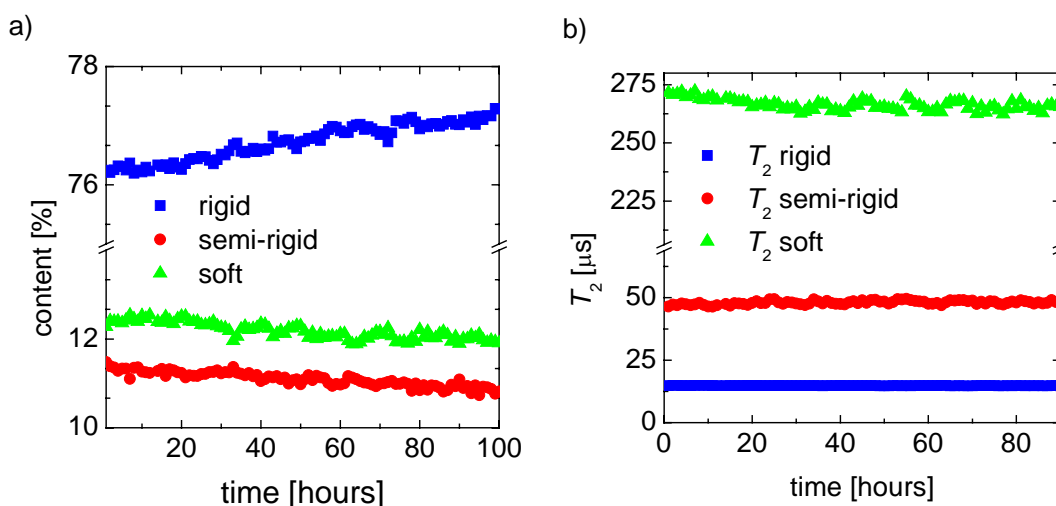
Fig. 4.5. a) The amounts of crystalline phase (% T_2^{rigid}), semi-rigid crystal-amorphous interface (% $T_2^{semi-rigid}$) and soft fraction of the amorphous phase (% T_2^{soft}) in HDPE as a function the annealing time at 121° C. b) The effect of annealing on molecular mobility, as determined by the T_2 relaxation time for the different phases of HDPE. Larger amplitude and/or frequency of molecular motions give rise to longer T_2 values.

The relaxation characteristics above are determined for the crystalline phase and the crystal-amorphous interface from the analysis of the FID and using the Hahn-echo data for the soft fraction of the amorphous phase, as described in experimental part. Due to annealing both the melting temperature as well as the melting enthalpy increase, namely: the melting peak shifts from 139.1° C to 145.4° C, and the melting enthalpy increase from 232.8 J/g to 273.9 J/g. The molecular mobility in the rigid, semi-rigid, and soft fractions of HDPE is also slightly affected by annealing at 121° C (Fig. 4.5b). The value of T_2 for the rigid fraction (T_2^{rigid})

decreases upon annealing from 15 μs to 14 μs due to perfection of crystals, as can be also concluded from large increase of the melting enthalpy at only 1 wt% crystallinity increase. The T_2-relaxation time for the semi-rigid fraction and soft amorphous phase decrease by a few percent. This decrease is likely to be caused by additional constraints imposed on to the amorphous phase due to the increased amount of crystalline phase.

The analysis of the temperature dependence of the T_2 relaxation and the annealing study show that 100° C is the optimum temperature for quantitative analysis of the phase composition in HDPE using the NMR experiments. At this temperature, the relaxation components T_2^{rigid}, $T_2^{semi-rigid}$, and T_2^{soft} (Fig. 4.4) largely originate from the crystalline phase, semi-rigid crystal-amorphous interface, and the soft fraction of the amorphous phase, respectively. The relative fraction of these components represent the corresponding weight fractions (Fig. 4.3a). The observation of three distinct T_2 relaxations rather than a wide distribution of the relaxation times indicate a fast loss of restrictions on rotational and translational chain mobility when moving away from the crystalline phase to the interface and to the soft fraction of the amorphous phase. Therefore, a step-wise change in the molecular mobility at the position between different phases is observed. Thus, we can conclude that the three-phase model describes the phase structure of HDPE well [Woo1993, Sch1999, Pav2005].

4.7 The thickness of domains in HDPE

The spin-diffusion experiments were performed for HDPE at 70° C, 100° C and 120° C before and after annealing for 100 hours at 121° C. In order to determine the size of the domains with different molecular mobilities, the spin-diffusion curves (Fig. 4.6) were fitted with equations that have been obtained using analytical solutions of the spin-diffusion equation for three distinct phases characterized by different spin diffusivities [Bud2003]. The values of the proton densities for the different phases of HDPE, which are required for the calculation [Bud2003], are determined from the densities of crystalline and amorphous phases of HDPE, i.e $\rho_c = 0.99$ g/cm^3 and $\rho_a = 0.87$ g/cm^3. It is suggested that the density of the interface, $\rho_i = 0.93$ g/cm^3, is the mean value of the densities for the crystalline and amorphous phases.
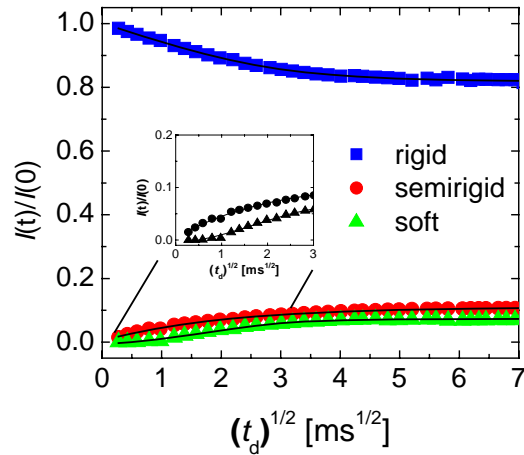
Fig. 4.6. Proton spin-diffusion data for the rigid (■), semi-rigid (●), and soft fractions (▲) of HDPE at 100° C. The experiment was performed on a low-field NMR spectrometer. The solid lines are the best fit with 1D solutions of spin-diffusion equations [Bud2003]. The data of short t_d are shown in the inset.

Table 4.1. The thickness of rigid (d_{rigid}), semi-rigid ($d_{semi-rigid}$) and soft domains (d_{soft}) at different temperatures in non-annealed HDPE. The domain thickness was obtained from ^{1}H spin-diffusion experiments with a DQ filter.[a,b]

The thickness of domains	Temperature		
	70 °C	100 °C	120 °C
d_{rigid} (nm)	18.0 (19.0)	17.0 (17.0)	13 (12.5)
$d_{semi-rigid}$ (nm)	1.1 (1.1)	1.3 (1.4)	1.2 (1.3)
d_{soft} (nm)	0.6 (0.5)	0.7 (0.8)	1.0 (1.1)
Long period from NMR: $\Sigma\ d$ (nm)	20.8 (21.7)	20.3 (20.6)	16.4 (16.2)

[a] Measured using 500 MHz and 20 MHz (in brackets) NMR spectrometers.
[b] The relative error of the data, is estimated to about 15 %.

The thickness of HDPE domains before annealing was determined using the time-domain and the frequency-domain spin-diffusion experiments, both methods yielding results that are in good agreement with each other (Table 4.1). The result for the long period is almost constant below 100° C (Fig. 4.7a). Moreover, below 100° C, the thickness of the rigid fraction d_{rigid} slightly exceeds the lamella thickness determined by TEM and SAXS. This is due to the fact that the interfacial layer with intermediate mobility on the lamellae surface is largely immobilized below 100 °C, as can be seen by comparing the amount of the rigid fraction with the sample crystallinity measured by SAXS (Fig. 4.3). The thickness of the rigid domain slightly decreases with increasing temperature and at approximately 100° C reaches the lamella thickness as measured by TEM and SAXS, i.e. 16 – 18 nm. Thus, the thickness of rigid domain at 100° C represents lamellae thickness. The lamellae thickness at 120° C is

smaller than that at 100° C, which could be caused by partial melting of the sample. Moreover, fragmentation of lamellae upon melting could also cause an apparent decrease in lamellar thickness due to an increase in the efficiency of the spin-diffusion. As far as the soft domain is concerned, its thickness increases with increasing temperature at the expense of the rigid domains. The thickness of the interface is nearly constant in the studied temperature range and equals 1.1 – 1.3 nm (Fig.4.3c). This value is in the same range as previously estimated by Monte Carlo simulations [Gau2000, Bal2000, Man1990]. The simulations have shown that density, orientational order and transverse structure parallel to the lamella surface change from those of the crystalline phase to the disordered amorphous phase within a layer of 1.0 – 1.2 nm thickness that is adjacent to the lamellae surface. It should be noted that the interface thickness is close to the length of the statistical segment for PE chains, which consists of 7 – 7 carbon – carbon bonds [Aha1983] and equals to 0.8 nm for fully extended PE chain. Therefore, distinct differences in chain mobility in different fractions of HDPE are apparently caused by short-range correlations of chain motion due to the short length of statistical segments.
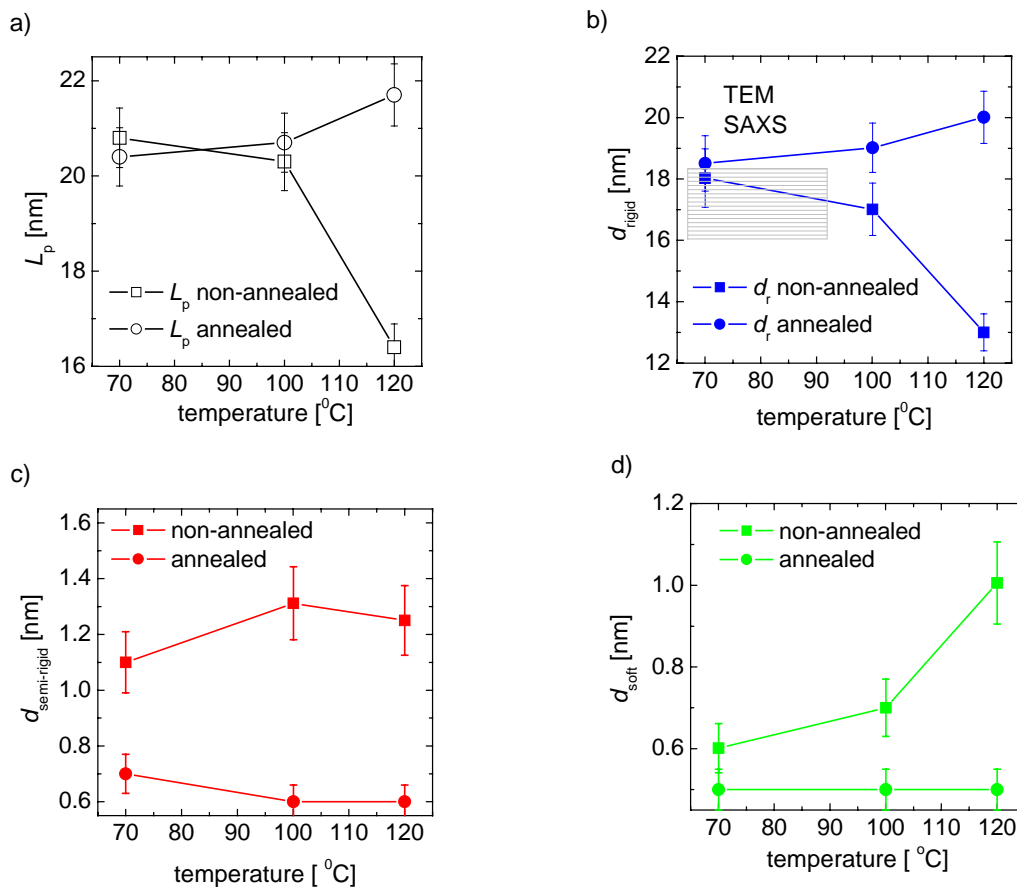
Fig. 4.7. The temperature dependence of the long period from NMR (a), the thickness of rigid (b), semi-rigid (c), and soft (d) domains of HDPE. The experiments were performed on low-field NMR spectrometer for a compression moulded plate before and after annealing at 121° C for 100 hours. The shaded area shows the lamellar thickness measured by SAXS and TEM.

4.8   The effect of annealing on the thickness of domains and molecular mobility

In order to determine the effect of annealing on the thickness of the rigid, semi-rigid, and soft domains, a compression moulded HDPE plate was annealed at 121° C for 100 hours. The thickness of domains was determined at 70° C, 100° C and 120° C and the results for the annealed sample are compared to those of the sample not annealed (Fig. 4.7). Annealing causes a significant decrease in the thickness of the interfacial layer and the soft amorphous phase, and an increase in the lamellar thickness, which can clearly be seen for the results measured at 120° C. The annealing causes only minor changes in molecular mobility (Fig. 4.5b).

The annealing study suggests the following mechanism of morphological changes due to annealing at elevated temperatures. Upon approaching the melting temperature, the molecular mobility increases both in the amorphous regions, the crystal-amorphous interface, and in the crystalline phase (α-relaxation) (Fig. 4.4). Previous ^{13}C NMR studies have suggested two types of crystalline environments with distinctly different molecular mobilities: a more perfect one and one with defects [Hil1998, Hu2000]. It might be suggested that chain mobility increases at elevated temperatures in the less ordered, surface layer of lamellae, as follows from a decrease in the lamella thickness above 100° C for the non-annealed sample (Fig. 4.7b). An increase in the molecular mobility is accompanied by partial melting of small crystals and less ordered fragments of the lamellae. An increased mobility in the amorphous phase and chain diffusion in- and out of the crystals (α - relaxation) [Sch1991] facilitate to some extent morphological changes towards a more thermodynamically stable, better-ordered crystalline structure and thicker lamellae. It should be mentioned in this respect that the root-mean-square displacement of chains in PE lamellae amounts to more than 10 nm at 100° C within 100 seconds [Sch1991]. Chain rearrangements upon prolonged annealing at 121° C for 100 hours result in a decrease in molecular mobility in the crystalline phase, as follows from a slight decrease of T_2^{rigid} during annealing and large increase in the melting enthalpy (from 232.8 J/g to 273.9 J/g) at only 1 wt% increase in the crystallinity (Fig. 4.5b). This might suggest perfection of the crystalline order. Lamellae thickening and a slight increase in the crystallinity would cause additional slippage of chain entanglements towards the inner part of inter-lamellar amorphous regions causing additional immobilization of the soft fraction of the

amorphous phases, as can be concluded from the decrease of the thickness of this layer (Fig. 4.7c) and the decrease in T_2^1 (Fig. 4.5b). Thus, our observations reveal that annealing is accompanied by a continuous shift of the crystal-amorphous interface towards the inner part of the amorphous regions and a reduction of the thickness of the amorphous layer [Che1994, Mat2001, Bas1973, Str1997].

4.9 Conclusions

The effects of temperature and annealing on the following molecular and morphological characteristics of HDPE were studied by time- and frequency- domain proton solid-state NMR: (i) the amount of rigid, semi-rigid, and soft fractions of HDPE, (ii) the thickness of the domains with different molecular mobilities, and (iii) the molecular mobility in these domains.

This study focused on two areas, namely (1) the improvement of low-field solid-state NMR methods for determining the thickness of domains in heterogeneous polymers, and (2) a better understanding of the phenomena that occur upon annealing of HDPE. (1) The novel spin-diffusion experiments that are based on the double-quantum dipolar filter provided reliable information about the thickness of lamellae, crystal-amorphous interface and soft fraction of the amorphous phase. The applied method allows a better discrimination between the HDPE phases and, therefore, a more accurate analysis of the thickness of the domains. In order to improve the accuracy of the method, the temperature dependence of the spin diffusivities in all three phases was determined, which allowed us to obtain reliable information about changes in the domain thickness as a function of temperature. The lamellae thickness and the long period determined by NMR, are in good agreement with the results of classical methods, i.e. TEM and SAXS, which proves the reliability of the NMR method. This study has also showed that spin-diffusion experiments with advanced dipolar filters can be performed with a low cost, low-field NMR spectrometer, which broadens the range of applications of this equipment.

(2) This study shows that the three-phase model is the most appropriate description of the phase composition in HDPE at least as revealed by ^{1}H NMR data. The spin-diffusion experiments show that rigid and soft fractions of HDPE are separated by a thin layer with intermediate molecular mobility. The thickness of this interface is nearly constant in the temperature range from 70° C to 120° C and its value is comparable to the length of the statistical segment of the PE chains. This suggests that the interfacial layer largely originates

from constraints on rotational and translational motions of chain fragments adjacent to the lamellae surface.

The crystalline phase, the semi-rigid crystalline-amorphous interface, and the soft fraction of the amorphous phase exhibit a larger contrast in molecular mobility at temperatures above 90° C. Upon increasing the temperature, the molecular mobility begins to increase in the inner/softer part of the amorphous phase towards the lamellae surface. Annealing causes a significant decrease in the thickness of the interfacial layer and the soft amorphous phase, and an increase in the lamellar thickness. It is suggested that annealing is accompanied by structural reorganizations at the frontier between the crystalline and amorphous phases, and these reorganizations are largely influenced by the chain dynamics in the crystalline and amorphous phases. Annealing leads to improving perfections of the crystalline order (presumably in a layer close to the lamellae surface), and a continuous shift of the interface towards the inner part of the amorphous regions reducing the thickness of the soft amorphous layer. These observations are in agreement with a previously proposed mechanism of partial melting and surface crystallization upon annealing of HDPE at premelting temperatures [Str1997].

Chapter 5

Isotactic Polypropylene (iPP)

5.1 Introduction and motivation

The physical and mechanical properties of semi-crystalline polymers (like isotactic polypropylene), and their practical lifetime, are significantly influenced by both the changes in the degree of crystallinity [Pop1987, Hal1972, Boy1979, Boy1983,Boy1984, Boy1985, Str1980, Man1964, Man1985, Neg1992, Wor1996], and the orientation distribution of the crystalline volume portion [Bel1993, Gos1996]. Both quantities typically change when the sample is exposed to temperatures well above the glass transition due to annealing [Hik1997, Alo1999, Aki1999, Mar2000, Iij2000, Mai2000, Weg2000, Ali2001, Lab2001]. This means that the degree of the crystallinity and the orientation distribution depend on processing conditions, crystallization, annealing, and thermal history in such materials. It is known that annealing of semi-crystalline polymers after fabrication causes changes in the structure and properties of the materials. This process has been employed to improve the final properties of polymers via healing of defects and diminishing residual stress and strain. In addition, lamellae thickening and rearrangement of the chain during heating also occur upon annealing.

For establishing structure-property relationships of semi-crystalline polymers, the characterization of lamellar thickness in bulk materials is a necessity, because their thermal and physical properties depend largely on the characteristic of the lamellae. Traditionally, transmission electron micrograph (TEM) and small-angle X-ray scattering (SAXS) are two major techniques used to determine the lamellar thickness. The former offers the advantage of direct access to the morphology. SAXS is a well-developed method to quantitatively determine the thicknesses of alternating layers of the crystalline and amorphous regions that are formed in semi-crystalline polymers. The morphological parameters can be deduced from SAXS data based on a model calculation. Although an indirect approach is applied, SAXS provides volume average characteristic.

Proton NMR spin-diffusion experiments have been used to provide information about the thickness of domains with different molecular mobility in polymers [Bri1993, Pac1984] [Hu2000, Bud2003, Bud2004, Van1996].

The main aim of this chapter is to study the change in the rigid fraction/crystallinity, semi-rigid, and soft fractions, and lamellae thicknesses for both annealed and non-annealed

iPP samples. This was done using a combination of DSC, SAXS, WAXD, TEM, and ^{1}H solid-state NMR, including spin-diffusion NMR. The ^{1}H NMR spin-diffusion methods, which explore both double-quantum (DQ) dipolar filter [Bud2003, Ba1998, Che2005] and the Goldman-Shen (GS) filter [Gol1961, Dem1996], were used for the first time to provide a more accurate analysis of the domain thickness of iPP. It is thought that TEM, SAXS, and NMR are complementary techniques, providing morphological evidence on the nanometer scale. The most probable morphology was established by comparing the ^{1}H spin-diffusion data with the multidimensional evaluation of the magnetization by spin-diffusion. The results are compared under the given conditions, which include the annealing time and annealing temperature. A simple model of crystal thickening as a function of the annealing time is discussed. The correlation between transverse relaxation rates and thickness of the rigid domain is presented, i.e., microscopic and mesoscopic properties.

5.2 Materials

Isotactic polypropylene homopolymer was obtained from SABIC Europe BV and used in our experiments. The material was injected in an Engel 45A machine. The melt temperature was set to 235° C, the holding pressure to 40 MPa, the holding time to 20 s, the cooling time to 20 s, and the overall cycle time to 49.5 s. For the annealing study, the sample was further annealed in the NMR probe at 134° C, 143° C and 153° C, for several times between 15 minutes and 30 hours.

5.3 Crystallinity by DSC

Quantities like the enthalpy, derived from heat capacity measurements, can provide important information about the physical state of the material. The heat capacities of iPP annealed for 10 hours at 143° C and iPP annealed for 10 hours at 153° C, are presented in Fig.5.1 as a function of temperature. Parts a and c of Figure 5.1 show the heat capacity c_p and crystallinity W data for the first heating curve and the second heating/cooling curve, respectively. The observed differences between the first heating curves for non-annealed and iPP annealed for 10 hours at 143° C and 153° C (Figure 5.1a) are due to the thermal treatment (thermal history) of the sample. For completion, heat capacity measurements of the cooling and second heating curve are presented as well in order to verify whether or not the thermal treatment modifies the polymer material. The thermal history of iPP is erased after the first heating scan and by keeping the polymer for 5 minutes in the molten state (200° C) (Fig. 5.1d).

Litvinov and Soliman showed that annealing of iPP gives rise to shoulders in the DSC thermograms [Lit2005]. In order to compare the annealed samples with non-annealed iPP, an offset temperature is defined in this study. The offset temperature corresponds to a drastic increase of the heat capacity due to melting of the polymer (see Fig. 5.1b). Offset temperatures of 144° C and 153° C are observed for iPP annealed at 143° C and 153° C for 10 hours, respectively. An apparent offset temperature of 134° C (increase of C_p in comparison to the baseline) is observed for non-annealed iPP. The determined offset temperatures for the annealed samples correlate with the applied annealing temperatures. These observations are in agreement with the NMR data discussed below.

d)
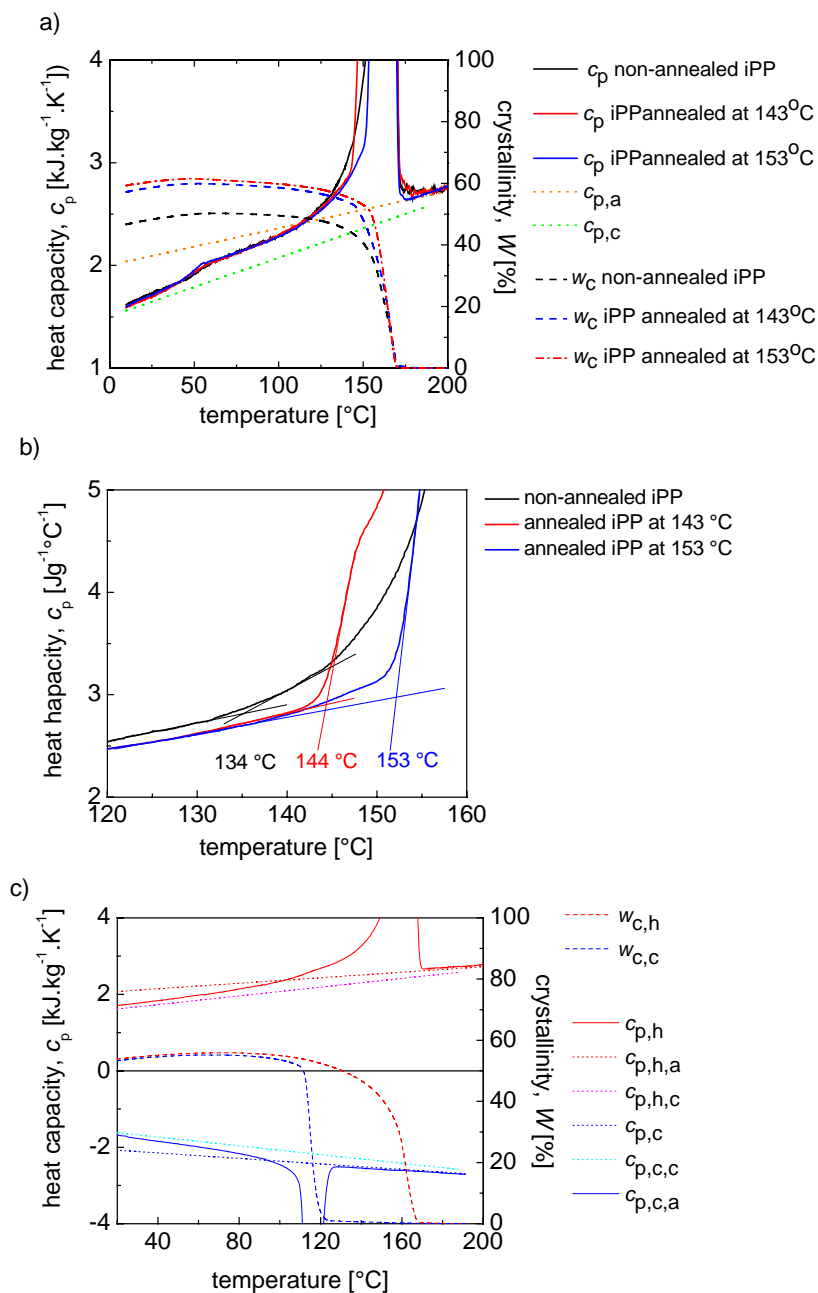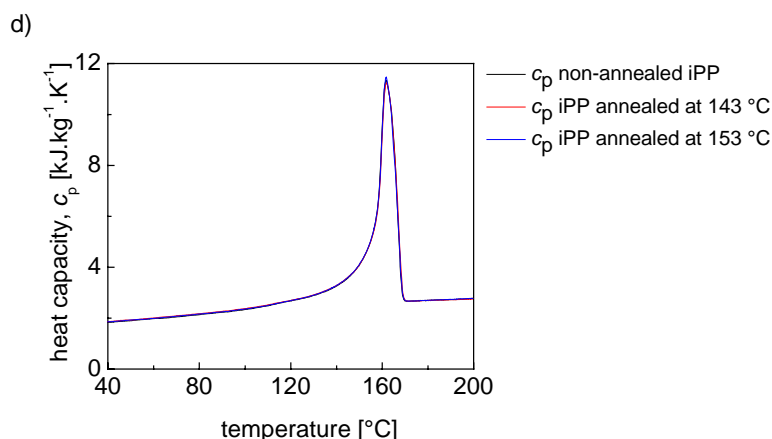
Figure 5.1. (a) Heat capacity (c_p) and crystallinity (W) data recorded during the first heating of non-annealed iPP (black solid and dashed lines), annealed at 143 $°$C iPP (red solid and dashed lines), and annealed at 153 $°$C iPP (blue solid and dashed lines). The annealing time was 10 hours. The green and orange dotted lines represent the heat capacity for the crystalline ($c_{p,c}$) and amorphous ($c_{p,a}$) phases, respectively. (b) Heat capacity and onset of melting for non-annealed iPP (black line), annealed at 143 $°$C (red line) and annealed at 153 $°$C iPP (blue line), respectively. The annealing time was 10 hours. (c) Heat capacity (solid lines) and crystallinity (dashed lines) recorded during the second heating ($c_{p,h,a}$ and $c_{p,h,c}$, $W_{c,h}$) and cooling ($W_{c,c}$, $c_{p,c,a}$ and $c_{p,c,c}$) of iPP. The dotted lines represent the heat capacity for the amorphous and crystalline phases for the second heating and cooling, respectively. (d) Heat capacity curves recorded for the second heating curves for non-annealed iPP (black line), annealed at 143 $°$C (red line) and annealed at 153 $°$C iPP (blue line). The annealing time was 10 hours.

A complete heat capacity analysis is performed. The extreme states in which the material can be found (100% crystalline and 100% amorphous) are referred to as reference states. These data are reported for a large number of polymers in the ATHAS Data Bank [Pyd1994].

Mathot has shown that the polymer can be regarded as consisting of regions having the same thermal properties as the reference states, and a simple two-phase model can be used in order to determine the enthalpy-based mass fraction crystallinity [Mat1944]. This means that no transition layers between the regions and no contributions from interfaces are taken into account for the analysis of DSC data in this study. We observed that the crystallinity of iPP, determined at 80° C ($W_{80°C}$), increases as expected with the annealing temperature: $W_{80°C}$ = 50 wt% for non-annealed iPP, 59 wt% for iPP annealed at 143° C and 61 wt% for iPP annealed at 153° C, (Fig.5.2).
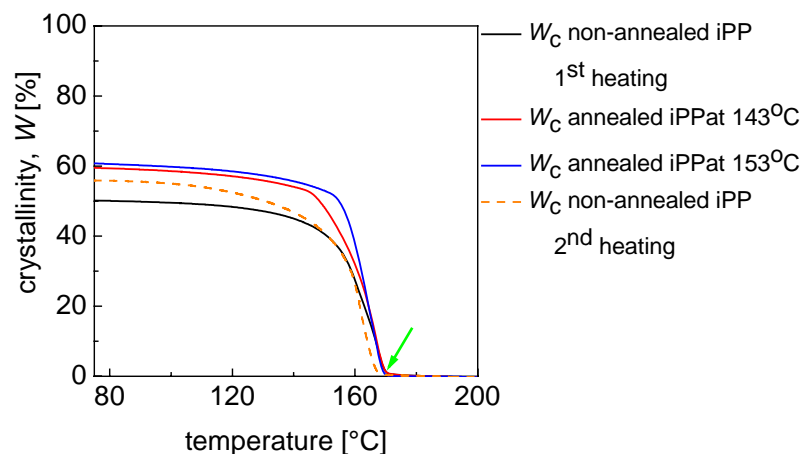
Figure 5.2. Crystallinity of iPP at the first heating curves (solid lines) of non-annealed iPP (black), iPP annealed at 143° C (red) and 153° C (blue). The annealing time was 10 hours. The crystallinity at second heating curve is shown by the orange dashed line.

After erasing the thermal history by melting, the crystallinity of iPP (Fig. 5.2 - second heating curve; the dashed, orange line) is somewhat higher than the crystallinity of non-annealed iPP (Fig. 5.2 - first heating curve; the straight, black line), but still lower than the crystallinity of both annealed iPP samples ($W_{80°C}$ = 55 wt% for the second heating curve). Thus, the crystallinity of iPP derived from the first heating curve shows a thermal history different from the one derived from the second heating curve (Figure 5.1d). The end of the melting behaviour of the annealed samples is located at a higher temperature than that of the second heating curve (indicated in Fig. 5.2 by the green arrow). This is expected when crystal thickening and crystal perfection occur. NMR experiments also show an improvement of crystal perfection upon annealing, as will be shown below. Crystal thickening is observed by NMR and TEM during annealing of iPP samples. Thus, the results of NMR and TEM are in line with the heat capacity data.

5.4 Morphology of iPP by TEM

The transmission electron micrograph is used to determine the type of the morphology in the studied samples. A TEM image of the non-annealed iPP sample is shown in (Fig. 5.3a). Stacked lamellar crystals separated by a thin amorphous layer can be observed. The iPP samples annealed at 143° C and 153° C for 10 hours reveal a cross-hatched morphology (Fig. 5.3b and 5.3c) consisting of radial and transverse lamellae. The thickness of the lamellae increases with increasing the annealing temperature.
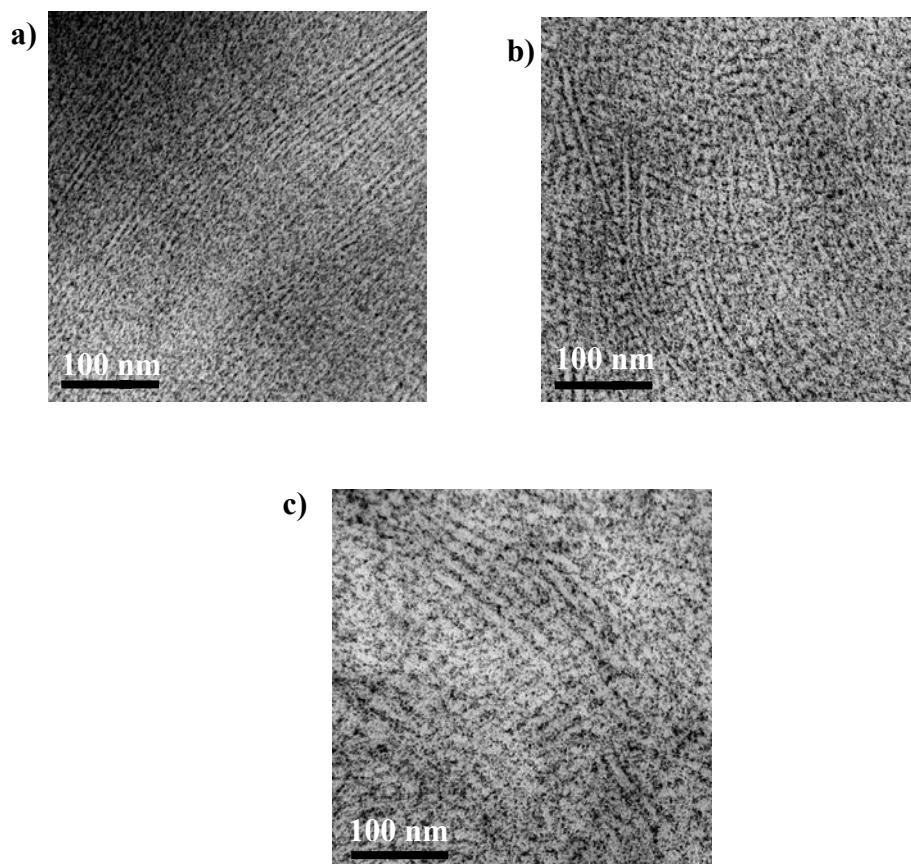
Figure 5.3. TEM image for non-annealed iPP (a), iPP annealed at 143° C (b), and 153° C (c). The annealing time was 10 hours. The scales of the images are show in the figures.

5.5   Crystallinity and Morphology by SAXS

The crystallinity of both annealed and non-annealed iPP samples has been determined by SAXS.
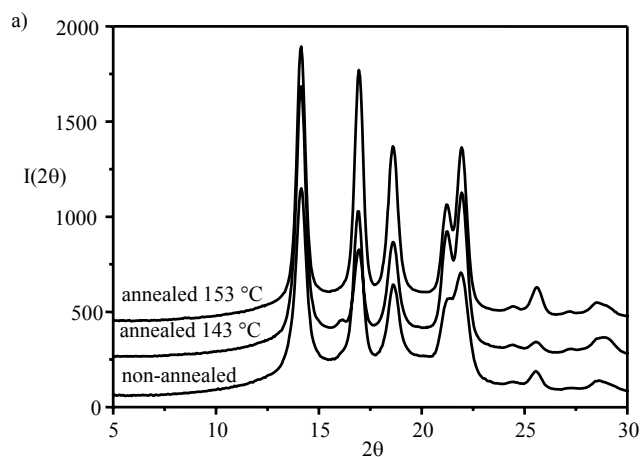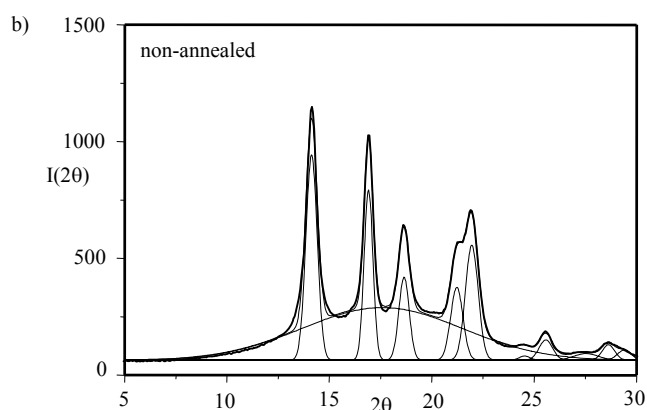
Figure 5.4. a) One-dimensional WAXD intensities obtained via integration of two-dimensional WAXD patterns for non-annealed iPP, and iPP annealed at 143° C and 153° C for 10 hours. b) Deconvolution of WAXD pattern for crystalline and amorphous phases for non-annealed iPP.

Integration of the 2D-WAXD pattern over a pie-shaped area yielded the intensity profiles displayed in Fig. 5.4a. In all cases, the sequence of the detected diffraction maxima is consistent with the monoclinic α-structure of polypropylene. The contributions arising from the crystalline and the non-crystalline components are extracted via peak fitting of the diffraction pattern (Fig.5.4b). The latter yielded the (X-ray) crystallinity which showed a 9% increase from a value of 0.49 ± 0.05 for the non-annealed system to 0.58 ± 0.05 for a sample annealed at 153° C. These values are in good agreement with DSC crystallinity.
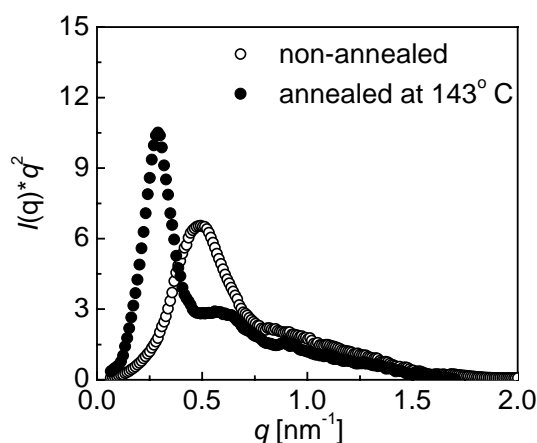
Figure 5.5. One-dimensional SAXS intensity $I(q)=I(q)*q^2$ recorded for non-annealed iPP and iPP annealed for 10 hours at 143 °C.

The SAXS patterns reveal well-defined interference maxima owing to a quasi-periodic arrangement of the crystalline domains. More details about the scattering and correlation functions are discussed in Ref. [Hed2007]. The one-dimensional scattering intensities

$I(q)^* q^2$ are shown in Fig. 5.5, where $q = (2/\lambda)^* \sin\theta$, λ is the wavelength of the X-ray radiation and, θ is the scattering angle and q is the scattering vector.

It follows from the results in Fig. 5.5 that annealing has a strong influence on the lamellae thickness. After annealing, the position of the interference maximum shifts towards lower scattering angles which indicates an increase of the effective long period. This is also reflected by the linear correlation functions, calculated from the scattering intensities (Fig. 5.6).
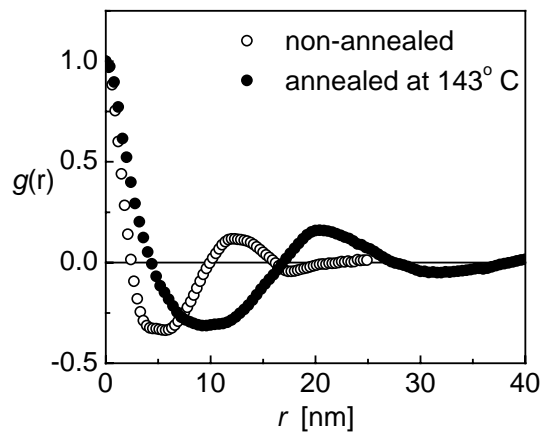
Figure 5.6. Normalized linear correlation function $\gamma(r)$ revealing an increase in the long period and phase dimensions due to annealing at 134° C, 143°C and 153° C for 10 hours.

In this case, the position of the first side maximum indicates the changes in the value of the long period following different thermal histories. Moreover, the inner part of the correlation function provides insight into the thickness of one of the phases. However, it cannot be concluded directly whether or not the corresponding value reflects the thicknesses of the crystalline or the amorphous domains.

5.6 Solid-state NMR study of phase composition, molecular mobility, and domain thickness

5.6.1 Temperature dependence of phase composition and chain mobility

A quantitative analysis of the FID and wide-line NMR spectra in terms of crystalline phase, semi-rigid phase, and soft phase was performed at a temperature well above T_g. The amounts of the rigid, semi-rigid and soft fractions of iPP obtained from low- and high- field NMR are shown (Fig. 5.7). At room temperature, a significant fraction of the soft phase is rigid, and contributes to both the intensity of the broad line of the NMR spectra, and the short T_2 relaxation component of the FID. At elevated temperature, the amount of the rigid fraction, which comprises the crystalline phase and the rigid fraction of the soft phase, slowly decreases. While the amount of the soft fraction increases under the same conditions, the amount of the semi-rigid fraction is almost constant in the temperature range from 70° C to 100° C (Fig. 5.7).
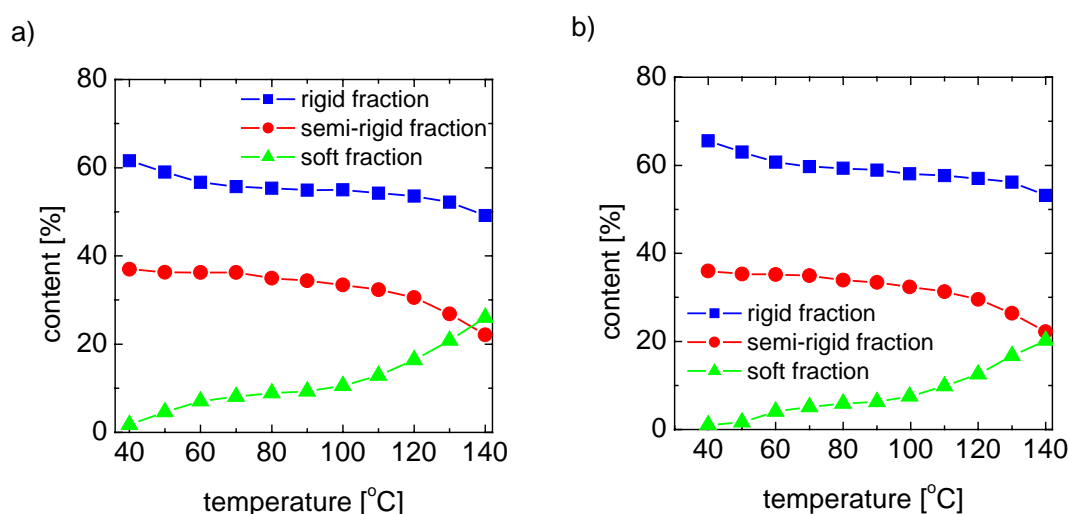
Figure 5.7. Temperature dependences of the amounts of rigid, semi-rigid, and soft fractions of non-annealed iPP measured with low-field (a) and high-field (b) NMR spectrometers.

The data in Fig. 5.8 show nearly constant values for T_2^{rigid} and $\Delta\nu_{1/2}^{\text{rigid}}$ with temperature increasing up to 100° C, indicating that the molecular motion in the rigid fraction is almost unchanged. The small increase in T_2^{rigid} above 100° C may be related to the motion in the crystalline phase (α relaxation process) which occurs prior to melting and to the thermal

expansion of crystal lattice [Sch1994]. In the temperature range from $40^{°}$ C to $60^{°}$ C, the transverse relaxation time of the semi-rigid and soft fractions increases largely, whilst $\Delta v^{semi-rigid}_{1/2}$, and $\Delta v^{soft}_{1/2}$ largely decrease (Fig. 5.8). These changes are due to the high-frequency (ca. 10 kHz) manifestation of the glass transition of the amorphous phase. The temperature dependences of the T_2^{soft} and of $\Delta v_{1/2}^{soft}$ can be correlated by the relationship $\Delta v_{1/2}^{soft} \approx \dfrac{1}{\pi T_2}$, valid for a Lorentzian line shape (Fig. 5.8). In the temperature range from $100^{°}$ C to $140^{°}$ C, an increase in the T_2 relaxation time of the semi-rigid and soft fractions is due to partial melting of isotactic polypropylene. That reduces hindrances of the chain mobility in the soft phase.
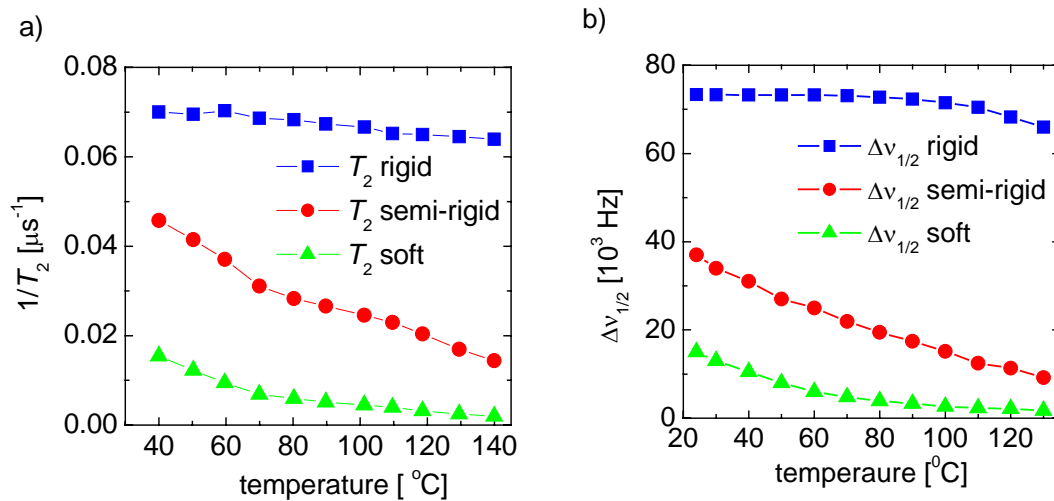
Figure 5.8. Temperature dependence of the ^{1}H $1/T_2$ relaxation rates (a), and line-width $\Delta v_{1/2}$ (b) for non-annealed iPP. The assignment of the parameters to the rigid, semi-rigid, and soft fractions of iPP is shown in the figure.

In conclusion, the temperature range from 70° C to $100^{°}$ C appears to be most suitable for accurate determination of the phase composition. In this temperature range, the differences in molecular mobility in different fractions of iPP are higher, and annealing can be lately avoided during the NMR experiment, as shown below. In the temperature range from 70° C to $100^{°}$ C, the amount of the rigid fraction is largely independent of temperature, and its values is closed to that of the crystallinity measured by DSC and X-ray scattering, as discussed below.

5.6.2 The effect of annealing temperature and annealing time on the phase composition and molecular mobility

To determine the temperature at which annealing causes changes in the morphology, two different types of annealing studies were performed. The annealing was studied at isothermal conditions in the temperature range from 70° C to 130° C in real time. The data were recorded each hour for 30 hours. No annealing effects were detected by NMR for iPP samples exposed to $70°$ C, $90°$ C and $110°$ C for 30 hours. In the temperature range from 110° C to 130° C, small changes in the molecular mobility and the phase composition were observed over a time of 500 hours. Annealing at 130° C for 500 hours causes ≈ 5 wt% increase in the amount of the rigid fraction at the expense of the soft phase. The amount of the semi-rigid phase remains almost constant (Fig. 5.9a). Figure 5.9b show that the molecular mobility in the crystalline phase of iPP is hardly affected by annealing at 130° C, whereas the molecular mobility of the semi-rigid fraction decreases and the molecular mobility in the soft fraction increases during the annealing.
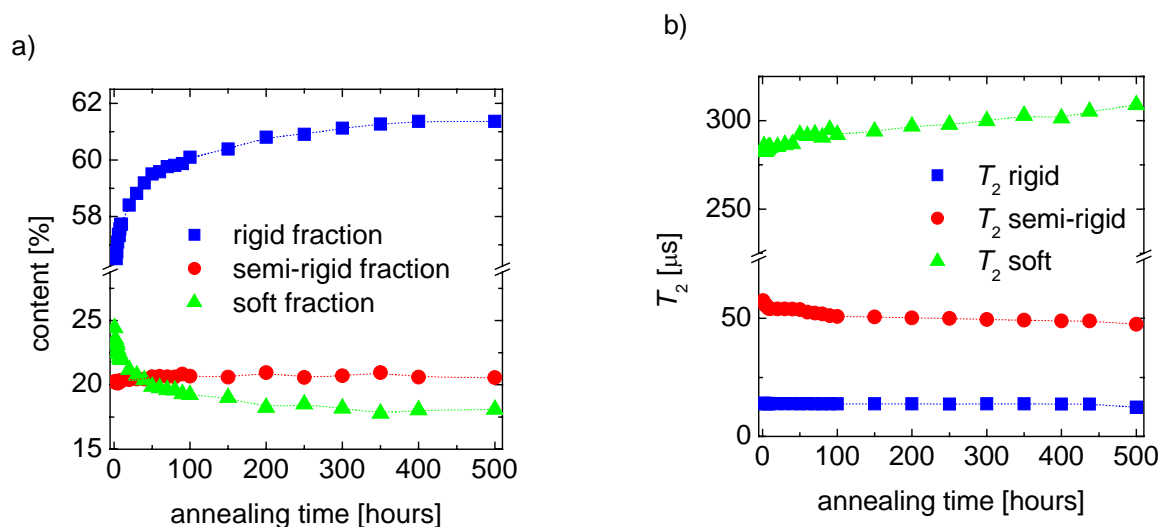
Figure 5.9. (a) The amounts of rigid phase, semi-rigid interface, and soft fraction of iPP as a function of the annealing time at $130°$ C. (b) The effect of the annealing on molecular mobility, as determined by the T_2 relaxation time for the different fractions of iPP. Larger amplitude and/or frequency of molecular motions lead to longer T_2 values. The relaxation characteristics were determined by the analysis of the FID (rigid and semi-rigid fractions), and Hahn-echo (soft fraction), as described in experimental section. The experiments were performed with low-field NMR spectrometer.

From the above results, we can conclude that exposure of iPP to temperatures between 100 - 130° C influences the NMR results, due to annealing of the samples during NMR experiments. These experiments were used to determine the maximum temperature at which no annealing occurs.

The effects of the annealing time and the annealing temperature on the phase composition and molecular mobility were studied for iPP samples annealed at 134° C, 143° C, and 153° C. The annealing times are taken in the range from 15 minutes to 30 hours. After annealing at the indicated temperatures, the NMR experiments were performed at 70° C. A fast increase in the amount of the rigid fraction is observed during the first five hours of annealing at 134° C, 143° C, and 153° C (Fig. 5.10a). The amount of the rigid fraction increases by a few wt% at the expense of the soft fraction. The amount of the semi-rigid fractions remains almost constant. It is also observed that the molecular mobility in the rigid and semi-rigid fractions of iPP decreases, while the molecular mobility of the soft fraction increases during the annealing. This increase is due to the better organised morphology of iPP during annealing. This is shown by the decrease in the T_2 values for the rigid fraction (T_2^{rigid}) (Fig. 5.10b), the semi-rigid fraction ($T_2^{\text{semi-rigid}}$), and the increase in the T_2 values for soft fraction (T_2^{soft}). The observed changes during annealing can take place for the following reasons: formation of thin lamellae between the primary lamellae, lamella thickening, and improvement of the ordering in different phases [Weg2000, Ito1992].
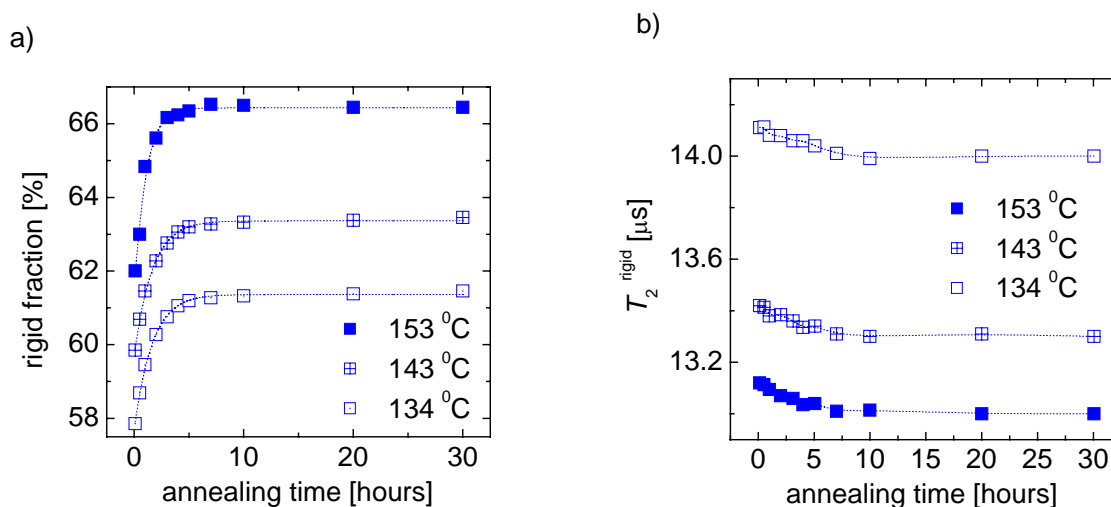
Figure 5.10. The effect of annealing time and annealing temperature on (a) the amount of the rigid fraction (% T_2^{rigid}), and (b) ^{1}H relaxation time (T_2^{rigid}) of this fraction of iPP.

5.6.3 Comparison of the amounts of rigid fraction/crystallinity obtained by NMR, SAXS, and DSC

It can be anticipated that the crystallinity values determined by different methods for the same sample are not exactly the same. By comparing the results of different methods, the complex morphology of semi-crystalline polymers can be understood better. The difference between the amounts of the rigid fraction that is obtained by the NMR experiment at 70° C and the degree of crystallinity obtained from DSC and SAXS for both annealed and non-annealed iPP does not exceed 10% (Table 5.1). All methods used show an increase in the amount of the rigid fraction/degree of crystallinity with increasing annealing temperature.

Table 5.1. The amounts of the rigid fraction/crystallinity obtained by NMR, SAXS, and DSC for non-annealed and iPP samples annealed for 10 hours.

	NMR 70 ^{o}C (wt%)			SAXS (vol%)		DSC (wt%)	
	rigid	semi-rigid	soft	crystalline	amorphous	crystalline	amorphous
non-annealed	56	36	8	51	49	51	49
annealed at 143° C	67	26	7	55	45	59	41
annealed at 153° C	70	24	6	58	42	61	39

The reasons for the apparent differences between the results obtained by NMR, DSC, and SAXS have been discussed in the previous chapter [Hed2007].

5.6.4 Comparison of the domain thicknesses measured by the DQ and the Goldman-Shen dipolar filters in spin-diffusion experiments

The confidence in both the values of the domain thickness and the effective dimensionality of the ^{1}H spin-diffusion process can be enhanced if the experiments are performed on the same iPP sample using different dipolar filters. In this case, we employed DQ and Goldman-Shen (GS) filters. These dipolar filters select the initial magnetization in the rigid and amorphous domains, respectively.

a)   b)
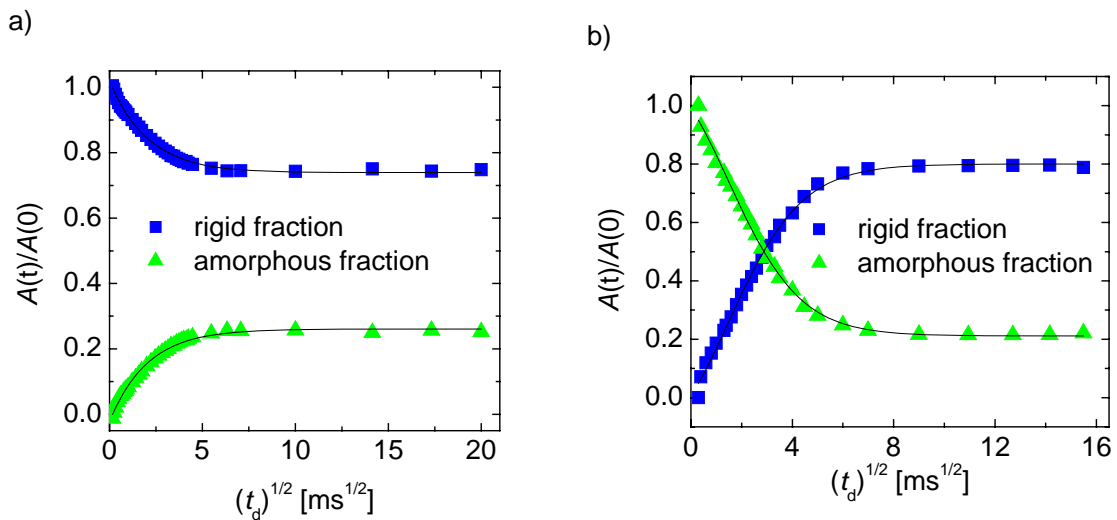
Figure 5.11. Proton spin-diffusion decay and build-up curves for the rigid (■) and amorphous (●) fractions of non-annealed iPP recorded using the DQ (a) and GS (b) dipolar filters. These filters select the magnetization of the rigid and amorphous fractions of iPP, respectively. The time-domain data were recorded at 70 °C with a low-field NMR spectrometer and fitted with one Abragam function and one exponential function. The filter time for the GS was set to 100 μs. The solid lines represent the best fit for the 1D solutions of the spin-diffusion data for the two-phase morphology.

The measurements of ^{1}H spin diffusion using both dipolar filters were performed on the non-annealed iPP sample at $70^{°}$ C with low-field NMR. The spin-diffusion build-up and decay spin-diffusion curves are shown in Fig.5.11.

From these data it is evident that the spin-diffusion process reaches the quasi-equilibrium state after a diffusion time of the order of $t_d \approx 70$ms for both filters. Moreover, for the DQ filter, the quasi-equilibrium of the relative magnetization for the rigid and amorphous phases equals 0.73 and 0.27, respectively. In the case of GS dipolar filter, the corresponding phase fractions are 0.79 and 0.21. In the limit of experimental errors, these two results prove that both dipolar filters provide similar values of domain thickness. Small differences exist because the efficiency of the dipolar filters in selecting the magnetization just from one domain is not 100%, and the shape of the relaxation components biases the accuracy of the FID deconvolution procedure.

The thicknesses of the rigid (d_r) and amorphous (d_a) domains are determined from fits of the spin-diffusion data (Fig. 5.11) with the 1D solutions of the spin-diffusion equations. The approximation of two phases should not have a large effect on the extracted domain thicknesses, taking into account the small amount ≈ 4 wt% of the soft fraction. The time dependence of the analytical spin-diffusion signals for the GS filter can be obtained from those of the DQ filter, by interchanging the indices r and a of the quantities present in the spin-diffusion solutions. The domain thicknesses obtained by fits of the spin-diffusion data of Fig. 5.11 are given in Table 5.2.

Table 5.2. The thicknesses of the rigid (d_r) and amorphous (d_a) domains of non-Annealed iPP measured at 70° C using spin-diffusion experiments with double-quantum (DQ) and Goldman-Shen (GS) dipolar filters (Fig. 5.11).

dipolar filter	d_r [nm]	d_a [nm]
DQ	10	2.5
GS	9	3

The time domain data were fitted with a combination of one Gaussian and one exponential function, and with a combination of one Abragam and one exponential function. The domain thickness with values closest to that measured by SAXS, is that obtained from the free induction decay deconvoluted with the sum of one Abragam and one exponential function. Moreover, both dipolar filters provide a volume ratio of the rigid and amorphous domains that is close to the mass fraction of these phases, as determined from the FID at different temperatures, i.e., $d_r / d_a \approx 2-5$ and $\%T_2^{rigid} / \%T_2^{amorphous} \approx 3-4.8$. These results provide additional proof of validity of the method for domain thickness determination, as well as the type of morphology. The thicknesses of the iPP domains determined by time-domain and frequency domain spin-diffusion experiments are in good agreement (Table 5.2).

5.6.5 Temperature dependence of the domain thickness

In order to estimate the domain thickness of the rigid and amorphous fractions, the spin-diffusion experiment was performed for non-annealed iPP samples at three different temperatures, 70° C, 100° C, and 130° C. The thickness of rigid and amorphous domains as well as the long period increase with increasing temperature (Table 5.3). These changes can be explained by melting of the small disordered crystals upon increasing temperature and by lamellae thickening.

Table 5.3. Long period (L_p), the thickness of rigid (d_c), and amorphous (d_a) domains, at different temperatures for non-annealed iPP samples. The domain thicknesses were determined from ^{1}H spin-diffusion experiments with a DQ filter measured at low- and high field (in brackets) NMR spectrometers, respectively.

thickness	temperature		
	70° C	100° C	130° C
d_r (nm)	10 (10.5)	11.4 (12)	12 (12.5)
d_a (nm)	2.5 (2.1)	3.5 (3)	7 (7)
L_p (nm)	12.5 (12.6)	14.9 (15)	19(19.5)

5.6.6 The effect of annealing temperature and annealing time on the domain thickness of iPP samples

The long period L_p, and the thickness of the rigid d_r and amorphous d_a domains, was studied as a function of annealing temperature and annealing time. The spin-diffusion experiments were performed at $70^{°}$ C for the iPP samples, annealed at three different temperatures, and different annealing times. The values of the long period before and after annealing, determined by NMR spin-diffusion experiment and SAXS, are in a good agreement (Table 5.4).

Table 5.4. The long period[a] of non-annealed iPP and iPP that was annealed for 10 hours at 143° C and 153° C as determined by NMR and SAXS.

	non-annealed	annealed at 143° C	annealed at 153° C
NMR ($70\ ^oC$)	12.5 nm	19.9 nm	21.3 nm
SAXS data	12.9 nm	21 nm	21.8 nm
SAXS, linear correlation function	12.5 nm	20 nm	21 nm

[a]The average errors are of the order of 15%

Figure 5.12 shows the changes of L_p, d_c, and d_a with annealing time. A rapid initial increase in the long period and in the thickness of the rigid domains is observed for the iPP samples during first 10 hours of annealing (Fig.5.12ab). The rapid increase in the crystal thickness with annealing is confirmed by the increase in the crystallinity (Fig. 5.10a, Table 5.1, and Table 5.4). For long annealing times, ranging between $10 - 30$ hours, L_p and d_c do not seem to change significantly, showing a stabilization of the iPP morphology (Fig.5.12ab) [Pou1998].

a)

b)

c)
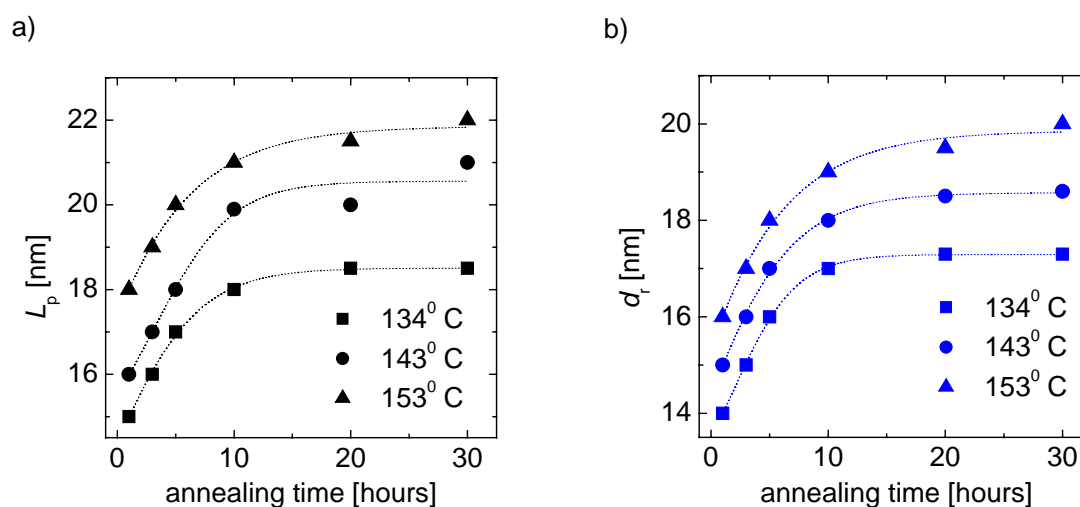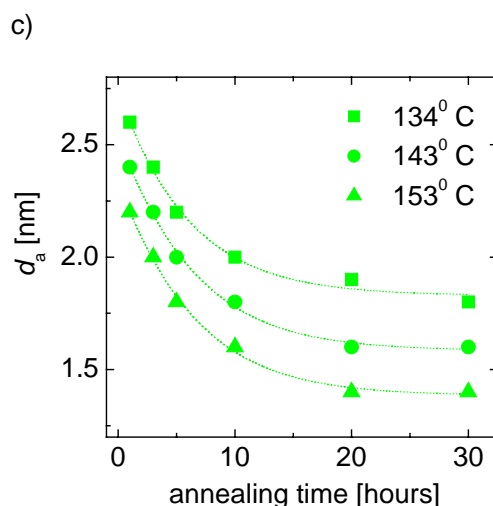
Figure 5.12. Changes of the (a) long period L_p, (b) thickness d_r of rigid domains, and (c) thickness d_a of amorphous domain of iPP as a function of annealing temperature and annealing time. The domain thicknesses were determined from ^{1}H spin diffusion experiments exploring a DQ filter. The experiments were performed with a low-field NMR spectrometer.

The thickness of the amorphous domains slightly decreases with increasing the annealing temperature and annealing time (Fig. 5.12c). Chain dynamics and thermodynamic factors play an important role in the annealing process. The growth of lamellae involves translational motion of the polymer chains [Fer1984]. Faster chain diffusion through iPP crystals, and higher chain mobility in the amorphous phase upon increasing the temperature facilitate the structural reorganization towards thermodynamically more stable thicker crystals [Sch1991, San1973] Previous studies have also shown that the annealing of iPP samples at sufficiently high temperature increases the thickness of the lamellae [Pou1998, Mar1998, Fer1984].

5.6.7 Thickening of crystalline domains during annealing

The spin diffusion NMR experiment measures the smallest dimension of the crystalline regions, i.e., the thickness of the crystal. This quantity changes during annealing, and this process is known as crystal thickening.

The polymer crystals when annealed isothermally are thermodynamically metastable since they are formed with high surface-to-volume ratios. The thickening can be considered as a process of going from a state of high to a state of low free energy. For thin polymer crystals, a thermodynamic force capable of driving the thickening phenomena arises from the unequal free energies of the fold and lateral surfaces. This process is an irreversible thermodynamic process that can be described by the non-linear differential equation [San1973]

$$\frac{dy}{dt} = \frac{2}{\tau_t}\left(\frac{1-y^{3/2}}{y}\right),$$ (5.1)

where $y = d_r/d_{r0}$, d_{r0} is the equilibrium thickness of the crystal, $\tau_t = k d_{r0}^2$ and k is a proportionality constant. The temperature dependence of the thickening rate should enter the theory through k, or equivalently τ_t. When τ_t is assumed to be independent of d_r, the above equation can be integrated analytically, and the transverse crystal thickness d_r exhibits a sigmoidal shape as a function of $\log(t_a/\tau_t)$ [San1973, Sat1961, Fis1962, San1974, Pet1963, Pet1967]. At the intermediate values of $\log(t_a/\tau_t)$, the crystal thickness increases approximately linearly with a higher rate at higher temperatures. Therefore, in the intermediate range of the annealing time t_a, the rigid domain thickness d_r measured by spin-diffusion can be described by the relationship

$$d_r \approx d_{r0} + B\log(t_a/\tau_t).$$ (5.2)

For an annealing time $t_a = \tau_t$ we get from the above equation $d_r \approx d_{r0}$. When $t_a = e\tau_t$ we get the significance of the constant B, i.e., $B \approx d_r - d_{r0}$.

The dependence of the rigid domain thickness for annealed iPP at three different temperatures is shown in Fig. 5.13 as a function of $\log(t_a)$. At all annealing temperatures, the data can be fitted with a straight line in agreement with Eq. (5.2). Therefore, the process of crystal thickening upon annealing for iPP can be described in the linear approximation by the Eq. (5.2) with can be derived from Eq 5.1 [San1973, San1974]. A strong temperature dependence of the thickening rate is not detected (cf. Fig. 5.13) probably due to the limited range of annealing temperatures. Moreover, the thickening rate is primarily a function of undercooling $\Delta T = T_m^0 - T$, where T_m^0 is the equilibrium melting point of the crystal (about 182^0 C for iPP [Yam2003]), rather than the absolute temperature T.
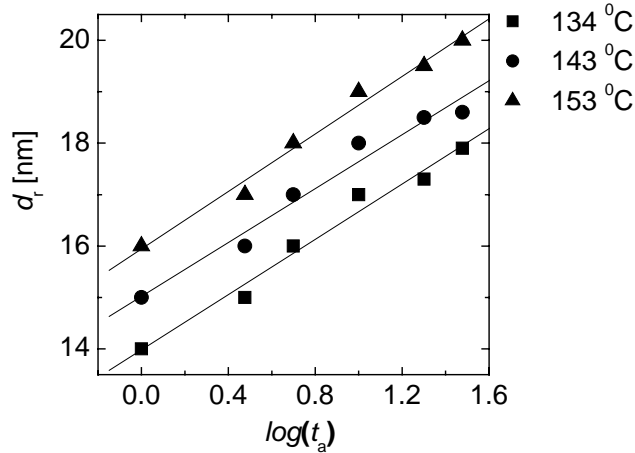
Figure 5.13. Change of the thickness d_r of the rigid domains with the annealing time t_a at three different annealing temperatures. The straight lines are a least-squares fit of the data using Eq. (5.2).

5.6.8 Correlation between the ^{1}H transverse relaxation rate and the domain thickness of the crystalline domains.

The microscopic properties of iPP are represented by several parameters that describe the polymer chain dynamics. These dynamics correlate with the local structure on the nanoscale range and are revealed *inter alia* by the ^{1}H transverse magnetization relaxation rates. The morphology and domain thickness characterize the materials on the mesoscopic scale, i.e., on the scale of tenth or hundreds of nanometers.

The values of the ^{1}H effective transverse magnetization relaxation rate ($1/T_2^{rigid}$) for the rigid domain is related to the residual second van Vleck moment $\langle M_2 \rangle$, i.e., $1/T_2^{rigid} \propto \langle M_2 \rangle$. This is evident from the fact that the free induction decay $G(t)$ of the rigid domains in the short time domain is described in a good approximation by the Gauss function $G(t) \propto \exp\left(-\dfrac{\langle M_2 \rangle}{2}t^2\right)$. An effective short relaxation time T_2^{rigid} can be introduced to describe this decay by the function $G(t) \propto \exp\left[-\left(\dfrac{t}{T_2^{rigid}}\right)^2\right]$, and hence we obtain

$$\frac{1}{T_2^{rigid}} = \left(\frac{\langle M_2 \rangle}{2}\right)^{1/2}. \qquad (5.3)$$

Consequently, faster transverse relaxation rates correspond to larger values of $\langle M_2 \rangle$ due to larger strength of the dipolar couplings. This is the case of slower chain motions, and

increased interchain dipolar interactions due to denser chain packing and/or better crystal organization.
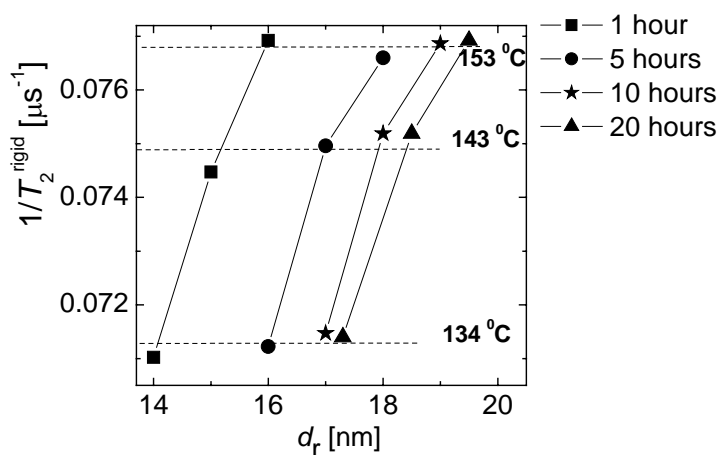
Figure 5.14. Correlation between the ^{1}H transverse magnetization relaxation rate ($1/T_2^{rigid}$) and the thickness of the rigid domains for iPP that was annealed at 134° C, 143° C, and 153° C for 1, 5, 10, and 20 hours. The NMR measurements were performed at 70° C using a low-field NMR spectrometer. The lines are a guide for the eye.

A phenomenological attempt to correlate $1/T_2^{rigid}$ and d_r for different annealing temperatures and annealing times is shown in Fig. 5.14. The transverse magnetization relaxation and spin-diffusion measurements were made at the same temperature of 70 °C. Therefore, the changes in the values of $1/T_2^{rigid}$ are due to the crystal thickening and perfection of the crystalline order during annealing. The theory of polymer annealing [San1973, San1974, Pet1963, Pet1967] predicts that for a given annealing temperature the crystalline domain thickness increases linearly with log(t_a) (see Eq. (5.2)), where t_a is the annealing time. This is evident from the values of d_r measured as a function of t_a at different annealing temperatures (Fig. 5.14). Only small changes in the values of $1/T_2^{rigid}$ are detected at each annealing temperature as a function of annealing time. This parameter increases slightly with annealing time due to an increase in the density (perfection) of the crystalline regions during annealing [San1973]. This leads to an increase in $1/T_2^{rigid}$, due to an increase in the ^{1}H dipolar couplings, and consequently in $\langle M_2 \rangle$. Higher annealing temperatures lead to more perfect and better-packed crystals in which fast small-angle fluctuations are reduced. Moreover, we note that this major effect occurs rapidly, and only minor further changes are observed during the course of annealing. This shows that there is no simple correlation between $1/T_2^{rigid}$ and crystalline the domain thickness.

5.7 Conclusions

Changes in phase composition (namely the amounts of rigid fraction/crystallinity, semi-rigid, and soft fractions), molecular mobility and domain thickness of both annealed and non-annealed iPP samples were investigated by ^{1}H NMR, SAXS, and DSC at different temperatures and different annealing times. The amounts of the rigid fraction as determined by NMR, exceeds by 5-10% the crystallinity from DSC and SAXS. This difference can quantitatively be explained by the effect of the interface, which is not taken into account in the analysis of the DSC and SAXS data.

According to TEM, the morphology of non-annealed iPP is mainly lamellar. For iPP samples that have been annealed at different temperatures and different times, the cross-hatching morphology can be observed. However, the predominant morphology remains lamellar. This is confirmed by the comparison of the phase composition with the domain thickness ratio that is determined by simulation of the results of the spin-diffusion data using 1D, 2D, and 3D solutions of the spin-diffusion equations. In an approximation of the two-phase model, the long periods obtained by NMR and SAXS are in good agreement with each other.

An important feature of the spin-diffusion experiments reported in this investigation is the temperature dependence of the proton spin diffusivities, which decrease with increasing temperature. The temperature dependence of the spin diffusivity of the amorphous phase was derived from the spectral line width. In the approximation of a single correlation time described by the Williams-Landel-Ferry (WLF) equation, the temperature dependence of the spin diffusivities was established, and the obtained WLF coefficients are in the range that is typical for the amorphous phase in semi-crystalline polymers and amorphous polymers.

The thicknesses of the rigid domains for iPP that has been annealed at different temperatures and different times has been discussed as a function of the logarithm of the annealing time. A linear relationship holds for all cases in good agreement between theory and the experimental results for other polymers [San1973, San1974].

The existence of a phenomenological correlation between microscopic and mesoscopic properties of iPP is reported. Microscopic properties are described by ^{1}H transverse relaxation rates or second van Vleck moment characterizing mainly the proton dipolar network. The morphology and domain thickness characterize the polymer on the mesoscopic scale. The correlation is complex and explained by the improvement of the crystalline order during the crystal thickening.

Chapter 6

Aging on Isotactic Polypropylene

6.1 Introduction and motivation

Physical aging of semi-crystalline polymers, which has been studied extensively in the past [Cru1984, Cha1980, Tom1996, Uzo1997, Ibh1996, Hel1997] from many aspects, refers to the evolution towards an equilibrium state and the associated changes in the morphological organization and physical properties. Above the glass transition the physical aging at different temperatures and different times involves the densification of the amorphous fraction (reduction in free volume) [Son1987], constraints in the chain mobility [Aga1981], lamellar perfection or densification, lamellar thickening, crystallization of constrained polymer chains forming small crystals or fringed micelles, and melting-recrystallization. The exact origin of the changes in iPP samples (and in other semi-crystalline polymers) with aging time and aging temperature is still under dispute [Cru1984, Cha1980, Tom1996, Uzo1997, Ibh1996, Hel1997, Son1987, Aga1981]. One reason of the dispute lies in the limitations of different techniques used to probe the structure of these materials and the discrepancies between their results.

Differential scanning calorimetry (DSC) rarely provides similar values for crystallinity as other techniques [Isa1999, Zho1997]; wide-angle X-ray diffraction (WAXD) requires an estimation of the amorphous fraction and the lattice imperfection factor [Rul1961]; and small-angle X-Ray diffraction (SAXS) is extremely model dependent [Bal1989]. It should be noted that the problems with SAXS analyses are enhanced in the case of iPP due to the crosshatched lamellar morphology [Oll1989].

One feature that is generally agreed upon by most researchers as important for aging behaviour is whether the annealing temperatures are above or below the crystalline dielectric relaxation α_c. The crystalline relaxation α_c is associated with the rotational-translational motion travelling along the crystal stem [Boy1985, Boy1985, Spi1991, Hu1999] that can grow from the soft fraction in a crystal thickening process. The responsible mechanism for crystallinity increase due to aging is the secondary crystallization by which the new lamellae are inserted between those formed during the primary crystallization. This mechanism occurs since the regions remaining amorphous still have the potential to partially crystallize. The

newly formed lamellae are constrained by those formed during primary crystallization. They are thicker as they are formed at higher temperatures. Because an additional driving force is needed, the newly formed lamellae at lower temperature upon further non-isothermal cooling are thinner. They may thicken if a low temperature active process is plausible. It is not only a matter of aging temperature, with respect to the glass transition temperatures of the crystalline and amorphous phases, for the new formed lamella, but also depends on the initial iPP morphology.

The first aim of this chapter is to study in detail the effects of aging temperature and aging time on the phase composition, crystallinity, melting and crystallization temperatures, chain mobility and mechanical properties of injection molded, crystallized from the melt, and quenched homopolymeric iPP by ^{1}H low field solid state NMR, DSC and X-ray. The second goal of this chapter is to show that the ^{1}H low-field solid-state NMR technique is capable of detecting the small changes in the phase composition and chain mobility due to aging at different times and different temperatures. Moreover, a correlation between the changes in the NMR, and DSC parameters due to aging and mechanical data is presented and discussed.

6.2 Materials

Three homopolymeric isotactic polypropylene (iPP) samples were used in our investigations. All the samples are commercial Ziegler-Natta-catalyzed PP manufactured by SABIC Europe BV. The first sample is an injection molded homopolymeric iPP. The materials were injected in an Engel 45A machine. The melt temperature was set to 235° C, the holding pressure to 40 MPa, the holding time to 20 s, the cooling time to 20 s, and the overall cycle time to 49.5 s. The second sample is melt-crystallized homopolymer iPP. The injection molded plates were melted at 230° C for 30 minutes in an oven under nitrogen flow, in order to avoid the oxidation of the samples, and finally crystallized at a slow cooling rate. The third sample is a quenched homopolymeric iPP sample. The sample has been brought to 250° C, kept 30 minutes at that temperature and than quenched from the melt at -195° C between two metal plates.

For the aging study at 28° C, all the homopolymeric iPP samples were further annealed in the NMR probe, for times between 10 minutes and 1000 hours after preparation. For the aging study at different temperatures the iPP samples crystallized from the melt was annealed in the NMR probe for the temperature range from 70° C to 130° C, for times between 10 minutes and 150 hours after preparation. The temperature of the NMR experiments coincides with the annealing temperature. All NMR measurements were repeated

with an interval of one hour. The samples were not removed from the NMR probe for 150 hours and 1000 hours, respectively.

6.3 NMR data processing.

At 28° C the FID of homopolymer iPP samples was fitted with a linear combination of one Abragam and one Gaussian function;

$$A(t) = A(0)^{rigid} \exp[-(t/2T_2^{rigid})^2] \cdot [\sin(at)/at] + A(0)^{soft} \exp[-(t/T_2^{soft})^2]. \tag{1}$$

At temperatures higher then 70° C the FID of homopolymer iPP samples was fitted with a linear combination of one Abragam, one Gaussian and one exponential function, i.e.,

$$A(t) = A(0)^{rigid} \exp[-(t/T_2^{rigid})^2] \cdot [\sin(at)/at] + A(0)^{semi-rigid} \exp[-(t/T_2^{semi-rigidt})^2]$$
$$+ A(0)^{soft} \exp[-(t/T_2^{soft})] \tag{2}$$

The parameter a is related to the second and fourth van Vleck moments. The transverse relaxation times (T_2), which are characteristic of different slopes in the magnetization decay curve, are related to the mobility in each fraction. The relative fractions of the relaxation components, $\{A(0)^k/[A(0)^{rigid} + A(0)^{semi-rigid} + A(0)^{soft}]\} \times 100\%$, represent the relative amounts of hydrogen atoms (mass fractions) of iPP phases/fractions with different molecular mobility. Repeated experiments for the same sample indicated that the relative error of the extracted relaxation parameters was about 1 %.

6.4 Mechanical results

To determine the influence of aging on the mechanical properties of homopolymer iPP, the effect of aging on the flexural modulus, impact strength, and shrinkage were investigated. Figure 6.1 shows the results of tensile modulus (parallel and perpendicular) plotted against the aging time and obtained from samples aged at 28 °C. The modulus increases with aging time. Compared to the value reached after one hour, the modulus has increased by approximately ≈13.5% after 200 hours.
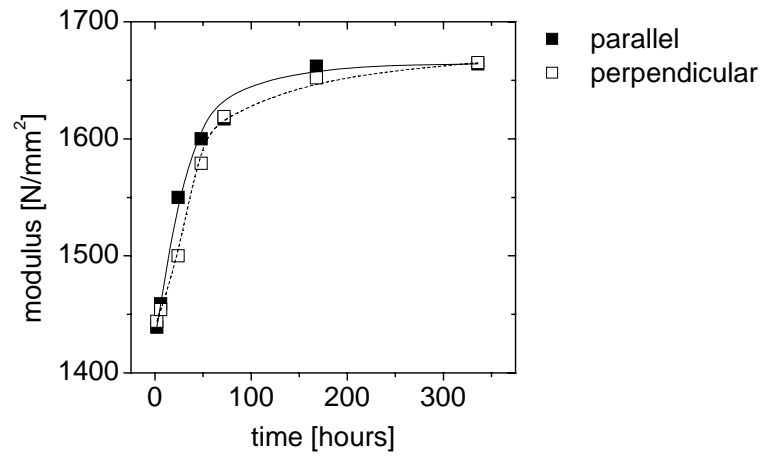
Figure 6.1. Flexural modulus as a function of aging time at 23° C for homopolymer iPP sample.
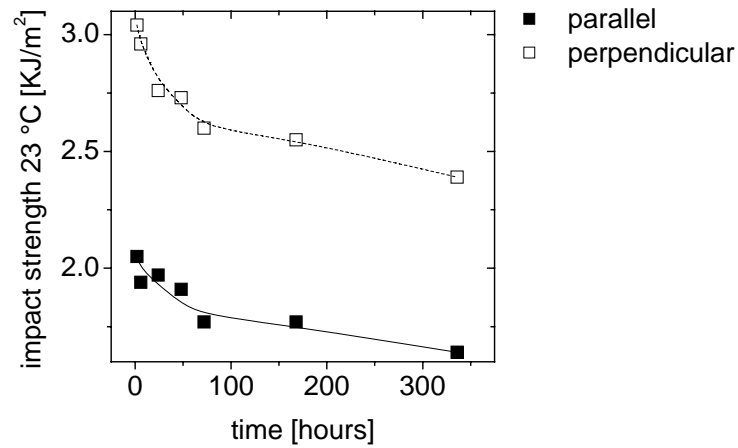
Figure 6.2. Impact strength in parallel and perpendicular directions at 23° C as a function of aging time for a homopolymeric iPP sample.
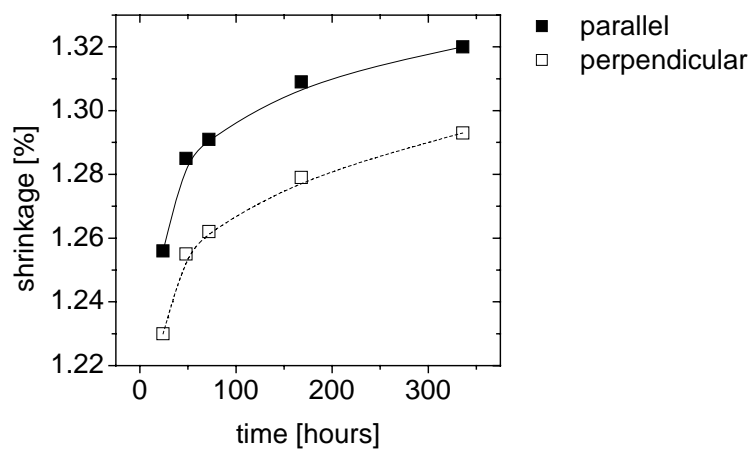
Figure 6.3. Relative shrinkage in parallel and perpendicular direction versus aging time for homopolymer iPP sample.

The decrease in impact strength in both directions (parallel and perpendicular), measured at 23° C with aging time can be observed in Fig. 6.2. Free shrinkage experiments were performed to investigate the changes of the organization of the amorphous phase depending of the aging time. Fig. 6.3 shows the change of the degree of shrinkage in time. In general, the shrinkage behaviour is non-linear and increases with increasing aging time.

6.5 X-ray results

Figure 6.4 shows the X-ray patterns of crystallized from the melt homopolimeric iPP samples aged for 10 minutes and 20 hours. Compare the diffraction patterns of the sample aged for 10 minutes and sample aged for 20 hours, no significant differences were observed as a function of time in the lattice parameters. The d-spacing values are almost constant for the observed crystallographic planes, which indicate no changes in the crystal packing. The significant changes of the mechanical properties during aging cannot be attributed to the changes in the crystallinity, seems not changes in X-ray patters were observed in time.
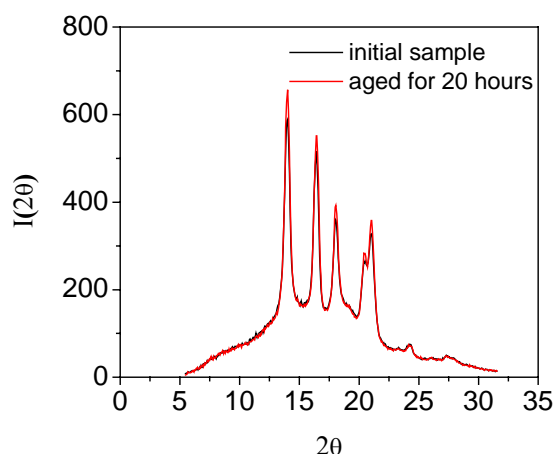
Figure 6.4. X-ray patterns of both initial and aged homopolymeric iPP samples

6.6 DSC results

Differential scanning calorimetric measurements have been performed to investigate the influence of time/temperature treatment on the crystallization and melting behaviour of homopolymeric PP samples. The applied temperature profiles are described bellow. All samples were kept for 15 minutes at 250° C, where after they were cooled at 10° C/min to 25° C. After an isothermal stay for 1 min at 25° C the PP homopolymer was heated at 10° C/min to 28, 70 and 130° C, and kept for 10, 60, 120, 480 and 1440 minutes at these programmed

temperatures. This pre-treatment can be compared with the thermal treatment used to measure the PP samples by solid-state NMR. After this isothermal treatment, the samples were cooled with 10° C/min to 0° C, where they were kept for 5 minutes to equilibrate and then heated at 10° C/min to 200° C (~ 1st heating curve), kept for 5 minutes at this temperature and cooled at 10° C/min to 0° C (~ cooling curve), after equilibration time of 5 minutes at 0° C the samples were finally reheated at 10° C/min to 200° C (2nd heating curve). The so-called 1st heating curve provides information concerning the thermal treatment (a certain time at a certain temperature), whereas both the cooling curve as the 2nd heating curve are being used to verify whether or not the thermal treatment has influenced the thermal response of the material, i.e. molecular and/or morphological changes.

Isothermal Measurements. The isothermal measurements have been analyzed. No crystallization phenomena could be detected. Although crystallization is present, the DSC does not record a crystallization signal during the isothermal treatment. The crystallization is that slow, it can not be seen due to the noise of the baseline (signal/noise ratio too small).

Dynamic Measurements. An offset and melting temperature, $T_{m'}$, can be calculated by the 1st heating curve. All results are presented in Table 6.1. In order to compare the thermal pre-treated samples with non-treated PP, offset and apparent offset temperatures are being used based on the previous article [Hed2007]. The crystallization temperature, T_c, the enthalpy of crystallization, ΔH_c and the melting temperature, $T_{m''}$ (2nd heating curve), are also presented in Table 6.1. The enthalpy of the cooling curve is being used to verify the reproducibility of the enthalpy of all samples. Table 6.1 shows that by calculating the mean crystallization temperature, $T_{c, average} = 121.0 \pm 0.3°$ C, the mean crystallization enthalpy, $\Delta H_{c, average} = 98 \pm 1$ J/g and the mean $T_{m''}$ (= 164.0 ± 0.6° C) one may conclude that the thermal treatment does not change the thermal response of the material after erasing the thermal history. The thermal treatment is a reversible process, which means that no structural changes took place within the homopolymeric iPP sample.

Table 6.1. Changes in offset temperature T_{offset}, crystallization temperature T_c, the enthalpy of crystallization ΔH_c, and melting temperature T_m of homopolymeric iPP samples as a function of aging time and aging temperature

Dynamic measurements						
Thermal treatment					110-130° C	
Time (min)	Temp (^{o}C)	T_{offset} (^{o}C)	$T_m^{1st}H$ (^{o}C)	T_c (^{o}C)	ΔH_c (J/g)	$T_m^{2st}H$ (^{o}C)
5	0	/	162.9	121.2	100	163.3
10		132	164.1	120.9	98	164.2
60		133.4	164.9	121.3	97	164.7
120	130	133.7	164.8	121.1	97	164
480		134.2	164	120.5	98	163.2
1440		134.9	164.8	120.6	98	163.7
10		74.4	164.2	120.9	98	164.4
60		75.7	163.8	121.4	98	164.4
120	70	78.3	163	120.7	99	164.2
480		77.1	162.9	120.7	99	163.2
1440		80.5	164.2	120.8	97	164.3
10		31.4	163.9	121.1	98	164.2
60		34	164.7	121.1	97	165
120		35.8	164.2	121.1	98	164.5
480	28	36.9	163.3	121.4	98	163.8
1440		40.2	162.8	121.5	98	164
Average			163.9	121	98	164.0
STDEV			0.7	0.3	1	0.5

For the samples kept at respectively 28 and 70° C, it is very difficult to determine the T_{offset} due to the small Cp step and the baseline curvature. The offset temperature of the transition related to the thermal treatment seems to shift to higher temperatures when more time is applied at this isothermal temperature (Table 6.1). The offset temperature values are plotted as a function of the log time and the data are linearly fitted (Figure 6.5). The slope of these lines present the variation of the offset temperature with time, which is the largest for the sample kept isothermal at the lowest temperature (28° C). The offset temperature differences between 1440 minutes and 10 minutes at a well-defined temperature (130, 70 and 28° C) are presented in the Table 6.2. The lower the applied isothermal temperature, the larger the difference is of the offset temperature (slope in Figure 6.5).
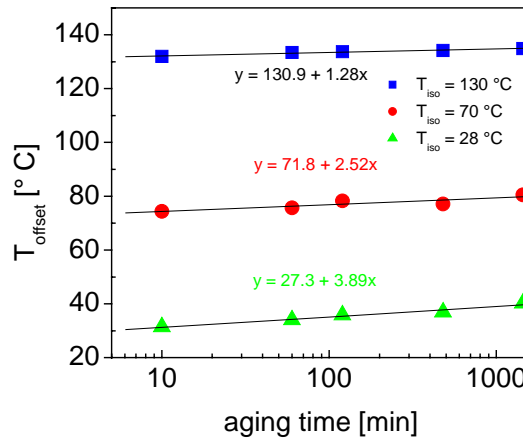
Figure 6.5. Offset temperature values as a function of log aging time for homopolymeric PP samples annealed different temperatures

Table 6.2. Offset temperature difference between 1440 minutes and 10 minutes for annealed PP samples at 28, 70, and 130° C.

temperature (° C)	$\Delta[1440 - 10]$ (° C)
130	2.9
70	6.1
28	8.8

These results clearly indicate long term changes when keeping homopolymeric PP samples for elaborate times at a well defined temperature. The changes are recorded as an increase of the Cp, which may indicate that the amorphous phase is changing rather than the crystalline phase. Most likely the amorphous and rigid-amorphous phases are seriously influenced by time and temperature effects. The question rises to which extent these long term changes influence the crystalline and/or the amorphous phase.
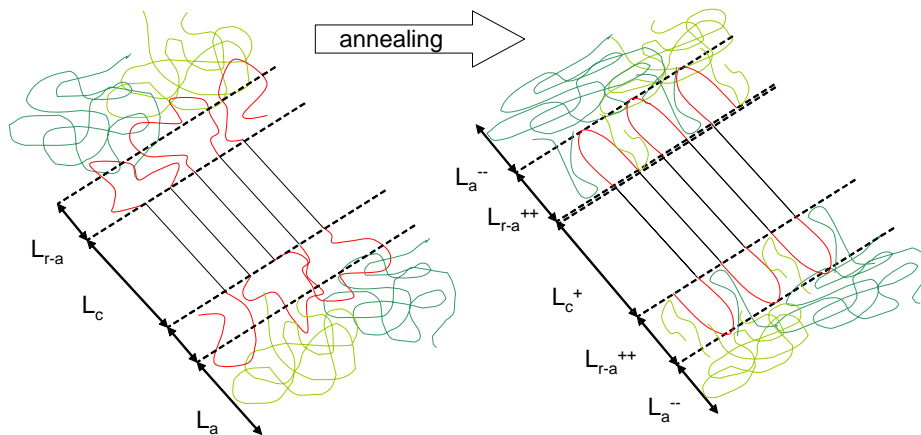
Figure 6.6. Changes in the morphology of homopolymeric iPP samples due to aging/annealing.

Figure 6.6 presents a hypothesis how annealing influences the amorphous (L_a), rigid-amorphous (L_{r-a}) and crystalline phases (L_c). Rigid-amorphous phase increases, L_{r-a}^{++}, amorphous phase decreases, L_a^{--}, and the crystalline phase increases slightly, L_c^{+} (3% of crystallinity increase), with time/temperature treatment. These results are in line with the observed NMR results.

6.7 Changes induced by aging at 28° C in the phase composition and chain mobility of homopolymeric iPP samples

Analyses of FID of injection-molded, crystallized form the melt and quenched homopolymeric iPP samples, in terms of rigid and soft fractions were performed at a temperature above T_g (0° C) of 28° C. At this temperature we are claiming that the contrast in chain mobility of the rigid and soft fractions of iPP is enhanced, and the aging process at this temperature can be followed over time with excellent sensitivity. The high amount of the rigid fraction detected by NMR at 28° C is due to the contribution of the immobilized soft fraction to the amount of the crystalline phase. Aging at $28^{°}$ C for 1000 hours causes $\approx 1-2$ wt% increase in the amount of the rigid fraction at the expense of the soft fraction (Fig. 6.7a).

a)

73

b)
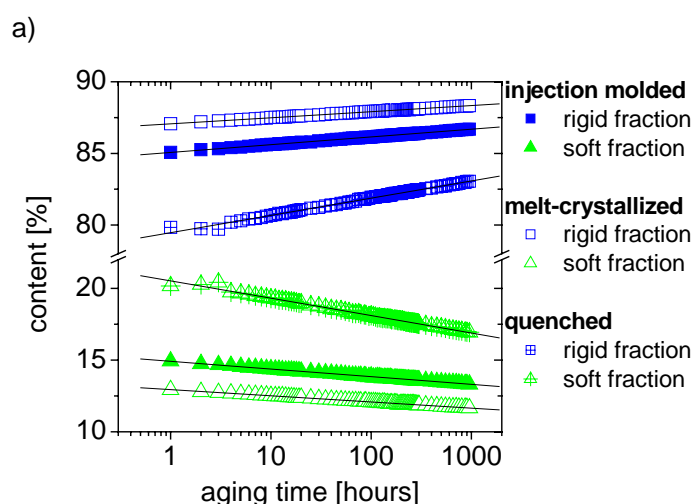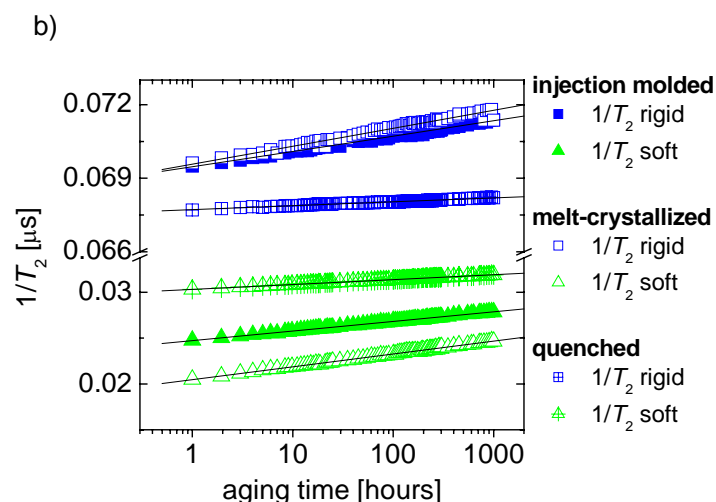
Figure 6.7. (a) The amounts of rigid and soft fraction of injection molded, crystallized from the melt and quenched homopolymeric iPP samples as a function of the aging time at 28° C. (b) The effect of aging at 28° C on chain mobility, as determined by the T_2 relaxation time for the different fractions of injection molded, crystallized from the melt, and quenched samples.

For all homopolymeric iPP samples the recorded amounts of the rigid phase increased systematically with increasing aging time (Fig. 6.7a). The systematic changes in the phase composition show that the aging persists for long times with no evidence of reaching an equilibrium state. The chain mobility of the rigid fractions (T_2^{rigid}) of iPP is affected by aging at 28° C during 1000 hours, whereas the chain mobility in the soft fraction (T_2^{soft}) decreases over time (Fig.6.7b). The decrease in the chain mobility of the soft fraction due to the aging was also observed by Agarwal [Aga1962] and VanderHart [Van2003].

To calculate a relative rates of aging, the amounts of the rigid and soft fractions, and the chain mobility ($1/T_2^{rigid}$, $1/T_2^{soft}$) data were plotted against aging time on a log scale, and a linear fit was made to the data. The changes in the phase content and chain mobility due to the aging at 28° C are approximately linear on a logarithmic scale over a time of 1000 hours. The overall slopes observed in Fig. 6.7a on a log time scale are not much different for the injection molded (slope = 0.53), melt-crystallized (slope=0.42) and quenched (slope = 1.2) samples. In the case of chain mobility in soft fractions the difference in the slopes are bigger (Fig. 6.7b).

6.8 Changes induced by aging at 70 – 130° C in the phase composition and chain mobility of homopolymer iPP samples

At temperatures between 70° C to 130° C the proton NMR free induction decay (FID) measured for homopolymeric iPP samples crystallized from the melt is decomposed into three components assigned to three fractions with different chain mobilities, manifested in the transverse magnetization times, i.e., the rigid (T_2^{rigid}), semi-rigid ($T_2^{semi-rigid}$), and soft (T_2^{soft}) fractions. At this temperature the contrast in the chain mobility of the rigid, semi-rigid and soft fractions of all homopolymeric iPP samples is enhanced and a quantitative analysis can be performed. Aging in the temperature range from 70° C to 130° C for 150 hours causes $\approx 1-2$ wt% increase in the amount of the rigid fraction at the expense of the soft fraction (Fig. 6.8a). The amount of the semi-rigid fr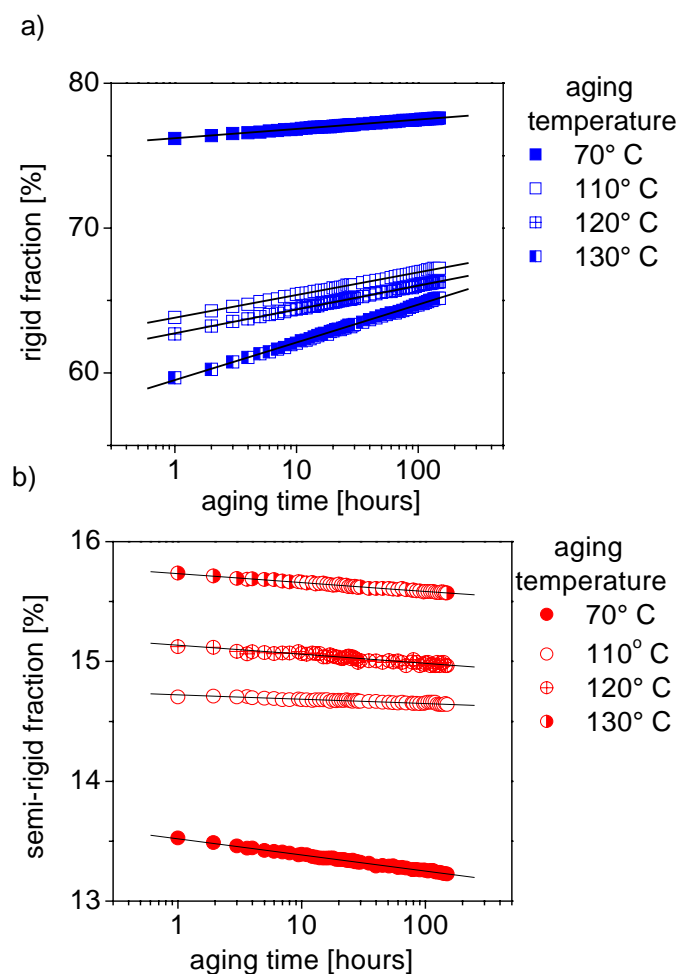action remains almost constant in all the cases (Fig. 6.8b). For all aging temperatures a decrease in the chain mobility of semi-rigid and soft fractions is observed. The chain mobility in the rigid fraction slightly decreases (Fig. 6.9).

a)

b)

c)
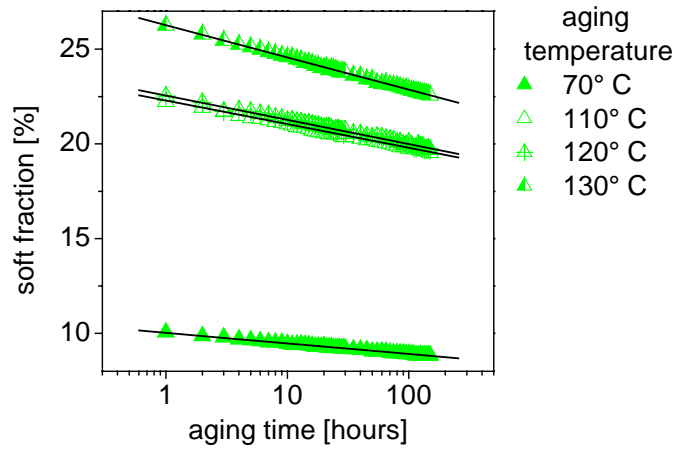
Figure 6.8. The amounts of rigid (a), semi-rigid (b), and soft (c) fractions of homopolymeric iPP samples crystallized from the melt as a function of the aging time for different aging temperatures.

a)

b)

c)
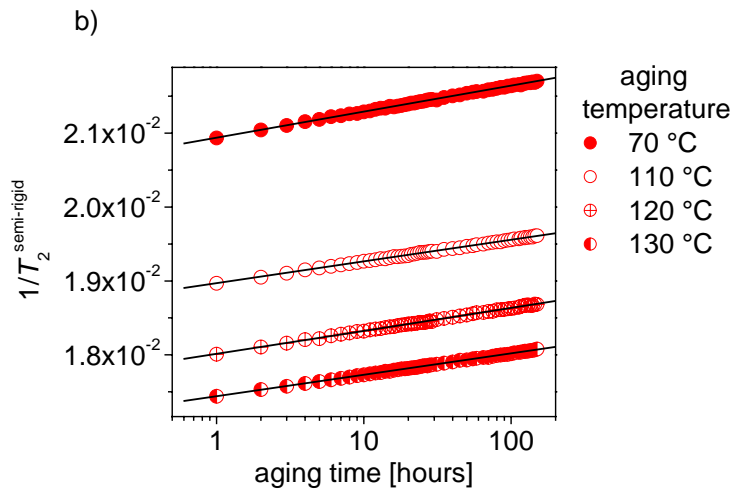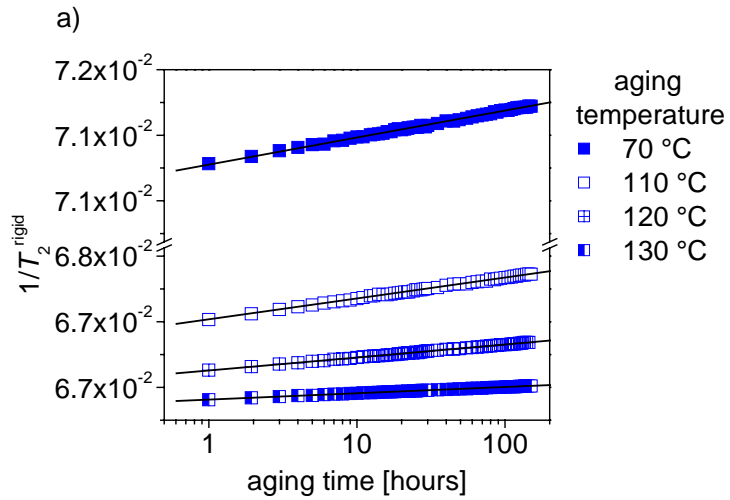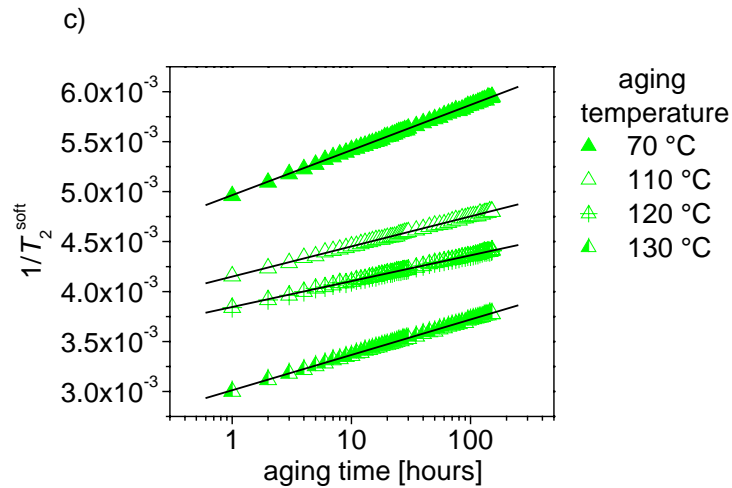
Figure 6.9. The effect of different aging temperatures on the chain mobility in the (a) rigid (T_2^{rigid}), (b) semi-rigid ($T_2^{semi\text{-}rigid}$), and (c) soft (T_2^{soft}) fractions of melt-crystallized homopolymeric iPP samples.

Using the same approach as in the previous paragraph it is possible to calculate the rates of aging, at different aging temperatures, in terms of the slopes of plots of the amounts of the rigid and soft fractions versus log *annealing time* and from the plots of T_2^{rigid}, $T_2^{semi-rigid}$, and T_2^{soft} versus log *annealing time*. In a good approximation all the plots yield a linear relationship at long aging time. The results obtained from those plots are summarized in Table 6.3 and Table 6.4.

Table 6.3. Overall slopes estimated from fitting of the dependences of the rigid and soft fractions on the logarithm of aging time at different aging temperatures.

aging temperature	slope	
	rigid fraction	soft fraction
70 °C	0.64	-0.55
110 °C	1.56	-1.24
120 °C	1.64	-1.27
130 °C	2.60	-1.7

Table 6.4. Overall slopes estimated from fitting of the dependences of the $1/T_2^{rigid}$ and $1/T_2^{soft}$ on the logarithm of aging time at different aging temperatures.

aging temperature	slope	
	rigid mobility	soft mobility
70 °C	-0.04	-14.01
110 °C	-0.01	-14.22
120 °C	-0.02	-14.51
130 °C	-0.01	-28.63

6.9 Discussion: physical aging in homopolymeric iPP samples by NMR and mechanical analysis

[Hed2007] has reported that the morphology of isotactic polypropylene at temperatures well above the glass transition can be described by a three phases model of rigid, semi-rigid and soft phases. At temperatures close to 25° C the morphology of iPP can be described by a two-phase model of rigid and soft fractions. The amounts and chain mobility of each fraction are important parameters regarding the physical and mechanical properties of iPP. Those quantities typically change when the sample is exposed to temperatures well above the glass transition due to aging and annealing [Hik1997, Ala1999, Aki1999, Mar2000, Iji2000, Mai2000, Weg2000, Ali2001, Lab2001]. It is known that the aging of iPP samples after the fabrication causes changes in the structure and properties of the materials. This process has been employed to improve the final properties of the polymers via healing of defects and relaxing residual stress and strain. The observed changes in the mechanical properties (Fig. 6.1, 6.2, 6.3) with the aging time indicate that micro-structural reorganization take place within the material. An increase in elastic modulus has been observed (Fig. 6.1), while the impact strength decreases (Fig. 6.2) with increasing aging time. The decrease in the impact strength is associated with an increasing the amount of the rigid fraction during aging. Property changes occurring upon aging are generally attributed to the relaxation process in the amorphous phase, leading to a reduction in free volume (Fig. 6.3), which will be recovered at higher temperatures, implying that aging is a fully thermoreversible process. The mechanical data imply that aging restricts the motion of the polymer chains, and a good way of probing such changes is to study isothermally the changes in the NMR signal for a long period of time.

In order to follow with high sensitivity the changes in the structure at 28° C the amounts and the chain mobility of the rigid and soft fractions are plotted versus log *annealing time*. When the sample is exposed at temperature of 28° C for 1000 hours after preparation the amount of the rigid fraction gradually increase in time at the expense of the soft fraction (Fig. 6.7ab). In contrast to the characteristic values describing the mechanical behaviour, the increase in the amount of the rigid fraction is not very pronounced and is not sufficient to attribute the significant enhancement of mechanical properties during aging just to the secondary crystallization. The chain mobility of the rigid fraction remains almost constant and the chain mobility of the soft fraction decreases with time.

Based on information from Fig. 6.7b, it is plausible to conclude that the aging at 28°C influences mainly the soft fraction of all homopolymer iPP samples, and the soft fraction becomes more restricted possibly due to molecular ordering. Our observations are in line with Struik's model [Str1987]. The information provided by Fig. 6.7(a) and (b), with the available level of resolution, indicates that the aging rate is higher in the case of injection moulded and quenched homopolymeric iPP compared to the material crystallized from the melt. From these results we can conclude that important factors determining aging are the morphology of the sample, and a relationship between the physical aging kinetics and the relative amount of the soft fraction. At 28 °C we cannot conclude about the changes in the semi-rigid fraction due to aging, because at this temperature the NMR signal can be decomposed into only two components.

In order to study the changes in the semi-rigid fraction due to aging, the temperature of the aging and NMR experiment was set within 70° C to 130° C. Increasing the aging temperature from 28° C to 70 - 130° C allows molecular motions to occur, which may lead to structural rearrangements and the observation of the phenomenon of physical aging. According to the results shown in Figure 6.5, Figure 6.8 and Figure 6.9, it is plausible to conclude that in homopolymeric iPP samples crystallized from the melt physical aging influences both the semi-rigid and soft fractions. These changes can be due to the small crystals formed by secondary-crystallization, which hinder the mobility of the soft fraction. The NMR data are consistent with the possibility of the formation of the small crystals, but do not prove this type of structure. Based on the chain mobility considerations, the formation of the new crystals, due to the secondary crystallization, takes place mainly in the semi-rigid and soft fractions, where the chain mobility decreases with increasing the aging time. No evidence of formation of thinner lamellae growing between the primary one due to aging is pointed out by X-ray data (Figure 6.4) Based on the results summarized in Table 6.3 and Table 6.4 the aging rates increase with increasing aging temperature.

The combination of results from NMR, DSC, X-ray and mechanical properties as a function of the age of the polymer on the basis of the current understanding of the dependence of those parameters on the polymer structure suggest an explicit interpretation of the changes in the structure, which accounts for the variation of the properties during aging. The structural changes are considered to be associated with a molecular rearrangement generally similar to secondary crystallization accompanied by a decrease in segmental chain mobility of the amorphous chains involved in the diffusion process. A decrease in the segmental chain mobility, by increasing the structural packing density in the amorphous or intercrystalline

regions due to the aging, results in an increase in the elastic modulus (see Fig. 6.1.). Tobolsky [Tob1965] states that for polypropylene and another semi-crystalline polymers, the crystalline regions act in part like crosslinks, thereby tending to increase the modulus by increasing the resiliency contributions of the amorphous or semi-rigid regions. The effect of the formations of small crystals due to secondary crystallization may therefore be viewed as effectively increasing the modulus.

6.10 Conclusions

In this chapter, we have investigated the influence of morphology, aging time, and aging temperature on the physical aging behaviour of homopolymeric iPP samples. We characterized the morphology in terms of the two- and three-phase model comprising rigid and soft phases, and rigid, semi-rigid and soft phases, respectively. Injection molded, crystallized from the melt, and quenched homopolymeric iPP samples provided us with specimens of widely differing morphologies. Crystallization from the melt resulted in a relatively lower amount of the soft fraction. This is consistent with a lower degree of constraints imposed by the crystallites on the mobility of the noncrystalline chain segments when crystallization occurs under conditions of high segmental mobility.

The extent and kinetics of physical aging in these samples were characterized following the changing in the phase content and chain mobility with time. These changes in the amounts of the rigid, semi-rigid, and soft fractions, and chain mobility in each fraction ($1/T_2^{rigid}$, $1/T_2^{semi-rigid}$ and $1/T_2^{soft}$) displayed a linear dependence on log(*aging time*). The changes in the phase content and chain mobility with time indicated that the extent of physical aging in semi-crystalline homopolymer iPP samples is significant and easily quantifiable. As a result, physical aging must be considered as an important factor when semi-crystalline iPP samples are designed for use in applications that involve prolonged exposure to above-ambient temperatures.

We have observed that the chain relaxation rate in semi-crystalline homopolymeric iPP is sensitive to the relative amounts of the semi-rigid and soft factions. Specifically, for a given aging history, the chain relaxation rate was observed to increase in the samples with a more stable thermodynamic morphology. This observation raises the possibility that the aging takes place primarily in regions of highest mobility that are more distant from the fold surface of the primary crystallites. The observation reported here also suggests that the conformational entropic state of the semi-rigid and soft fractions is more relevant to physical

aging in semi-crystalline polymers than the proximity of the aging temperature to their respective glass transition temperatures.

Chapter 7

Uniaxially Deformed Isotactic Polypropylene

7.1 Introduction and motivation

The mechanical properties of semi-crystalline polymers are strongly affected by changes in the degree of crystallinity due to variations in the molecular structure, different processing conditions and loading conditions [Pop1987, Hal1972, Boy1979, Boy1983, Str1980, Man1964, Man1985, Neg1992, Wor1996, Boy1984, Boy1985]. Loading conditions include the drawing temperature, draw ratio, and the strain rate [Bel1993, Gos1996, Sil1998]. The deformation process of semi-crystalline polymers has been extensively investigated for many years using a variety of methods [Fis1962, Pet1967, Hay1965, Pet1967, Pet1969, Fis1969, Ste1969]. When semi-crystalline polymers are highly drawn, the shear forces destroy the spherulites. This is followed by the reorganization of the spherulitic morphology to another type of morphology depending on the material drawn and the drawing conditions. Several modes of deformation above glass transition temperature have been identified in semi-crystalline polymers. According to Flory and Yoon [Flo1978], the plastic deformation occurs by partial melting and re-crystallization of the crystalline phase. However, according to Peterlin [Pet1973] the plastic deformation during the application of stress occurs in three stages. In the first stage, the plastic deformation of the original spherulitic structure occurs. The deformation occurs by strain of the interlamellar soft regions with a combination of interlamellar separation, lamellae stack rotation, interlamellar shear deformation and cavitation [Li1999, Lin1974, Zha2000]. In the second stage, the discontinuous transformation of the spherulitic structure to a fibrillar morphology takes place. During this stage, the lamellae in micronecks are fragmented and the broken crystal blocks are incorporated into newly formed microfibrils. In uniaxial drawing, the blocks are not only oriented into the drawing direction, but also in the direction perpendicular to it [Bra1986]. The chains connecting the broken crystal blocks in the lamellae serve as intramicrofibrillar tie molecules. In the third stage, the plastic deformation of the fibrilar structure occurs. The drawing of the microfibrillar structure [Pet1973] is completely different from the initial plastic deformation that transforms the lamellae into the microfibrillar morphology. The thickness of the fibrils changes almost proportionally to the draw ratio, as a consequence of the much smaller shear

displacement of the constituting microfibrils, caused by the shear stress on the fibrils [Pet 1987].

Crystallinity, molecular mobility, lamellar thickness and structural orientation in both soft and crystalline phases are important parameters regarding the physical and mechanical properties of stretched and non-stretched iPP. There are several methods for the structural characterization of the soft and crystalline phases of the polymers. One of the methods - solid-state NMR - is capable of characterizing the crystallinity, the molecular mobility, domain thickness and specifically the orientation distribution function of semi-crystalline polymers [Sch1994, Sch1991, Gun1992, Kiv1986, Bud2003, Ba1998, Che2005, Gol1961, Dem1996]. Another method is IR spectroscopy, widely used to determine the degree of crystallinity of iPP [Hei1959, Sam1981, Kis1983]. Knowledge of strain-induced order in the crystalline and soft phases of stretched iPP under various conditions is valuable information for understanding the structure reorganization mechanisms, and their relation to the mechanical properties of iPP.

Wide-angle X-ray diffraction (WAXD) provides information about the crystal lattice order, strain-induced changes in orientation of crystalline domains, and highly oriented crystalline structures in the fibrilar morphology generated in the neck part of uniaxially stretched polymers [Men2003]. Very little information about strain-induced changes in the soft component can be obtained from WAXD. Small angle X-ray scattering (SAXS) provides information about lamellae packing, orientation, and long period [Zhu2004, Wen1993, Zhu2005, Mez1994, Aur2001].

The spectroscopic evidence from infrared (IR) and NMR for structural reorganization during deformation is rather indirect as far as morphology is concerned. Transmission electron microscopy (TEM) yields direct access to the details of the lamellar morphology [Yam1998, Zho2005]. It is thought that IR and NMR are complementary techniques providing morphological evidence on nanometer scale phenomena for stretched iPP, the phase composition, molecular mobility and the orientation. In a recent investigation on iPP by NMR, SAXS, WAXD, DSC and TEM [Hed2007] the phase composition, chain mobility, and domain thicknesses were correlated.

The focus of this chapter is to study the change in the phase composition/crystallinity, molecular mobility, and lamellae thicknesses in iPP upon uniaxial drawing at different drawing temperatures and rates. Two complementary methods, ^{1}H solid-state NMR and IR, are used. The study largely focuses on strain-induced changes in the soft phase that have not been analyzed previously in detail.

7.2 Materials

The isotactic polypropylene (iPP-PP575P) homopolymer samples that were used for the present study were manufactured by SABIC Europe BV. The material is characterized by a melt flow index of 10g/10 min. It was injected moulded into plates of 12 cm x12 cm and 4 mm thickness using an Engel 45A machine. The melt temperature was set to 235° C, the holding pressure, the holding time, the cooling time and the overall cycle time were 40 MPa, 20 s, 20 s and 49.5 s, respectively.

Dog - bone shaped tensile bars with a length of 70 mm, thickness of 4 mm and gauge dimensions of 20 mm length were cut from the injection moulded iPP plates. The samples were uniaxially stretched at different temperatures (25° C, 80° C, and 110° C) and different rates (1, 10, 50, 100 mm/min) to draw ratios in the range of $\lambda = 7 - 16$ using a Zwick Z050 tensile machine. Based on the literature information [Pet1971] we assume that in this deformation range the spherulitic structure is transformed into fibrillar structure. Since no homogeneous neck formation was observed at $\lambda = 1 - 6$, samples in this range of strain were not studied. All the NMR and IR experiments in this study were performed on the neck part of stretched samples after 2 hours of strain recovery. New tensile bars were used for each NMR experiment as a function of temperature, strain and deformation rate.

7.3 Stress-strain characteristics

Figure 7.1a shows the stress-strain curves for iPP samples that were uniaxially stretched at a deformation rate of 10 mm/min in a temperature range between 25° C and 110° C. It can be observed that the deformation behavior of iPP is strongly affected by the temperature. For a drawing temperature range between 25° C and 110° C typical ductile deformation behavior with a yield point, neck formation, and propagation, and strain hardening is found. In the low temperature region a pronounced yield point occurs, which is related to necking and the inhomogeneous deformation of the iPP samples. At a microscopic scale this corresponds to the beginning of the transformation of the initial spherulitic morphology into fibrillar morphology. The higher values of the yield stress at low drawing temperatures can be explained with increasingly important contributions from the soft phase to strain-induced changes in the crystalline phase due to the low chain mobility in the soft phase. With increasing drawing temperature, the yield stress and strain hardening decrease. The strain-hardening region also becomes less well defined and the yield point becomes diffuse. At high

drawing temperatures, the increase in the chain mobility of iPP chains in the soft and crystalline regions (see below 7.5) results in a lower stress required for strain-induced morphological changes. Strain hardening is related to an increase in stress when the neck propagation over the whole length of the gauge part of the sample is achieved. The onset strain hardening seems to be slightly shifted to higher draw ratio with increasing temperature.
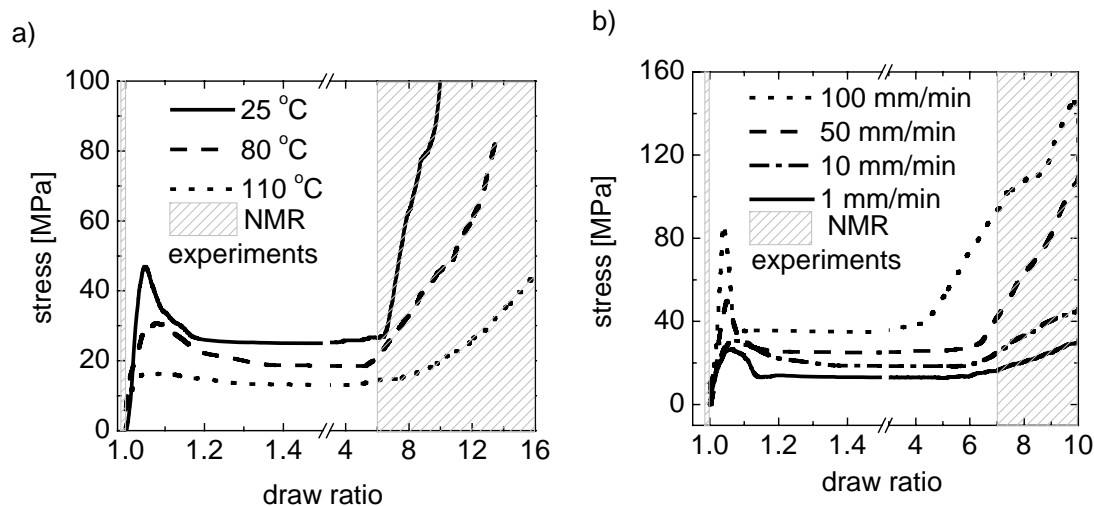
Figure 7.1. Stress-strain curve recorded (a) at 25° C, 80° C and 110° C at a constant drawing rate of 10 mm/min, and (b) with different drawing rates of 1, 10, 50, and 100 mm/min at 80° C. The hashed area corresponds to the draw ratio λ where the NMR experiments were performed for recovered after strain sample.

Figure 7.1b shows the stress-strain curves of iPP samples stretched at 80°C with different drawing rates of 1, 10, 50, and 100 mm/min. Both, the yield stress and the strain hardening increase with increasing strain rate at 80° C (see Figure 7.1b). These changes indicate that chain mobility plays an important role in the molecular rearrangements that are required for strain-induced morphological changes. Therefore, the strain increases with the deformation rate.

7.4 Crystallinity by IR

Infrared analyses were carried out on the samples draw to λ=7, 10 and 12.5 at 80° C and 10 mm/min. Dichroic and non-polarised spectra of one of the samples (λ=10) are provided in Figure 7.2. It is clear that orientation of the sample has a distinct effect on the acquired spectra, indicating that the sample is non isotropic. The peak heights of the relevant peaks were extracted from these spectra based on the definitions mentioned in the experimental section [Kis1983] and used to calculate the crystallinity (cf. Table 7.1). Due to the

experimental errors we cannot draw a conclusion about the dependence of the crystallinity on the draw ratio. However it is clear that the value of rigid fraction from NMR is in the same order of magnitude as the crystallinity measured by IR.

Table 7.1. Crystallinity of uniaxially stretched iPP determined by IR spectroscopy using the Kissin [Kis1983] method. The samples were uniaxially drawn at 80° C with 10 mm/min.

Sample	Crystallinity[a]
$\lambda = 7$	67
$\lambda = 10$	66
$\lambda = 12.5$	69

[a] The errors are of the order of 10%
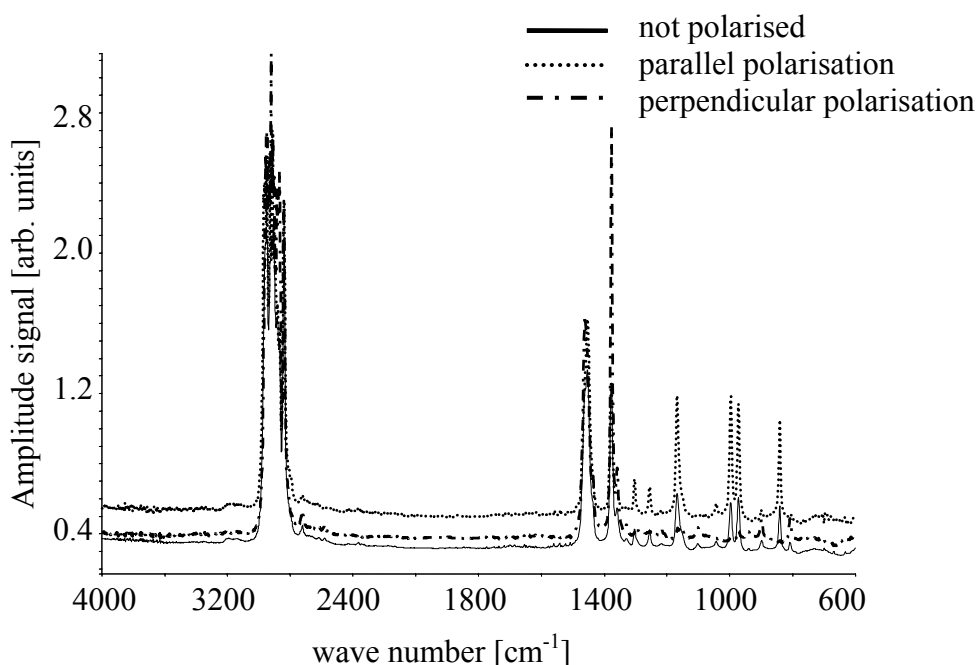
Figure 7.2. IR spectra of the iPP drawn to $\lambda=10$ at 80°C acquired with and Polarized and non-polarised lighter. The drawing rate was 10 mm/min.

7.5 Phase content and chain mobility by NMR at 70° C

The temperature dependence of the amount of the rigid, semi-rigid and soft fractions for iPP samples both non-stretched and uniaxially stretched at 80° C, and at three different drawing ratios ($\lambda=1$, 7, and 12.5) at a drawing rate of 10 mm/min are shown in Figure 7.3a. For the non-stretched iPP sample ($\lambda=1$) the content of the rigid fraction first decreases upon heating to 60° C, then it is almost constant in the temperature range from 60° C to 110° C, and finally

decreases from 120° C onward due to the partial melting. In the temperature range from 40° C to 60° C, a significant fraction of the soft phase is immobilized and contributes to the amount of the detected rigid fraction (see Figure 7.3a). In this temperature range, the amount of the rigid fraction is composed of the crystalline phase and immobilized fraction of the soft phase. The amount of the soft fraction increases upon increasing the temperature. This increase is accompanied by an increase in molecular mobility of the less constrained chain fragments in the soft phase as it follows from T_2^{soft}. In the temperature range from approximately 60° C to 100° C the amount of the rigid fraction is close to the crystallinity determined by SAXS and DSC [Hed2007]. Above 110° C, the amount of the rigid fraction of iPP decreases due to the partial melting of thin lamellae. The iPP samples, having recovered after strain show similar temperature dependence of the amount of each fraction as non-deformed iPP samples.
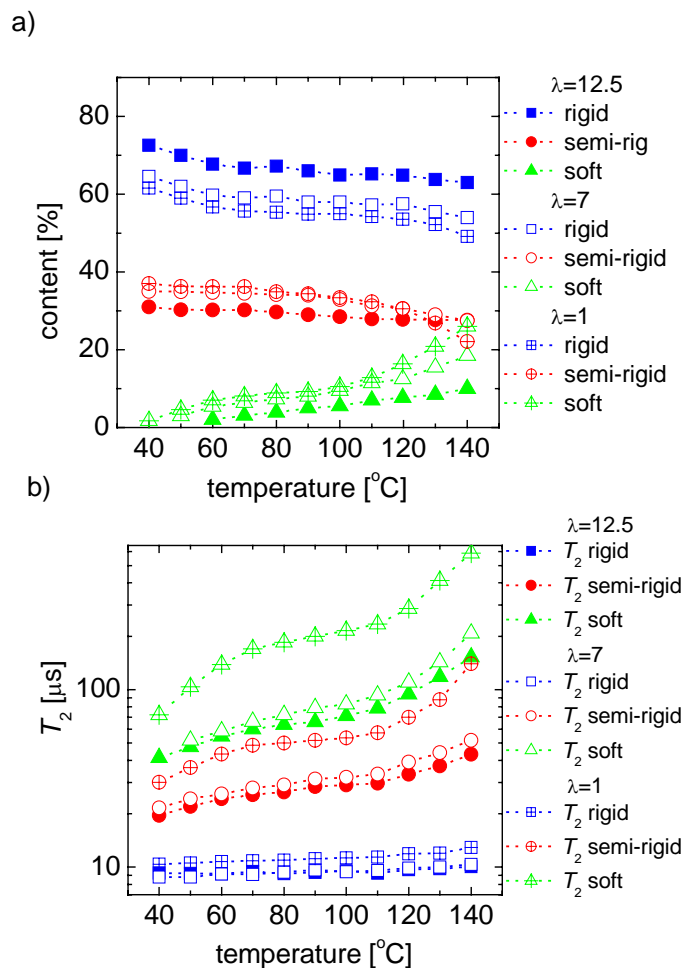
Figure 7.3. (a) Temperature dependence of the amounts of rigid, semi-rigid, and soft fractions of non-stretched iPP ($\lambda=1$) and uniaxially stretched iPP ($\lambda=7$ and 12.5). The samples was stretched at 80° C with a draw rate of 10 mm/min. (b) Temperature dependence of the ^{1}H T_2 relaxation times (T_2^{rigid}, $T_2^{semi-rigid}$ and T_2^{soft}) for both non-stretched and uniaxially stretched iPP samples. The NMR experiments were performed at 70° C.

Thus, above 40° C, three different fractions (Figure 7.3a) with different mobilities (Figure 7.3b) are detected. The characteristic decay time T_2 is related to the chain mobility in different fractions. The relaxation time (T_2^{rigid}) of the rigid fraction increases slightly with temperature in all the samples. The small increases in T_2^{rigid} with increasing temperature could be related to α_c relaxation process [Sch1991]. The intermediate $T_2^{semi-rigid}$ relaxation time increases with increasing temperature, but its value essentially does not exceed T_2^{rigid} for the same sample at a given temperature. This indicates that the segmental motion responsible for $T_2^{semi-rigid}$ is largely restricted. A significant difference in temperature dependence for the sample with different draw ratios is observed for the relaxation time T_2^{soft} of the soft fraction (Figure 7.3b). With increasing draw ratio the constraints on the segmental mobility in both soft and semi-rigid component increases. This leads to a decrease of $T_2^{semi-rigid}$ and T_2^{soft}, is especially in the strain-hardening region ($\lambda \sim 7$) of the samples.

7.6 Effect of drawing ratio on the phase composition and chain mobility

In order to study the structural changes caused by drawing, the amounts of rigid, semi-rigid, and soft fractions that was measured at 70° C is plotted as a function of the draw ratio for iPP samples which were uniaxially stretched at 80° C, with a drawing rate of 10 mm/min (Figure 7.4a). Drawing to $\lambda = 7$ cause a small increase in the amount of the rigid fraction, which indicates the presence of highly strained tie molecules. With the draw ratio increasing to 10 – 16, a further increase in the amount of the rigid fraction is observed. This increase can be attributed to strain-induced crystallization due to high straining of chains in the soft component and/or large immobilization of chains in the soft phase due to their elongation. In the deformation range from $\lambda=7$ to $\lambda=12.5$ the amount of the rigid fraction is in good correspondence with the degree of crystallinity obtained by IR (see Figure 7.4a). Thus, the increase in the amount of the rigid fraction is mainly due to strain – induced crystallization.

Figure 7.4. (a) Dependence of the amounts of rigid, semi-rigid, and soft fractions at 70° C on the draw ratio of iPP uniaxially stretched at 80° C ($\lambda=7\div16$). The drawing rate was 10 mm/min. The amount of the rigid fraction (■) determined by NMR at 70° C is compared with the degree of crystallinity (□) determined by IR. (b) Draw ratio dependence of the ^{1}H T_2 relaxation times for both non-stretched and stretched iPP samples. The T_2 values are assigned to the rigid, semi-rigid, and soft fractions of iPP as shown in the figure.

In order to reveal the effect of drawing on the mobility of the rigid, semi-rigid and soft fractions, T_2^{rigid}, $T_2^{semi\text{-}rigid}$ and T_2^{soft} are shown as a function of draw ratio in Figure 7.4b. At $\lambda = 7$, both $T_2^{semi\text{-}rigid}$ and T_2^{soft} are significantly shorter than for non-stretched iPP, indicating that the molecular mobility of the semi-rigid and soft fractions largely decreases upon drawing. At $\lambda > 7$, $T_2^{semi\text{-}rigid}$ is essentially unaffected by strain, while T_2^{soft} continuously decreases up to the highest draw ratio ($\lambda=16$). The semi-rigid fraction is not affected any more by deformation and the structural changes of the soft phase continue. All these results regarding mobility considerations have important implications for the understanding of the deformation mechanism, and the characteristic changes of the tensile modulus with the draw ratio, in terms of the corresponding changes in the morphology.

7.7 Effect of drawing rate on the phase composition and chain mobility

The effect of the drawing rate on the phase composition and molecular mobility is investigated for iPP samples uniaxially stretched at 80° C to a draw ratio $\lambda = 10$ with drawing rate $d\lambda/dt$ of 1, 10, 50 and 100 mm/min. The NMR experiments were performed at 70° C. The amounts of the rigid, semi-rigid, and soft fractions and the chain mobility in each fraction of uniaxially stretched iPP are hardly affected by the drawing rate within the limit of the

experimental errors (Figure 7.5 a and b). These results show that the changes in the morphology and chain rearrangements upon uniaxially drawing of iPP are fast compared to the total time scale of explored deformation. Another explanation can be the relaxation process which occurs when removing the sample from the tensile machine.
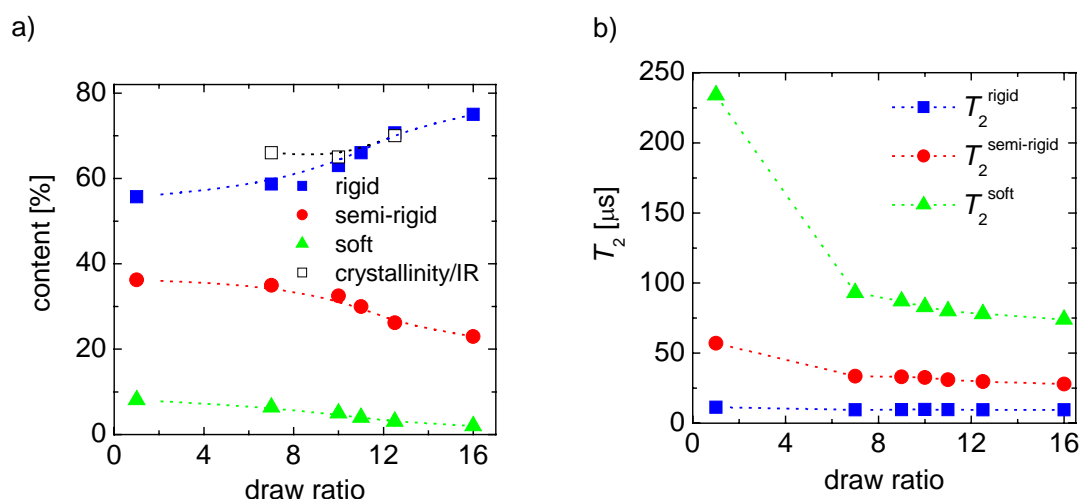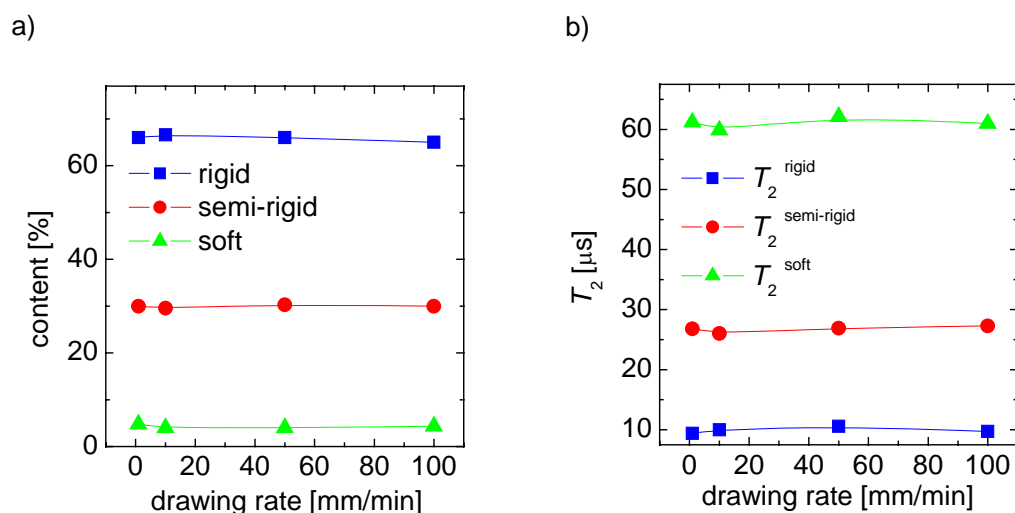

Figure 7.5. (a) Dependence of the amounts of rigid, semi-rigid, soft fractions on the drawing rate of iPP uniaxially stretched at 80° C and $\lambda = 10$. (b) Proton T_2 relaxation times for uniaxially stretched iPP samples as a function of drawing rate. The NMR experiments were performed at 70° C. The lines are guides for the eyes.

7.8 Effect of drawing temperature on the phase composition and chain mobility

Isotactic polypropylene samples uniaxially stretched with a drawing rate $d\lambda/dt$ of 10 mm/min, show differences in the phase composition and chain mobility depending on the drawing temperature. All the NMR experiments were performed at 70° C. In Figure 7.6ab, the T_2 relaxation times, and the amounts of the rigid, semi-rigid and soft fractions are shown as functions of both drawing temperature and drawing ratio. The amount of the rigid fraction increases with increasing drawing temperature for all draw ratios at the expense of both the semi-rigid and the soft fractions. The chain mobility in all fractions is lower at higher deformation temperatures.

The observed changes suggest that the α-relaxation influences morphological transformations via shearing and fragmentation of the lamellae upon deformation. The relative difference in imperfections of the crystalline structures can be identified by comparing the relaxation time T_2^{rigid}. T_2^{rigid} value is longer at lower deformation temperatures

at the same draw ratio λ. This indicates larger imperfections of the crystalline phase of iPP stretched at 25° C, as compared to the undeformed sample (Figure 7.6b).
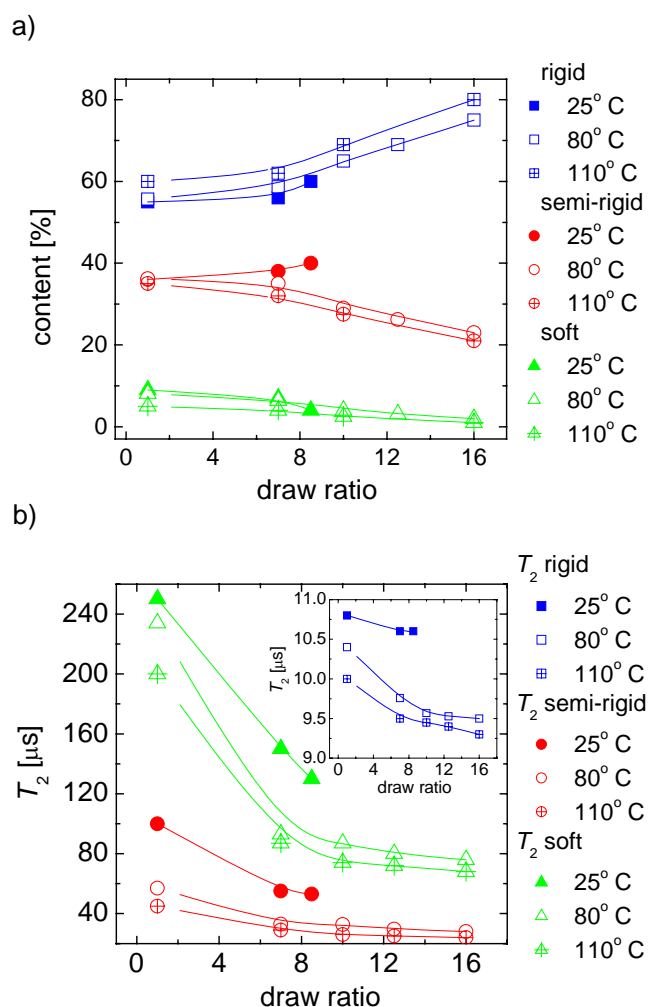
Figure 7.6. (a) Dependence of the amounts of rigid, semi-rigid, and soft fractions on drawing temperature and draw ratios for iPP uniaxially drawn at 25° C, 80° C, and 110° C. A drawing rate of 10 mm/min was used. The NMR measurements were performed at 70° C. (b) Dependence of the ^{1}H T_2 relaxation times on the drawing temperature and the draw ratio for iPP uniaxially stretched at different temperatures. The lines are guides for the eyes.

A small increase in the amount of the rigid fraction is observed at strain hardening deformations (λ>7) that can be due to a large extension of the tie chains. These results suggest that at higher deformation temperatures, higher strain-induced chain orientation and better ordered crystalline structures are formed upon deformation. This is because higher chain mobility facilitates the morphological transformations, and possibly partial melting and strain-induced crystallization occur at higher temperatures. The NMR measurements reveal that the drawing temperature has an important influence on the phase composition and molecular mobility of drawn iPP.

7.9 The effect of draw ratio and drawing temperature on the domain sizes of iPP

The long period L_p and the thickness of the rigid (d_r) and semi $-$ rigid $+$ soft (d_{srs}) domains were studied as a function of both draw ratio and drawing temperature. The values of L_p, d_r, and d_{srs} were determined from the analysis of the spin-diffusion data (measured at 70° C) (Figure 7.7) with the 1D (non-stretched iPP) and 2D (stretched iPP) spin-diffusion models [Hed2007].
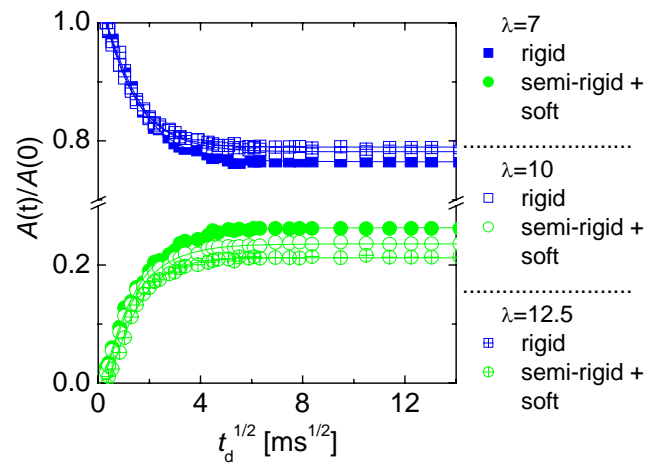
Figure 7.7. Proton spin-diffusion decay and build-up curves for the rigid and semi-rigid fractions of iPP uniaxially stretched to λ = 7, 10 and 12.5. The drawing temperature and drawing rate were 80° C and 10 mm/min, respectively. The NMR experiments were performed at 70° C. The DQ filter selects the magnetization of the rigid fractions of stretched iPP, as described in ref [Hed2007]. All experiments were performed at low field. The FID was fitted with the sum of one Abragam function and one exponential function. The solid lines represent the best fit to the 2D solutions of the spin-diffusion data for the two-phase morphology.

The different models are required because above yield strain, the spherulitic morphology is transformed into a fibrillar morphology typical for polymeric fibres. The chosen dimensionality of the spin diffusion process is established based on the morphology for non-stretched and stretched polyolefin's [Sch1991, Hu2000, Fis1962]. This is also confirmed by the analysis that was outlined in the Chapter 5 describing the morphology of non-stretched iPP [Hed2007], which shows that the dimensionality of the spin-diffusion process is 1D and 2D for initial sample and the uniaxially drawn iPP, respectively. The thickness of the rigid and combined semi-rigid plus soft domains are determined for uniaxially stretched iPP because the small amount of the soft fraction $\approx$ 2-5 wt.-% (Figure 7.4a) does not allow accurate determination of the thickness of this fraction.

The long period and the domain thicknesses obtained by the analysis of the spin-diffusion data which are shown in Figure 7.7 are given in Figure 7.8. This figure shows the changes of L_p, d_r, and d_{srr} upon uniaxial drawing to different draw ratios and at different drawing temperatures. At a drawing temperature of 25° C, that is below the α-relaxation temperature, the long period and the thickness of the rigid domains slightly decrease at the expense of the thickness of the semi-rigid plus soft domains (Figure 7.8). These dependences of the rigid domain thickness d_r and long period L_p on the deformation temperature can be explained by brakeage and disordering of crystals. During the uniaxial deformation of iPP at 25° C the probability of the broken crystals to recrystallize and form thicker crystals is small. Strain-induced immobilization of the soft phase hinders the displacements of chains in the soft and crystalline phases that are required for lamellae thickening. No significant strain-induced crystallization and/or annealing occur during deformation at 25° C. At higher deformation temperature faster chain mobility (Figure 7.3) can provide the required energy to facilitate the reorganization of chains to cause an increase in the amount of the rigid fraction (Figure 7.6). For higher drawing temperatures (80° C and 110° C), an increase in the long period and thickness of lamellae is observed upon increasing the draw ratio and drawing temperature (Figure 7.8).
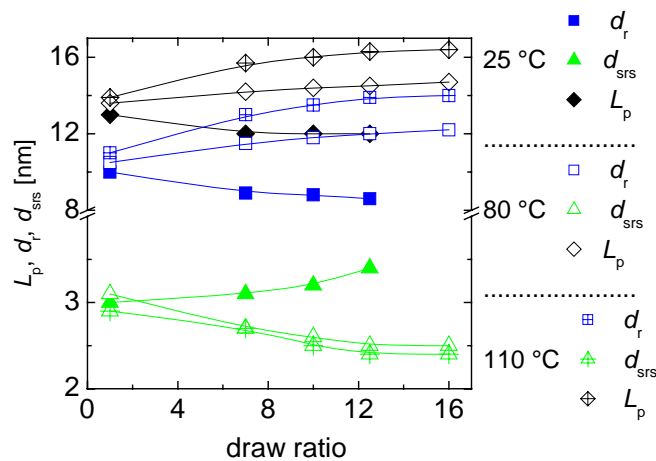
Figure 7.8. Dependence of long period L_p, the thickness d_r of the rigid and semi-rigid + soft (d_{srs}) domains on the drawing temperature and the draw ratio for iPP stretched to λ = 7, 10-16 at 25° C, 80° C, and 110° C with 10 mm/min.

The thickness d_{srs} of the semi-rigid plus soft layer slightly decreases with increasing the draw ratio and drawing temperature suggesting that the crystal thickening is caused by the chain reorganization in the soft phase adjacent to the crystal surface and the annealing process. Thus, deformation at temperatures above 60° C causes an increase in crystal thickness and long period, while deformation at lower temperatures causes a slight decrease in

crystal thickness and possibly long period. The main difference between deformation at high and low temperature is attributed to the rate of molecular motion with respect to the rate of molecular displacement with increasing strain.

7.10 Correlation between the amount of the rigid fraction and the thickness of the rigid domains

Figure 7.9 shows the correlations between the amount of the rigid fraction and the domain thickness d_r of the rigid phase for all iPP samples uniaxially stretched at different temperatures. For the limited drawing temperature range 80° C - 110° C, the dependence of the amount of the rigid fraction on d_r is apparent described by a linear function.
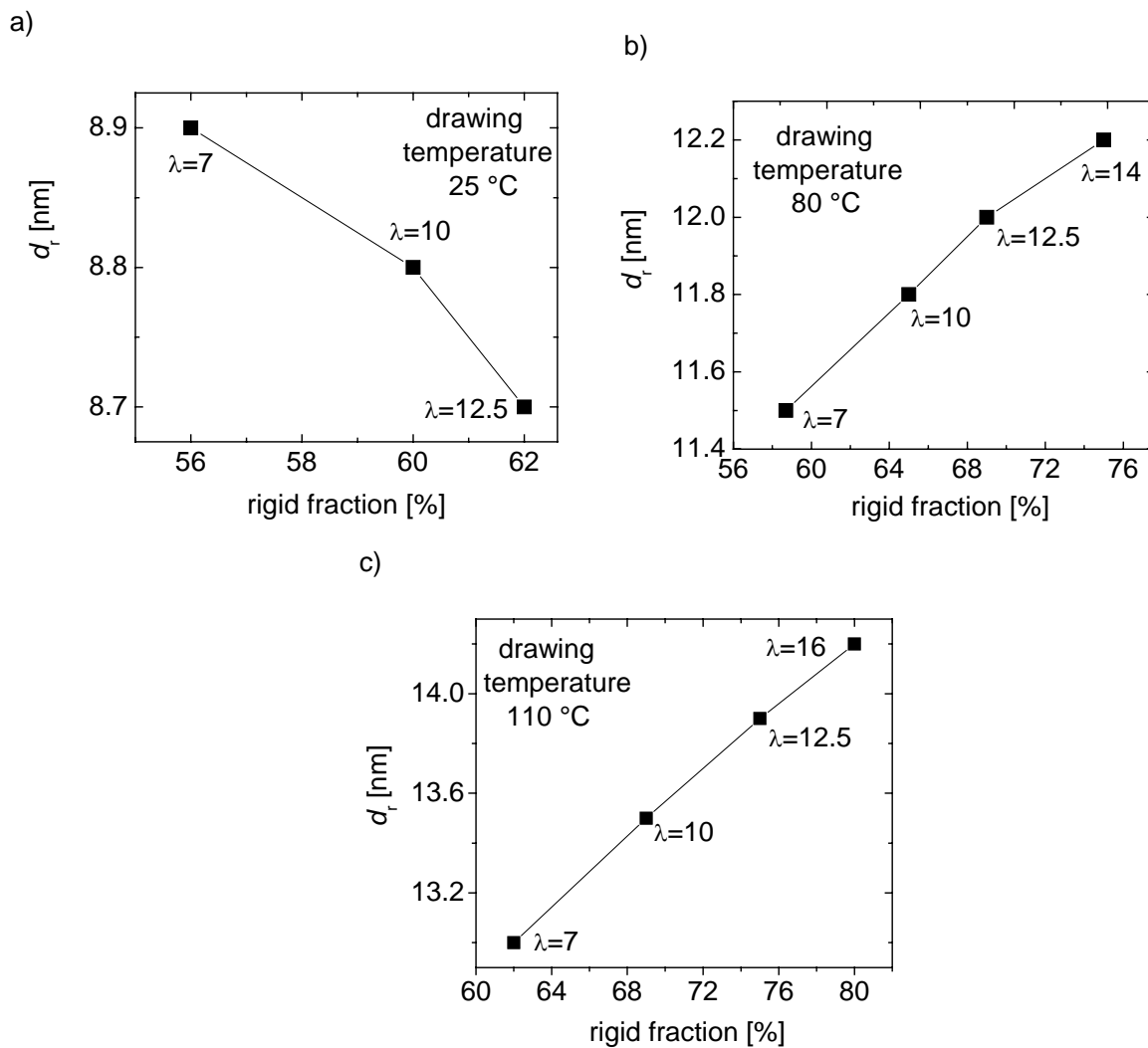
a)

b)

c)

Figure 7.9. Correlation of the thickness of the rigid domains with the amount of the rigid fraction/crystallinity for iPP uniaxially drawn at 25° C (a), 80° C (b) and 110° C (c) with 10 mm/min.

The behavior of the long period presented in Figure 7.10 (see below) is in qualitative agreement with that reported in Ref. [Bal1969]. As proven by SAXS [Bal 1969] for polypropylene, drawing at a temperature higher than 60^0 C yields an increase of long period whereas deformation below these temperatures causes a decrease of the long period. This is evident from Figure 7.9b and c and Figure 7.9a, respectively. Nevertheless, in our case the correlation is established between the thickness d_r of the rigid fraction and the content of the rigid fraction measured by ^{1}H spin diffusion at different drawing temperatures and draw ratios.

We shall consider in the following a semiquantitative model to establish the correlation between the thickness d_r of the rigid fraction and the content C_r of the rigid fraction in the high drawing temperature regime (Figure 7.9b and c). The changes produced by deformation in polymer morphology are enhanced at higher drawing temperatures. This is due to large mobility of polymer chains at the interface and in the soft fraction. Hence, the thickness of the rigid fraction and its content will increase at higher drawing temperatures. At such conditions the original morphological structure is completely destroyed and every single lamella is broken up into small folded chain blocks. The blocks are then incorporated into long microfibriles. We assume that the spin diffusion process in these microfibriles can be described by a 2D morphology as proposed for polyethylene in Ref. [Hu 2000]. In the approximation of a square section of microfibriles of size d_r and length h_r the volume is $V_{rigid}^{microfibril} \approx d_r^2 h_r$. The total volume of the rigid fraction at the end of the drawing process is $V_{rigid} = N_{microfiblils} V_{rigid}^{microfibril} \approx N_{microfiblils} d_r^2 h_r$. Therefore the rigid fraction content is $C_r \propto V_{rigid}$, and finally $C_r \propto d_r^2$ or $d_r \propto (C_r)^{1/2}$. These simple arguments explain semiquantitatively the correlation between d_r and C_r (Figure 7.9b and c). Apparently a linear dependence is shown by the data that we believe is due to the limited range of C_r explored in the experiments. Finally, we shall point out that NMR measurements that establish the thickness of the rigid domain and the phase composition are independent.

7.11 Correlation between the long period and the drawing temperatures

The long periods (L_p) were measured for different iPP samples drawn at different draw ratio $\lambda = 7 \div 16$ in the temperature (T_d) range from 25° C to 110° C using the ^{1}H spin-diffusion method. Our particular interest is the influence of the drawing temperature on the long period

(Fig. 7.10). The long period first increases rather slowly with temperature and finally increases rapidly near the melting point. Such investigation was reported before on polyethylene [Bal1969, Pet1965, Cor1967 55].
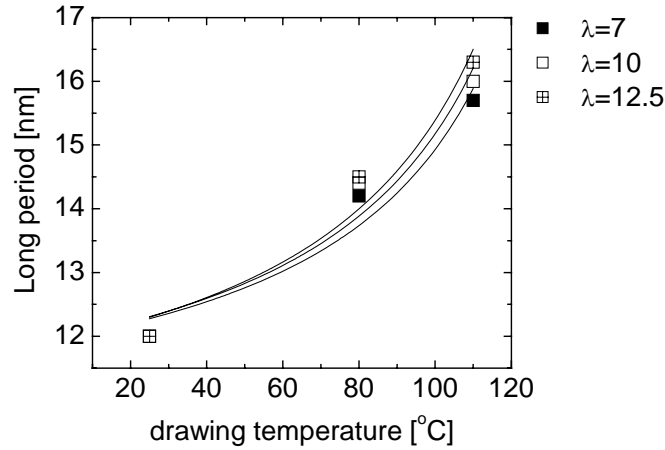
Figure 7.10. The long period of iPP samples uniaxially drawn with 10 mm/min and measured by ^{1}H spin-diffusion NMR as a function of the drawing temperatures for different values of draw ratios. The solid lines represent the fit of the data with Eq. (7.1). The fit parameters A and B are reported in Table 7.2.

The long period of drawn iPP as a function of the drawing temperature is shown in Figure 7.10. This dependence can be represented approximately [Bal1969, Pet1965, Cor1967] by the equation:

$$L_p = A + \frac{B}{T_m^0 - T_d},$$ (7.1)

where T_m^0 is very close to the melting temperature (T_m=160° C) and T_d is the temperature of drawing. The continuous lines in Figure 7.10 represents the fit of the data with Equation. 7.1. The constants A and B are given in Table 7.2 for different draw ratios.

Table 7.2. The values of the constant A and B from Equation (7.2) obtained from a fit of the data shown in Figure 7.10.

Draw ratio	A [nm]	B [nm T]
7	9.7 ± 0.8	355.1 ± 69.9
10	9.5 ± 0.9	383.7 ± 77.6
12.5	9.3 ± 0.9	413.2 ± 74.5

They are in the same range of values as those reported for polyethylene [Pet 1965, Cor1967]. The long periods were measured in this case by SAXS. These results prove indirectly that the spin-diffusion measurements give a valid trend for the long periods.

One can conclude that the blocks of chains broken in the initial iPP morphology are subjected to such a high concentration of deformational energy that they melt and reorganize according to the temperature of drawing like in polyethylene [Cor1967]. The resultant long period is more characteristic of the drawing temperature than the initial state of the iPP sample. The change of the long period is abrupt, indicating a discontinuous step in the transformation form the original microspherulitic into the fibrillar structure [Bal1969].

7.12 Correlation between the ^{1}H transverse relaxation rate and the domain thickness of the rigid domains

Morphology of semi-crystalline polymers and domain thickness characterize the material on a scale ranging from nanometers to hundreds of nanometers and micrometers. The analysis of the chain dynamics, revealed *inter alia* by the ^{1}H transverse magnetization rate, is a useful tool to improve the understanding of the microscopic properties of heterogeneous polymers.

The value of the ^{1}H effective transverse magnetization relaxation rate ($1/T_2^{rigid}$) for the rigid domains is related to the type and frequency of chain motions, and to intrachain and interchain interactions in those domains. Faster transverse relaxation rates correspond to an increase in the dipolar coupling due to the denser chain packing and/or better crystal organization that could affect chain mobility in the rigid domains. The correlation between $1/T_2^{rigid}$ and domain thickness d_r for different draw ratios and drawing temperatures is shown in Figure 7.11. For iPP samples uniaxially stretched at 25° C, the increase in $1/T_2^{rigid}$ and decrease in d_r with increasing draw ratio are due to the immobilization of the polymer chains and the fragmentation of the crystalline blocks. At this drawing temperature, the chain mobility is lower and the reorganization of the morphology from spherulitic to fibrillar is restricted. The increase in the values of $1/T_2^{rigid}$ and d_r, for iPP samples uniaxially stretched at 80° C and 110° C, are due to a decrease in chain mobility. Moreover, at this deformation temperature the chain mobility is larger than at deformation temperature of 25° C, which facilitates the reorganization of the morphology. The perfection of the crystals can occur during the strain-induced recrystallization process and/or immobilization of the soft phase, which both occur at higher deformation temperatures.

We note that all NMR measurements were done at 70° C on stretched iPP samples recovered after strain. Therefore, the dependences shown in Figure 7.11 reflect changes in the thickness and chain reorganization of crystals due to irreversible iPP deformation at different temperatures.

a)

b)

c)
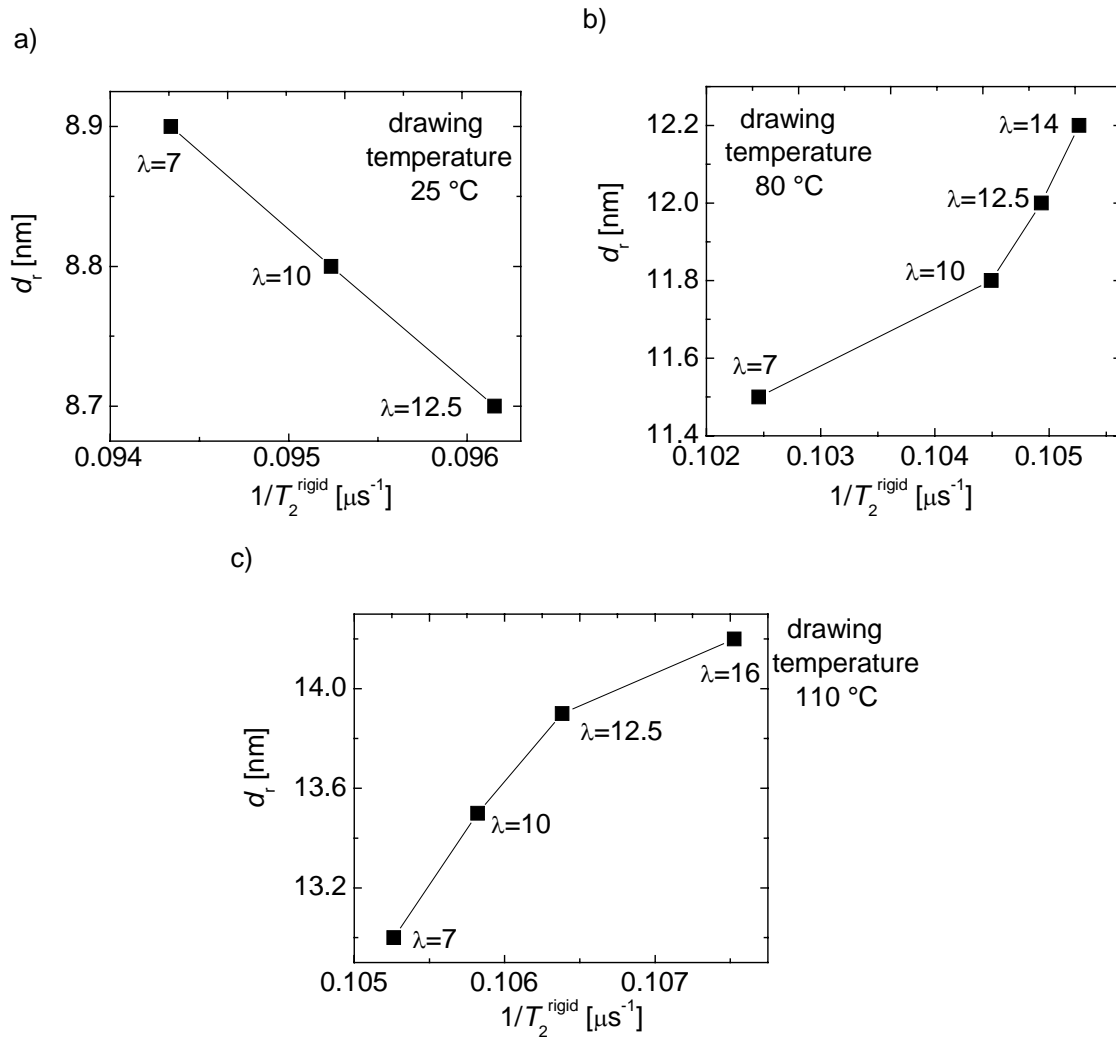
Figure 7.11. Correlation of the thickness of the rigid domains with the ^{1}H transverse magnetization relaxation rate of the rigid domains ($1/T_2^{rigid}$) for iPP that was uniaxially drawn at 25° C (a), 80° C (b) and 110° C (c) with 10 mm/min.

Elastic recovery in the soft phase can cause some changes in the phase composition, domain sizes and molecular mobility after removing the applied stress. However, these changes would not affect the conclusions about the effects of the draw ratio, drawing rate, and temperature on the structural reorganization during drawing of iPP.

7.13 Conclusion

In this present chapter, we have investigated by ^{1}H solid-state NMR the changes in the phase composition (namely the amounts of rigid fraction/crystallinity, semi-rigid, and soft amorphous fractions), chain mobility, and domain thickness for uniaxially drawn iPP at different draw ratios, drawing rates, and drawing temperatures. The values of the rigid

fraction/degree of crystallinity obtained by NMR and IR coincide within a few percent. The small difference can be explained by the analysis of NMR and IR data using three- and two-phase model, respectively. An increase in the drawing rate from 1 mm/min to 100 mm/min does not affect the phase composition and chain mobility for iPP stretched at 80° C. The drawing temperature was shown to have a significant effect on the phase composition, chain mobility, long period, and lamellar thickness. The results show that the amount of the rigid fraction/crystallinity increases as the draw ratio and drawing temperature increase for the entire range of draw ratios ($\lambda = 1, 7 - 16$). For example, the amount of the rigid fraction in non-drawn iPP is 55 wt.-% at 70° C. Its value at the same temperature increases up to 65 wt.-% for iPP stretched to $\lambda=12.5$. Higher draw ratio and drawing temperatures above 80 °C resulted in an increase of the thickness of the lamellae from 11 nm to 16.5 nm that can be explained by partial melting and recrystallization as well as immobilization of the soft phase. We can conclude that the phase composition, chain mobility and the thickness of domains largely depend on the deformation conditions, namely the draw ratio and the drawing temperature.

Correlations between the following molecular parameters were established: (1) the amount of the rigid domains and their thickness; (2) the chain mobility in the rigid domains and the thickness of these domains. A semiquantitative model was developed to describe the correlation between the amount of the rigid fraction and the thickness of the crystalline domain in the range of high drawing temperatures. Moreover, the correlation between the long period and the drawing temperature was analysed based on a phenomenological law applied before on polyethylene [Cor1967]. These relationships differ for iPP uniaxially drawn at 25° C and at higher deformation temperatures $\geq$ 80° C. The results reveal the important role of chain mobility during strain-induced transformation of the spherulitic morphology to a fibrillar one. At 25° C, the rate of molecular motion is not high enough to follow molecular displacements that are caused by macroscopic strain. This is conformed by the fact that the stress-strain dependence at 25° C largely depends on the deformation rate. High local forces that cause crystal slip damage crystalline structures as can be concluded from a small decrease in the lamellae thickness. At the same time the amount of the rigid fraction increases due to the immobilization of highly strained chain fragments in the soft phase. Deformation at temperatures of 80° C and higher, is not accompanied by high local forces due to more intensive chain motion. Moreover, a heat release during drawing causes partial melting followed by recrystallization. This results in thicker crystals and larger long periods. As far as the chain mobility is concerned, it decreases with increasing draw ratio both in the rigid and

soft phases. The decrease is more pronounced at higher deformation temperatures, which points out a more perfect structure reorganization due to partial melting followed by recrystallization at higher deformation temperatures.

Chapter 8

Impact Modified Copolymer Polypropylene

8.1 Introduction and motivation

Polypropylene (PP) is one of the most important commercial polymers available because of its extremely broad spectrum of applications. Homopolymeric PP however is too brittle for applications such as automotive components that require a polymer with high or medium impact resistance. The most widely used method to improve the impact properties of PP is through copolymerization with another α-olefin in a multi-stage reactor system or blending with ethylene propylene rubber (EPR), resulting in a system with dispersed ethylene propylene rubber particles (EPR) in a PP matrix [Ros1992, Kar1999]. The impact properties depend on the EPR rubber dispersion, composition and particle sizes and on the matrix crystallinity [Jan1993, Jan1994, Pre2000, Jan1996]. However, such modifications to improve the impact properties are often detrimental to other desired properties. The development of new systems that show an improved balance between properties represent therefore one of the major challenges to the PP industry. For instance, an improved balance between impact strength and stiffness, impact strength and transparency and impact strength and stress whitening is desired and are areas of continuous research. To partially compensate the decrease in stiffness due to the addition of EPR, addition of nucleating agents such as talc and ADK STAB NA-11 is recommended. Addition of nucleating agents increases the temperature of crystallization resulting in a decrease in cycle for injection moulding [Fil1994]. Nucleating agents increase the number of crystallization sites in polymers and reduce the spherulite size. They cause simultaneous growth and thus evenly sized crystals. Smaller evenly sized crystals improve the physical properties of the polymer like transparency and flexural modulus. A detailed knowledge of the phase morphology is a key parameter for improving the mechanical and optical properties, and for obtaining a proper balance between these properties for different applications.

A wide range of characterization methods has been applied to study the PP copolymers. A number of these techniques are suited to give information on the morphology of PP copolymers where the EPR domains typically extend form a few hundred nanometers to a few micrometers in size. Scanning electron microscopy (SEM) has been applied to study the EPR distribution in PP copolymers [Gre2002, Goi1992, Goi1993, Poe2000, Kim1998,

Cha2002, Cha2002, Cop1987, Pet1996, Bro1997, Kar1979, Ora2001, Bed2000, Yam1999, Ora1982]. TEM is another technique that has been widely applied to study the morphology in PP copolymers [Gre2002, Kim1998, Nor1995, Yok1997, Nys1999, Sta1998, San1986, Bed2002, Tom2000, Kim1996]. The prepared TEM samples show clear contrast between matrix and rubber inclusions. This technique has the advantage that the lamellae structure of the PP matrix as well as the rubber part can be studied [Poe2000, Ora2001, Sta1998, San1986].

Atomic force microscopy (AFM) is a convenient method compared to SEM and TEM in the sense that less sample preparation could be necessary and several investigations have employed AFM for morphology studies of rubber-modified PP [Cha2002, Cha2002, Nys1999, Bed2002, Nys1995, Swa2000,]. AFM directly reveals the presence of the rubber inclusions on the surface.

Nuclear magnetic resonance (NMR) relaxation provides an excellent microscopic probe of molecular or segmental motion in PP copolymer systems [Dou1979]. Sensitive indicators of molecular mobility in different fractions are the nuclear spin-lattice relaxation time T_1 and spin-spin relaxation time T_2. Previously, solid-state NMR relaxation has been used to study the changes in the phase content and the chain mobility in different fractions of polyethylene and polypropylene [Hed2007].

The first purpose of this chapter is to study the morphological features of impact modified PP copolymer by transmission electron microscopy (TEM), scanning electron microscopy (SEM) and atomic force microscopy (AFM). The second purpose is to study the changes in the phase content and chain mobility due to the change in the rubber content and the addition of nucleating agents (talc and ADK STAB NA-11). The third propose is to establish a correlation between the NMR parameters, DSC results, and mechanical data.

8.2 Materials

The impact modified copolymer polypropylene samples used in our experiments were manufactured by SABIC Europe BV. The material was first compounded at temperature between 244 - 262° C in a ZSK3033 extruder than injected in an Angel 45A machine. The melt temperature was set to 235° C, the holding pressure was 40 MPa, the holding time 20 s, the cooling time 20 s, and the overall cycle time 49.5 s. The mold chosen provides an injection molding plate (65 x 65 x3.2 mm) and a tensile bar (dumbbell shape). Three series of five samples were prepared with different rubber contents (from 0% to 33%) and different nucleating agents (Table 8.1).

Table 8.1. Listed details of impact modified PP copolymer samples that were examined in this study

Series 1	% wt RC	% Talcum	% ADK STAB NA-11	Series 2	% wt RC	% talcum	% ADK STAB NA-11	Series 3	% wt RC	% talcum	% ADK STAB NA-11
1	0	-	-	1	0	0.05	-	1	0	-	0.05
2	5	-	-	2	5	0.05	-	2	5	-	0.05
3	15	-	-	3	15	0.05	-	3	15	-	0.05
4	25	-	-	4	25	0.05	-	4	25	-	0.05
5	33	-	-	5	33	0.05	-	5	33	-	0.05

The first series of samples (Series 1) is a regular PP impact modified copolymer, the second series (Series 2) is a PP impact modified copolymer with talc nucleating agent and the third series of samples (Series 3) is a PP copolymer modified copolymer with an ADK STAB NA-11 nucleating agent, respectively. The injection molding plates were used for the impact test, stiffness text, CLTE, and NMR experiments. The tests on the injection molding plates were performed in two directions: parallel and perpendicular to the injection molding side because the values measured are significantly different for the two directions. The tensile bars were used for the tensile test.

8.3   Morphology by TEM and AFM

The shape, content, size, and size distribution of dispersed rubber particles are important factors affecting the toughening effect of PP impact modified copolymer, which relate to the micromorphological structure of the material. Transmission electron micrograph was used to determine the type of the morphology in the studied samples. TEM images of regular impact PP modified copolymer samples with rubber contents amounting to 5% and 33%, are shown in Figure 8.1ab and Figure 8.2ab.
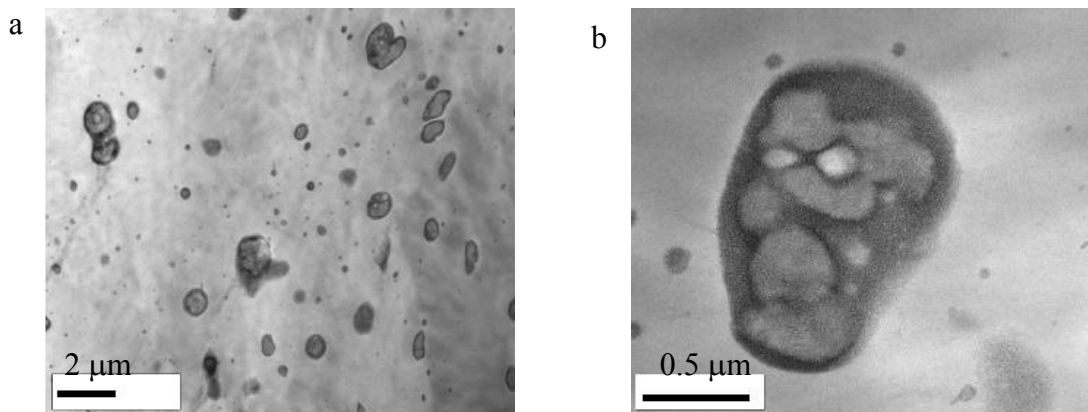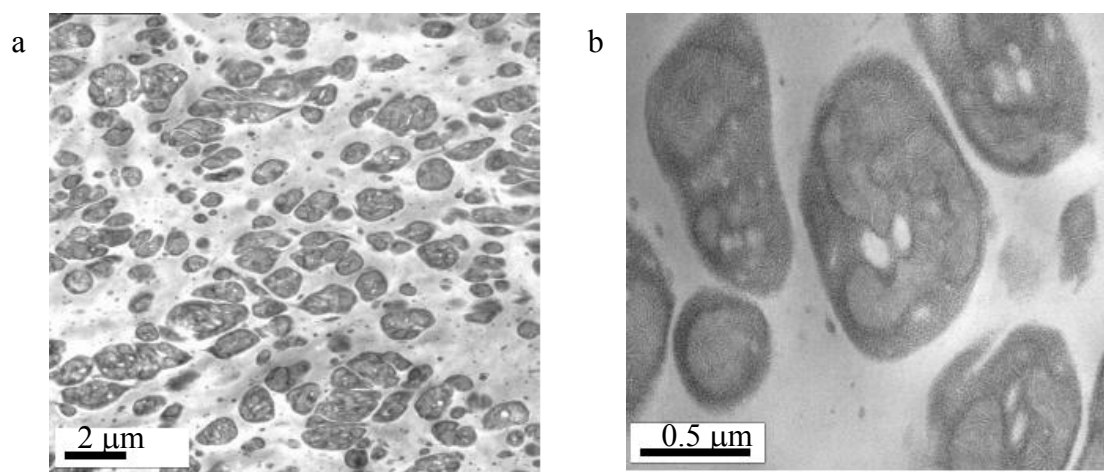

Figure 8.1. TEM picture of a regular PP impact copolymer sample with 5% of ethylene-propylene rubber (EPR)

Figure 8.1 and 8.2 demonstrate that EPR domains can clearly be seen within the PP matrix for both samples containing 5% EPR and 33% EPR, respectively. It was also observed that increasing the rubber content changes only the density and sizes of the rubber particles in the PP matrix. Because the EPR domains are soft relative to the surrounding PP matrix, lighter regions correspond to the PP matrix and darker regions correspond to EPR domains. It can be seen also that some EPR domains are dispersed and nonuniform in the cross section however, most of them can be approximated as having a rather spherical shape. Comparing the images of Fig. 8.1 and Fig. 8.2, it becomes clear that the rubber domains are more numerous for the sample with 33% rubber content. The average size of the rubber domains is between 0.2 µm and 2.4 µm for the samples with 5% rubber and between 0.2 µm and 3.4 µm for the samples with 33% rubber.

Figure 8.2. TEM picture of a regular PP impact copolymer sample with 33% of ethylene-propylene rubber (EPR)

Figure 8.1b and Fig. 8.2b further detail the morphology of the rubber domains of the regular impact copolymer PP samples with 5% and 33 % rubber content, respectively. For both samples the rubber domains can be better visualized, the presence of the dark amorphous phase (rubber) and relatively light crystalline phase (ethylene crystals) being clearer.

An additional technique used to visualise the overall shape of the dispersed rubber domains in the PP matrix is the AFM Phase Imaging (Figure 8.3). The lighter colour represents the homopolymer PP matrix whereas the darker colour represents the rubber phase. In both Figures 8.2 and 8.3 the presence of ethylene crystals in the rubber phase can be observed, i.e. the lighter regions within the darker ones.
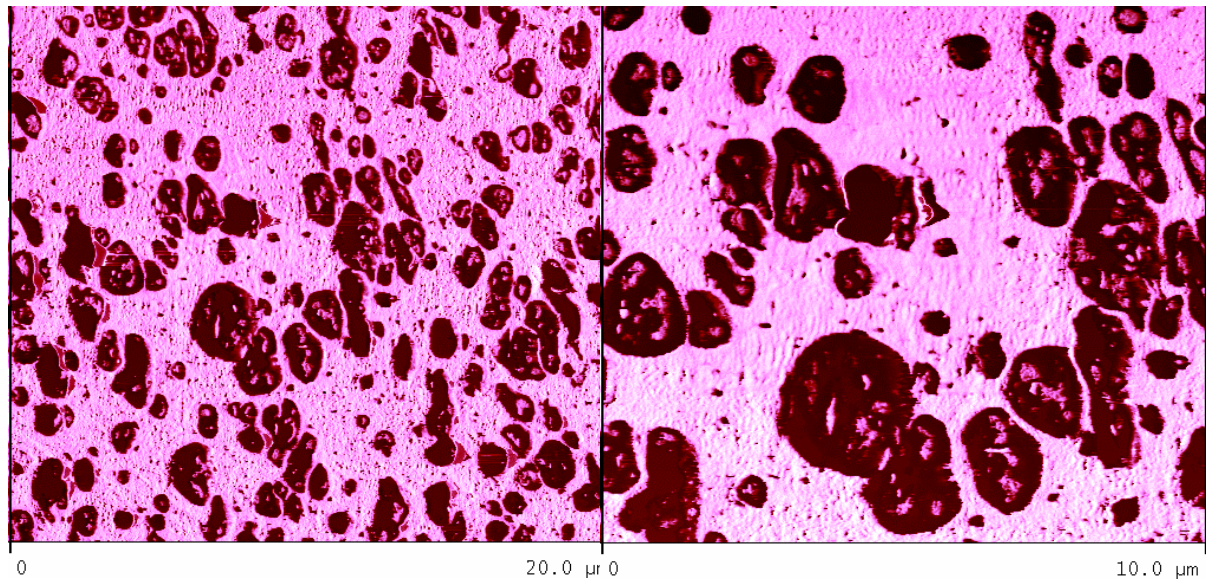
Figure 8.3. AFM phase image revealing distribution of rubber particles in an injection moulded plate of PP impact copolymer (33% rubber).

The size of the rubber domains provided by the AFM images is in good agreement with the size provided by TEM, i.e. between 0.2 μm and 3.4 μm for the 33% rubber content sample. The AFM scans also provided information with respect to the talcum particles, i.e. their flow-induced orientation and the fact that they are preferentially surrounded by the matrix.

Based on AFM scans of specific areas, the changes in the shape of the particles can be monitored throughout the sample's surface, even in systems containing high amounts of talcum particles (Figure 8.4). These systems were difficult to investigate by TEM.
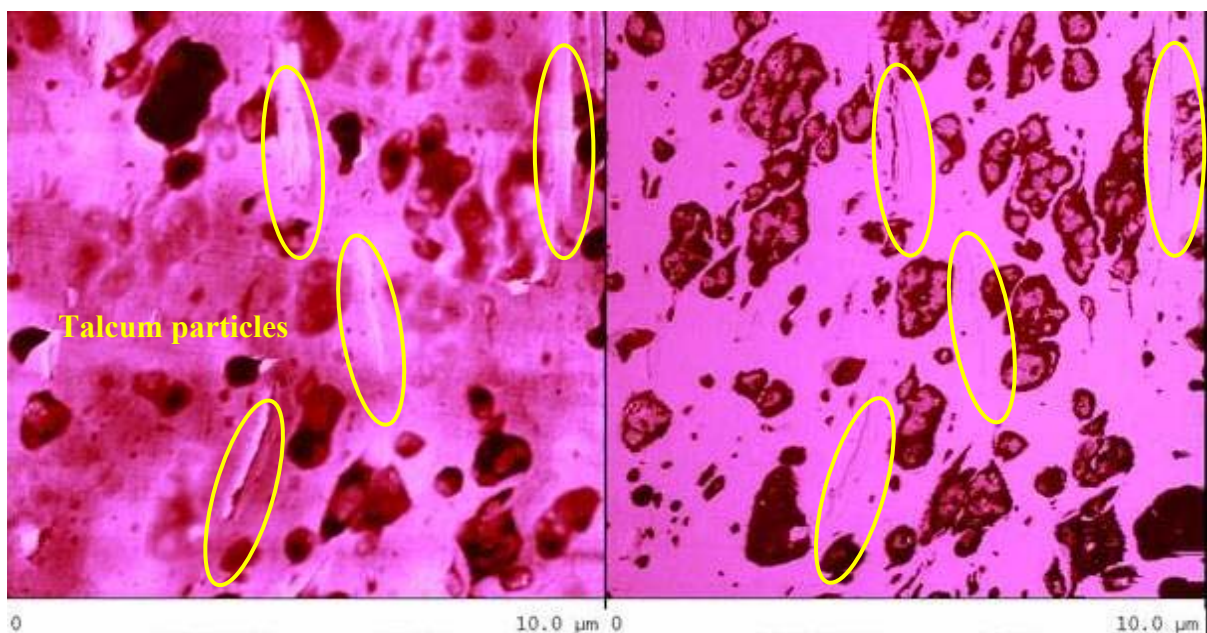
Figure 8.4. AFM height (left) and phase (right) images revealing distribution and orientation of rubber and talcum particles in an injection moulded plate of PP copolymer.

8.4 Temperature of crystallization and heat of fusion by DSC

DSC curves have been measured on injection molding plates of all series of PP samples. Fig. 8.5 shows the temperature of crystallization of all sample series vs. rubber content. No changes in temperature of crystallization of PP matrix with increasing ethylene-propylene-rubber (EPR) content can be detected by DSC for all series of samples as expected as the rubber and PP matrix crystallized separately. An increase in the temperature of crystallization is attributed to the nucleating agent which has an effect on the PP matrix. The nucleating agents improve the temperature of crystallization and decrease the cycle time.
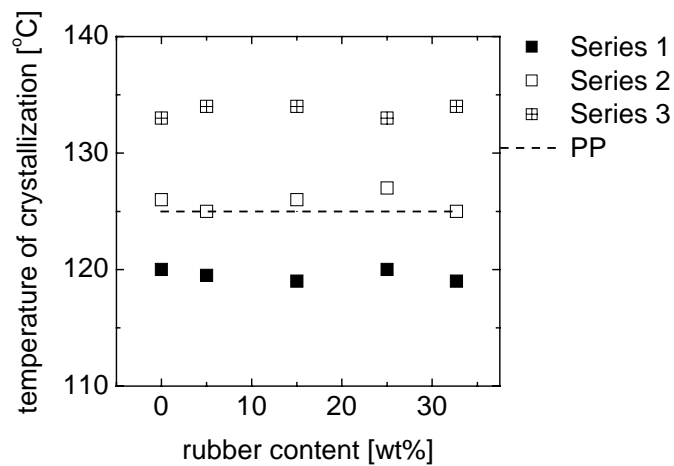

Figure 8.5. Temperature of crystallization of both homopolymer and PP copolymer versus rubber content
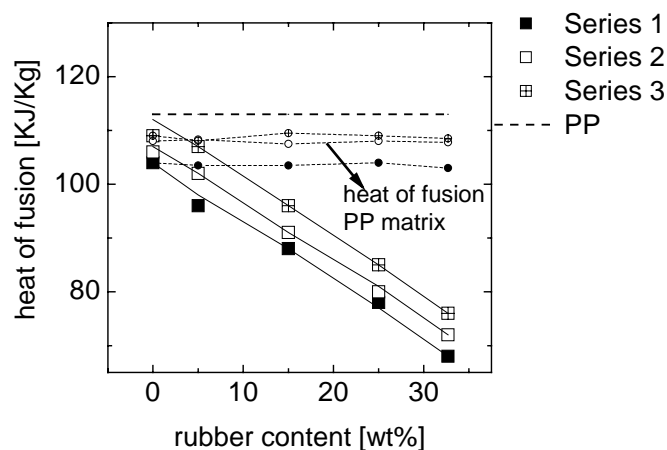
Figure 8.6. Heat of fusion of both, the homopolymer and all series of the PP modified copolymer versus rubber content

108

Figure 8.6 represents the heat of fusion of the second heating curve versus the rubber content. A decrease in the heat of fusion for all series impact copolymer PP samples can be observed with increasing rubber content. The heat of fusion of PP matrix is constant and independent of the rubber content. An increase in the heat of fusion is observed due to the presence of nucleating agent.

8.5 Mechanical properties

The improvement in toughness (impact strength) when EPR is added to PP matrix normally implies in a reduction of its stiffness, which is usually related to a decrease in flexural modulus, yield stress and an increase in the yield strain. A balance between toughness and stiffness is always required for optimum performance of the rubber-toughened polymer. The aim of tensile and flexural tests is to study the effect of rubber content and the addition of nucleating agents to the yield point and flexural modulus. The yield point is defined as the first point on the stress-strain curve at which an increase in strain occurs without a stress increase. A soft but tough material shows a low modulus and a low yield stress. We expect that the addition of rubber would decrease the yield stress whereas the addition of nucleating agents would increase the yield stress.

Figure 8.7 shows the dependences of yield stress on the rubber content. The yield stress decreases with the rubber content indicating that the softness increases. The impact modified copolymers tend to have lower stiffness and lower yield stress than the homopolymer as the presence of the ethylene reduces the crystallinity and stress level to produce shear yielding [Mes1995]. The addition of nucleating agents produce a finer spherulitic structure in the nucleated impact modified PP copolymers sample, which tend to give higher yield stress values in relation to non-nucleated sample. All the nucleating agents have almost the same effects.
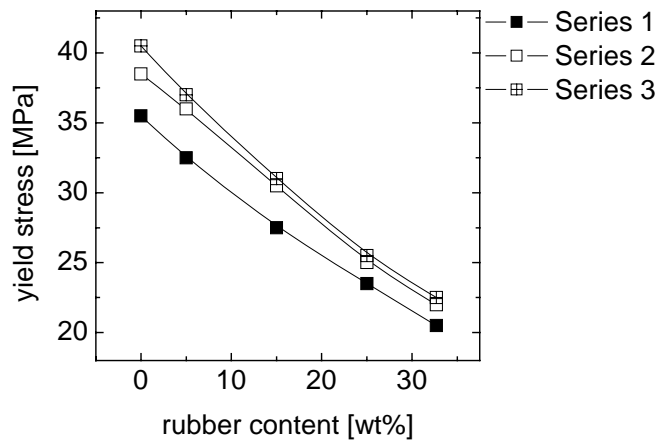
Figure 8.7. Yield stress of PP copolymer sample with different nucleating agent
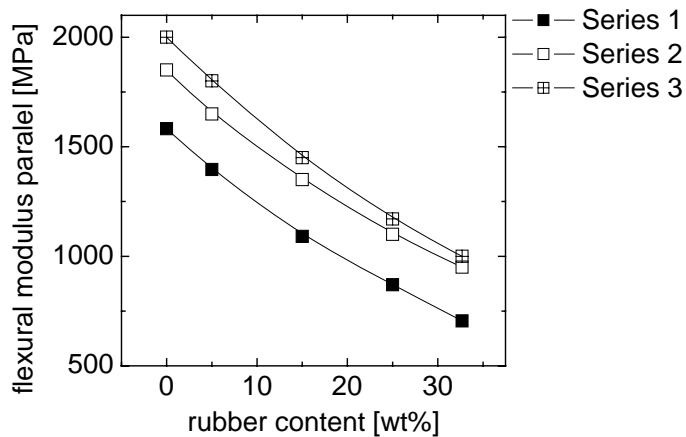
Figure 8.8. Flexural test of PP copolymer sample with different nucleating agents

A flexural test was conducted to determine the elastic modulus of each of the sample in the series. The principle of the flexural test is to bend the tested specimen in the middle until the fracture of the specimen or until the deformation reaches a predetermined value. During this procedure, the bending force applied to the specimen is measured. The tests have been performed in two directions.

Figure 8.8 represents the flexural modulus determined when the bending force was applied parallel to the injection direction in the injection molding process. It was observed that the flexural modulus decreases with increasing rubber content. Addition of the rubber increases the toughness, however, it is associated with a loss in stiffness.

The addition of nucleating agents increases the elastic modulus. The decrease in the modulus associated with the increase in the rubber content can be partly prevented by the

simple addition of nucleating agents. For example, the modulus of a sample containing 25% of rubber was brought to the value of the modulus corresponding to a sample with 15% rubber and no nucleating agents by adding nucleating agents.

8.6 Phase content and chain mobility by NMR at 70° C

Figure 8.9 shows the changes in the phase content and chain mobility in all series of impact PP modified copolymer samples due to both, the addition of different nucleating agents and the increase in the rubber content. The amounts of the rigid, semi-rigid, and soft fractions decrease with increasing rubber content. This can be explained by the decrease in the percentage of PP matrix in the sample with increasing rubber content. Since the PP matrix is semi-crystalline and the rubber domains are mainly amorphous, the amount of the rigid fraction decreases with increasing rubber content. However, it was observed that the crystallinity in the PP matrix is constant and independent of the rubber content. These results are in line with DSC results on heat of fusion.
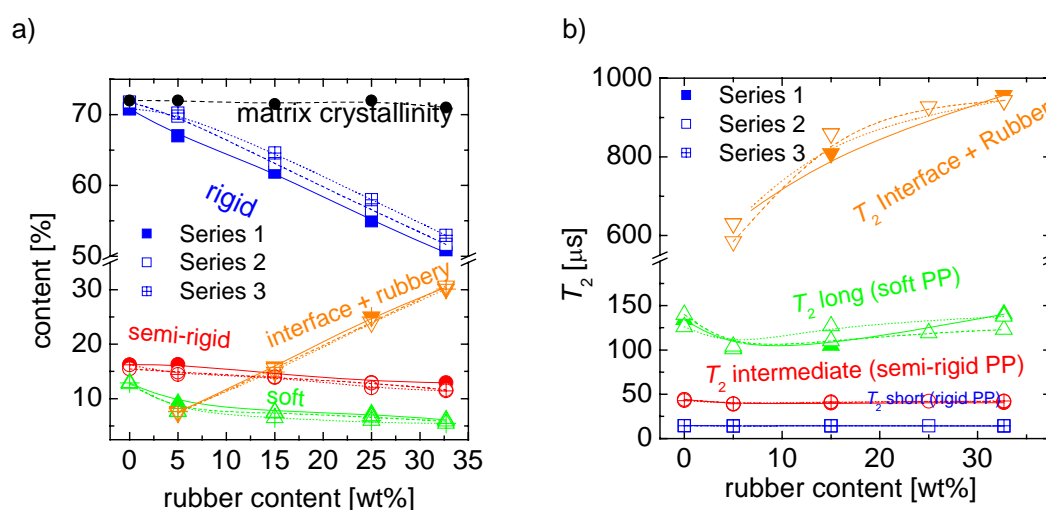
Figure 8.9. (a) The amounts of rigid phase, semi-rigid interface, soft fractions and rubber phase of all series of impact modified PP copolymers. (b) The effect of rubber content and nucleating agent on chain mobility, as determined by the T_2 relaxation time for the different fractions the copolymer. Larger amplitudes and/or frequencies of molecular motions lead to longer T_2 values. The relaxation characteristics were determined by the analysis of the FID, (rigid and semi-rigid fractions), and the Hahn-echo (soft and rubber fraction). The experiments were performed a with low-field NMR spectrometer.

At 70° C the NMR signal (FID) of all series of PP samples showed four different relaxation times (Fig. 8.9b). The shortest relaxation time T_2^{rigid} is associated with the chain mobility in the rigid fraction; the intermediate relaxation time $T_2^{semi-rigid}$ is associated with the chain mobility in semi-rigid fraction; the long relaxation time T_2^{soft} is associated with the

chain mobility in soft fraction, and the longest relaxation T_2^{rubber} time is associated with the interface and rubber fraction.

The chain mobility of the rigid (T_2^{rigid}) and semi-rigid ($T_2^{semi-rigid}$) fractions was found unaffected by increasing the rubber content. This shows that the ethylene-propylene rubber is well separated from the rigid and semi-rigid fractions, and cannot be present in those fractions. Similarly, the increase in the chain mobility of the soft fraction (T_2^{soft}) of the copolymer was explained by the presence of ethylene-propylene rubber mainly in the more mobile core part of the soft phase.

The longest relaxation time (T_2^{rubber}) related to the mobility of the rubber fraction was found to increase with increasing the ethylene-propylene rubber content. This is believed to be related to the average size and size distribution of ethylene-propylene rubber domains and the presence of small ethylene crystals in the rubber domains. In small rubber domains the chain mobility of the rubber molecules is more restricted due to the attachment of a large percentage of these molecules to the fraction of the PP chains in the amorphous phase. In larger rubber domains the percentage of the attached rubber molecules is lower and therefore the chain mobility is less restricted. Another explanation for increase in T_2^{rubber} with increasing the rubber content can be the better phase separation between the rubber domains and the amorphous PP phase for the sample with the highest amount of rubber. The large difference in the molecular mobility between PP matrix and rubber matrix is due to T_g much lower for ethylene-propylene rubber than for the PP homopolymer.

No significant changes in the phase content and chain mobility were detected by NMR for any of the series of impact modified PP copolymer samples upon addition of nucleating agents. The amount of rubber estimated by low-field NMR was found to be in good agreement with the results obtained from liquid-state NMR and the calculated chemical composition.

8.7 Aging in impact modified PP copolymer at 70° C by NMR

In the chapter 6 we reported that aging at 70° C causes changes in the morphology and chain mobility of homopolymeric PP. The observed changes in the phase content and chain mobility with aging time indicate that a micro-structural reorganization takes place within the material. In order to follow the micro-structural reorganization at 70° C in the structure of the impact

modified PP copolymer, the amounts and the chain mobility of rigid, semi-rigid, soft, and rubber fractions are plotted versus log *aging time* (Figure 8.10).
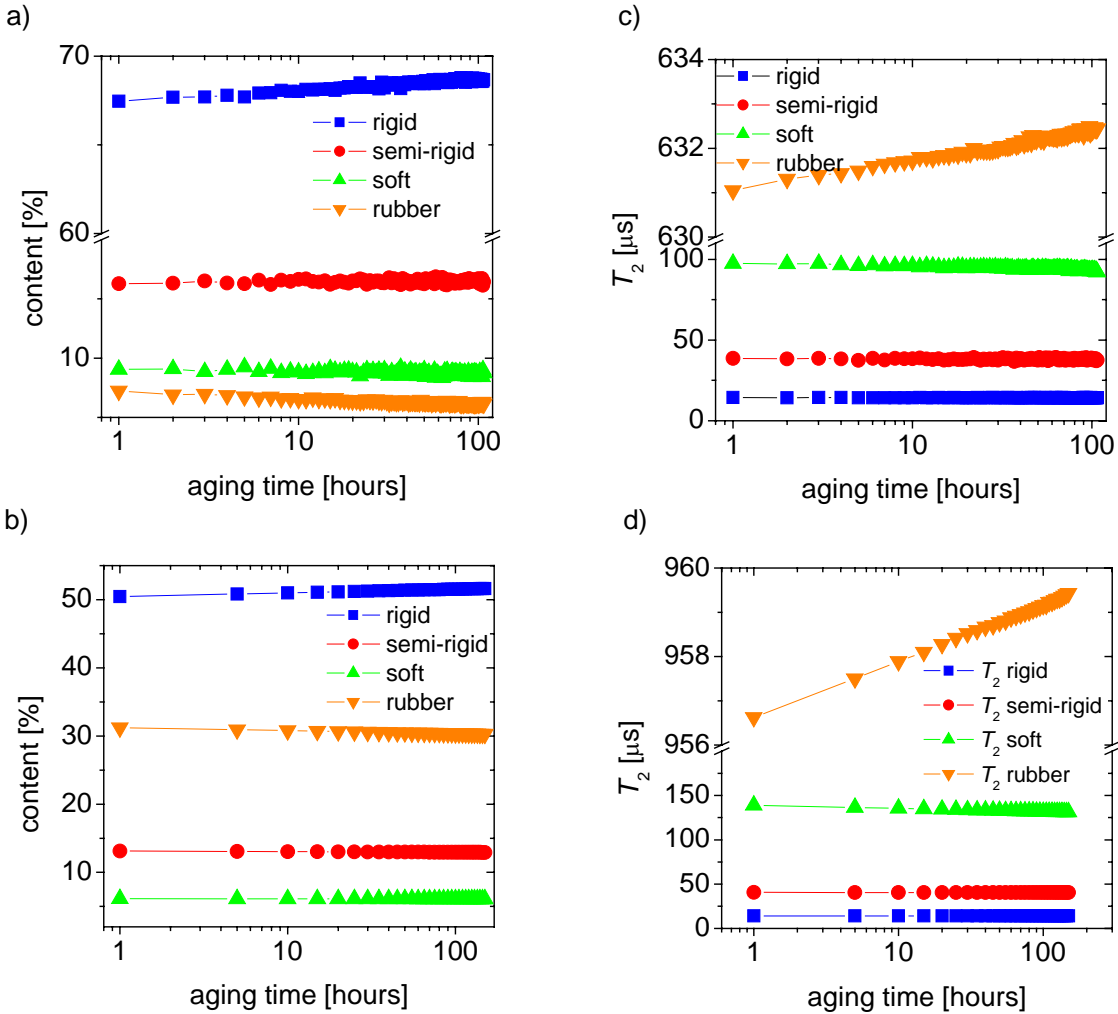
Figure 8.10. (a,b) The amounts of rigid, semi-rigid, soft and rubber fractions as a function of aging time for regular impact modified PP copolymer with 5wt% and 33 wt% rubber. (c,d) Chain mobility in rigid, semi – rigid, soft and rubber fraction of impact modified PPcopolymer with 5wt% and 33 wt% rubber .

Comparing the results shows in Figure 6.7 and 6.8, and the results of Figure 8.10 we concluded that the changes in the phase content and chain mobility of the PP matrix of the impact modified PP copolymers are the same as in the homopolymer PP samples. We also observed that in time the amount of the rubber fraction decreases whereas the chain mobility of the rubber phase increases, which is probably due to the ongoing separation between the rubber domains and the amorphous PP phase. The highest increase in chain mobility of the rubbery phase is observed for the sample with 33 wt% rubber. Based on chain mobility considerations, a better separation between the rubber domains and amorphous phase of PP will cause an increase in the chain mobility of the rubber domains. This can partly explain the results presented in Figure 8.9.

8.8   Phase content and chain mobility by NMR at 0° C

At 70° C the analysis of the NMR signal of the complex impact modified PP copolymer is not by any means trivial. To verify the correctness of the results obtained by NMR at 70° C, the amount of the rubber phase in the PP copolymer was also determined by low temperature NMR. At 0 °C the morphology of PP impact copolymer by NMR is less complex (Figure 8.11). At temperatures below the glass transition temperature (0 °C) of the homopolymer PP matrix, no difference in chain mobilities between different morphological phases of the PP matrix was detected. At this low temperature, the existence of only one fraction (rigid) with low chain mobility can be detected.
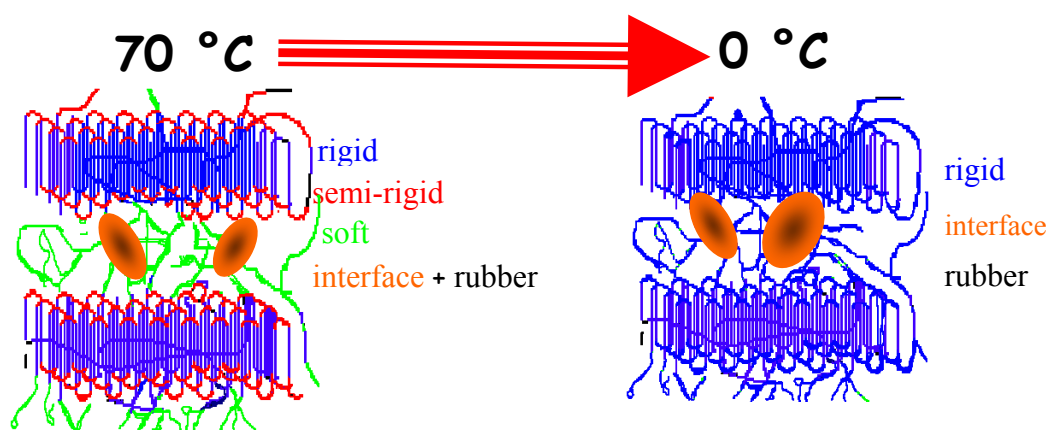
Figure 8.11. Schematic representation of morphology of impact modified PP copolymer at 70° C and 0° C

In contrast to the homopolymer PP matrix, the existence of three fractions with different mobilities is revealed at 0° C for the impact modified PP copolymer. Relaxation components were assigned to these three fractions of different molecular mobility, i.e for the PP matrix (T_2^{matrix}), interphase ($T_2^{interphase}$), and rubber (T_2^{rubber}) phases, respectively (Figure 8.12). It was observed by NMR that the amount of the interphase increases with increasing rubber content (Figure 8.12a). This is in line with the TEM picture which shows that the sample with 33% rubber content contains bigger rubber domains (Figure 8.1 and 8.2). The chain mobility in the PP matrix remains constant however, indicating that the EPR is well separated from the most crystalline part of the PP matrix (Figure 8.12b).

It was further observed that the chain mobility of the interface increases with increasing rubber content. This effect can be explained by a higher amount of mobile EPR chains that is present at the interface. On the other hand, the chain mobility of the rubber phase remains almost constant indicating that the EPR chains in the rubber domains have the same mobility. Using these findings at 0 °C, we can now explain better why the mobility at

70° C increases with increasing amount of rubber (Figure 8.9). We also assume that the ethylene crystals inside the rubber domains play an important role in the mobility of the EPR chains within these domains.
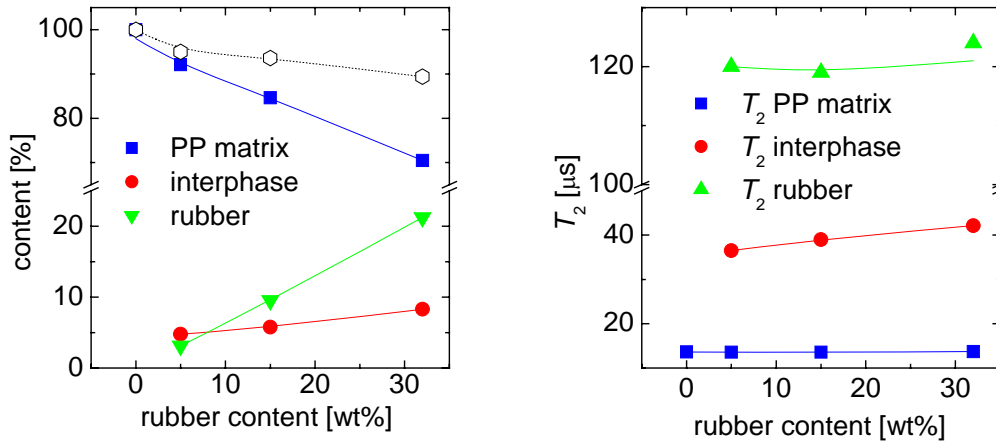
Figure 8.12. (a) The amounts of rigid phase, interface and rubber fractions at 0° C of regular impact modified PP copolymer with different rubber amounts (Series 1). (b) Chain mobility of the rigid (T_2^{matrix}), interphase ($T_2^{interphase}$), and rubber (T_2^{rubber}) fractions at 0° C of the regular impact modified PP copolymer with different rubber contents.

To further verify the accuracy of the data obtained at 0° C, the sum as determined by NMR of the amounts of the interphase and rubber phase was compared with the same data derived from the chemical composition (Figure 8.13). A good correlation between these data was obtained. The above described analysis by low temperature NMR helped to understanding the mechanical behaviour of the impact modified PP copolymer.
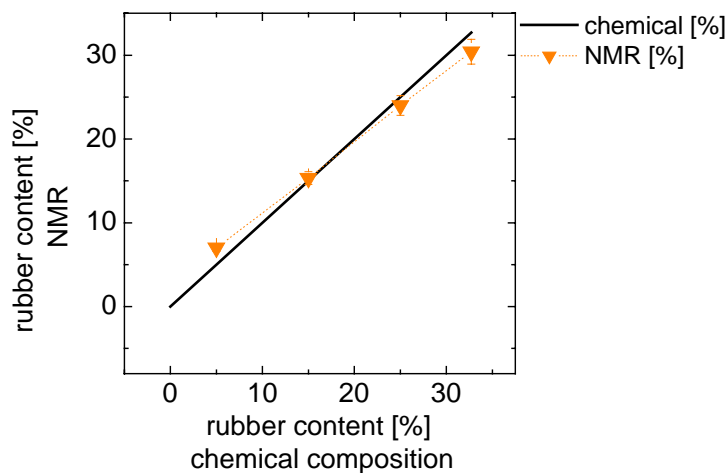
Figure 8.13. Comparison between the amounts of the rubber detected by NMR and the amounts of the rubber estimated from the chemical composition.

One of the disadvantages of known PP copolymers is their low impact strength at low temperatures. A method to improve the impact strength is to blend the PP with rubber, also known as rubber toughening. Figure 8.14 represent the impact strength versus temperature for regular impact modified PP copolymer with 5 wt% rubber. The letters indicate the different classifications given to the sample. A brittle sample (B) means that the sample break rapidly, whereas a tough sample (T) yields above a certain value of the applied force. In the transition regime, there are brittle-tough samples (B-T) and tough-brittle (T-B) samples. The sample is called brittle-tough when for the five sample tested there are more brittle than tough samples and the other way around for the tough-brittle samples.
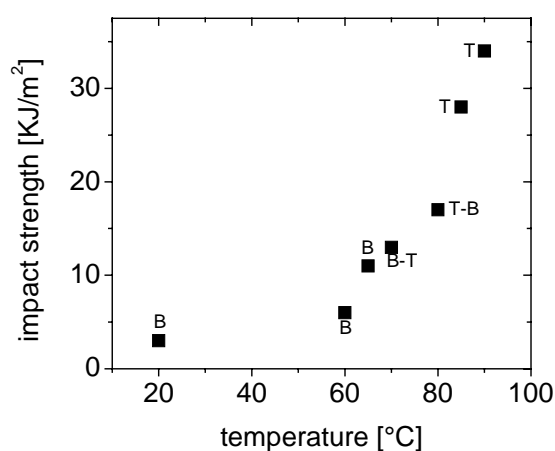
Figure 8.14. Impact strength of regular PP impact copolymer with 5 wt% rubber at different temperature

The impact strength at low temperatures depends on the behaviour of the rubber at those low temperatures. To study in detail the rubber behaviour with temperature in impact modified PP copolymer samples with 5 wt% rubber content, the NMR experiments were performed from -40° C and up to 70° C. In the temperature range from -40° C to -20° C (regime I in Figure 8.15ab) the NMR signal can be decomposed in two components with different chain mobility, i.e. a rigid component with low chain mobility and a soft component with higher chain mobility.

a)

b)

c)

I

II

III

rigid
soft

rigid
semi-rigid
soft

rigid
semi-rigid
soft
rubber
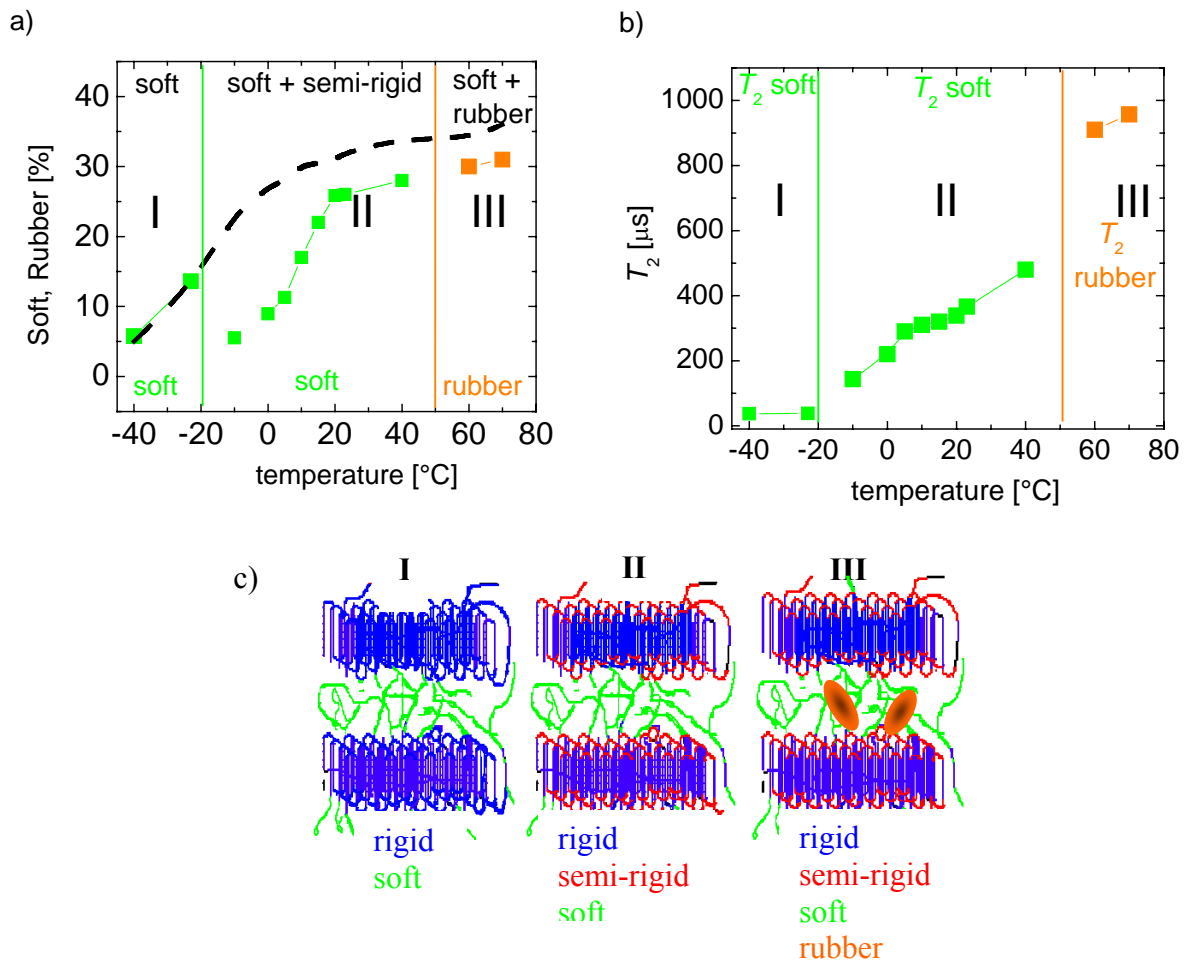
Figure 8.15. (a) The amounts of soft and rubber phase at different temperatures for regular impact modified PP copolymer with 33% rubber. (b) Chain mobility of the soft (T_2^{soft}) and rubber (T_2^{rubber}) fractions at different temperatures. (c) Schematic representation of the morphology at different temperatures by NMR.

In the temperature rage from -20° C to 40° C (regime II in Figure 8.15ab) three different components with different relaxation times can be identified, i.e. a rigid component with low chain mobility, a semi-rigid component with intermediate mobility and a soft component with higher chain mobility. Above 60° C (regime III in Figure 8.15ab) the NMR signal can be decomposed in four relaxation components i.e. a rigid component with low chain mobility, a semi-rigid component with intermediate mobility, a soft component with higher chain mobility, and a rubber component with the highest chain mobility.

It can be concluded that by increasing the temperature, the presence of the rubber phase in the impact modified PP copolymer becomes more significant because it provides the entire copolymer with a more rubber-like behaviour. As a consequence, the impact strength of the copolymer increases accordingly.

8.9 Conclusion

Improving the impact toughness and stiffness of PP has important practical meaning for extending the range of applications. Obviously the impact toughness of PP can be enhanced by rubber inclusion in the PP matrix. DSC, TEM, AFM, and NMR analysis confirmed that the impact modified PP copolymer consists of multiple phases: PP, EPR (crystalline and amorphous), and PE.

Because of the addition of rubber in homopolymeric PP, variations of the molecular structure can be induced. The effects of the addition of rubber and the addition of nucleating agents on the different properties are presented in the following Table 8.2.

Table 8.2. Effect of addition of rubber and nucleating agent on crystallization temperature, heat of fusion, yield stress, flexural modulus, phase composition and chain mobilities of impact modified PP copolymers.

Properties, phase content and chain mobilities	Increasing rubber content	Adding of nucleating agent
Crystallization temperature	No effect	Increase
Heat of fusion	Decrease	Increase
Yield stress	Decrease	Increase
Flexural modulus	Decrease	Increase
Toughness	Increase	Decrease
Rigid fraction	Decrease	Increase
Semi-rigid fraction	Decrease	No effect
Soft fraction	Decrease	No effect
Rubber fraction	Increase	No effect
Mobility in rigid fraction	No effect	No effect
Mobility in semi-rigid fraction	No effect	No effect
Mobility in soft fraction	Increase	No effect
Mobility in rubber fraction	Increase	No effect

Chapter 9

General Conclusions

Solid state Nuclear Magnetic Resonance has successfully been applied for the characterization of high-density polyethylene, isotactic polypropylene, and impact modified polypropylene copolymers. For the first time, NMR experiments on polyolefin materials have been performed at both low and high field. These NMR methods alone and in combination with DSC, X-ray, IR, TEM, and AFM were used to obtain information about the changes in the structure, molecular dynamics, and domain thickness of the investigated systems. These changes were caused by stretching and exposure of the sample at elevated temperature for a certain time, and addition of rubber and nucleating agents. The main conclusions of this work results are as follows:

1. The most appropriate description of the morphology of both homopolymer HDPE and iPP by NMR is a three-phase model (rigid, semi-rigid, and soft fractions). The amounts of the rigid, semi-rigid and soft fraction, and chain dynamics in each fraction of polyethylene and isotactic polypropylene have been investigated by ^{1}H solid state NMR as a function of temperature. The domain thicknesses as determined by NMR were compared with those measured by small-angle X-ray scattering (SAXS) and transmission electron microscopy (TEM) and are in a good agreement. This proves the reliability of the low-field NMR methods for the determination of domain thicknesses in heterogeneous polymers like those enumerated above. Annealing at higher temperatures causes an increase in the lamellae thickness and crystallinity and a decrease in the chain mobility in all fractions. It was shown that the thickening of the crystalline domains during annealing of iPP can be described by a model based on irreversible thermodynamics. A phenomenological correlation was established between the relaxation rate of ^{1}H transverse magnetization characteristic to the rigid fraction of iPP and the annealing temperatures.

2. The effects of deformation ratio, deformation rate, and deformation temperatures on the phase content, chain mobility, and domain thickness of homopolymeric iPP has been investigated using low-field solid state NMR. The amount of the rigid

fraction/degree of crystallinity obtained by NMR coincided within few percent with that obtained by IR. A decrease in the chain mobility has been observed in all fractions with increasing the drawing rate, draw ratio, and drawing temperature. The increase in the thickness of the lamellae with increasing draw ratio and drawing temperature can be explained by partial melting and recrystallization, as well as immobilization of the amorphous phase. We established correlations between the thicknesses of the rigid domains and the amount of the rigid fraction of unaxially stretched iPP, as well as between the thickness of the rigid domains and the chain mobility in the rigid fraction.

3. The effect of aging temperature and aging time on the phase composition, chain mobility and mechanical properties of iPP homopolymer has been studied in detail by ^{1}H low-field solid state NMR. The samples were obtained by a process involving injection molding, crystallization from the melt, and quenching. The aging effect on different morphologies of homopolymeric iPP samples was rationalized in terms of increased restrictions of the chain mobility in the semi-rigid and soft fractions. All samples exhibited physical aging at elevated temperatures and furthermore, it was observed that the physical aging kinetics depends by the morphology of the iPP and the aging temperature. The structural changes due to aging are considered to be associated with a molecular rearrangement generally similar to a secondary crystallization which is accompanied by a decrease in segmental chain mobility of the diffusing amorphous chains.

4. Changes in the morphology, phase content, chain mobility, and mechanical data of impact modified polypropylene copolymer have been investigated using a combination of different techniques such as NMR, X-Ray, TEM, AFM, and DSC. These changes were caused by the ethylene-propylene rubber and nucleating agents added to improve the impact strength and modulus of the polymer. A decrease in the heat of fusion, yield stress, flexural modulus has been observed with increasing rubber content. The addition of nucleating agents however, caused an increase in the crystallization temperature, heat of fusion, yield stress, flexural modulus, and rigid fraction.

Based on the above results, we can conclude that low and high field proton NMR can be successfully used to obtain information about the structure, molecular dynamics, and domain

thickness in the investigated homopolymers of HDPE, iPP, and copolymeric PP. However, the potential of these NMR techniques can be easily extended to other polymeric systems. Corroborating the NMR results with data obtained from other measurement techniques as those enumerated above, helped in gaining further insights in the microscopic properties of the materials under investigation. Therefore, the authors hopes that this thesis brings the reader a step closer to understanding at least part of the known multiple possibilities of NMR investigations and sets a solid base for those that are yet to be discovered.

References

[Abr1961]   A. Abragam, "Principles of Nuclear Magnetism", *Oxford University Press*, Oxford, 1961.

[Aga1962]   M. K.Agarwal, K. E. Helf, *Kolloid Z.* **180**, 114-118 (1962).

[Aga1981]   M. Agarwal, J. M. Schultz, *Polym. Eng. Sci.* **21**, 776 – 781 (1981).

[Aha1983]   S. M. Aharoni, *Macromolecules* **16**, 1722-1728 (1983).

[Aki1999]   A. Akizadeh, L. Richardson, J. Xu, S. McCartney, H. Marand, Y. W. Cheung, S. Chum, *Macromolecules* **32**, 6221 (1999).

[Ala1999]   R. G. Alamo, G. M. Brown, L. Mandelkern, A. Lehtinen, R. Paukkerri, *Polymer* **40**, 3933 (1999).

[Ale1969]   L. E. Alexander, *Diffraction Methods in Polymer Science*, John Wiley & Sons, Inc.: New York, 1969.

[Ali2001]   A. Alizahedh, S. Sohn, J. Quinn, H. Marand, L. C. Shank, H. D. Iler, *Macromolecules* **34**, 4066 (2001).

[Ass1978]   R. A. Assink, *Macromolecules* **11**, 1233 (1978).

[Ath1994]   ATHAS Data Bank. http://web.utk.edu/~athas/databank/ *Ed. M. Pyda*, 1994.

[Aur2000]   F. Auriemma, O.R. Ballesteros, C. De Rosa, P. Corradini, *Macromolecules* **33**, 8764, (2000).

[Aur2001]   F. Auriemma, C. De Rosa, T. Boscato, P. Corradini, *Macromolecules* **34**, 4815 (2001).

[Awa1998]   H. Awaya, *Polymer* **26**, 591, (1988).

[Axe1983]   D. E. Axelson, L. Mandelkern, R. Popli, P.J. Mathieu, *Polym. Sci.: Polym.Phys.* **2,** 2319 (1983).

[Ba1998]   Y. Ba, J. A. Ripmesster, *J. Chem. Phys.* **108,** 8589-8594 (1998).

[Bas1974]   D. C. Bassett, S. Block, G. J. Piermarini, *J. Appl. Phys.* **45**, 4146, (1974)

[Bal1989]   F. J. Balta-Calleja, C. G. Vonk, „X-ray Scattering of Synthetic Polymers" *Elsevier*, New York, 1989.

[Bal2000]   S. Balijepalli, G. C. Rutledge, *Comp. And Theoretical Pol. Sci.* **10,** 103-113 (2000).

[Bas1973]   D. C. Bassett, D. R. Carder, *Polymer* **24**, 387 (1973).

[Bed2000]   E.L. Bedia, N. Astrini, A. Sudarisman, F. Sumera and Y. Kashiro. *J Appl*

Polym Sci **78,** 1200 (2000).

[Bed2002]   E.L. Bedia, S. Murakami, K. Senoo and S. Kohjiya. *Polymer* **43,** 749 (2002).

[Bell1993] A. Bellare, R. E. Cohen, A. S. Argon, *Polymer* **34**, 1393 (1993).

[Ber1967]   K.Bergmann, K. Nawotki, *Z-Z Polym* **219**, 132 (1967).

[Ber1978]   K. Bergmann, *J.Polym.Sci., Polym. Phys.* **16,** 1611 (1978).

[Boy1979]   R.H. Boyd, *Polym. Engng. Sci.* **19**, 1010 (1979).

[Boy1983]   R.H. Boyd, *J. Polym. Sci. Polym. Phys.* **21**, 493 (1983).

[Boy1984]   R. H. Boyd, *Macromolecules* **17**, 903 (1984).

[Boy1985]   R. H. Boyd, *Polymer* **26**, 323 (1985).

[Bra1986]   J. M. Brady, E. L. Thomas, *Polymer Prep.* **27**, 1 (1986).

[Bra1999]   J. Brandrup, E. H. Immergut, E. A. Grulke, „Polymer Handbook" 1999.

[Bri1993]   J. V. McBrierty, K. J. Paker, "Nuclear Magnetic Resonance in Solid Polymers" *Cambridge Univ. Press*, Cambridge, 1993.

[Bro1997]   G.M. Brown and J.H. Butler. *Polymer* **38,** 3937 (1997).

[Bud2003]   A. Buda, D. E. Demco, M. Bertmer, B. Blümich, V. M. Litvinov, J. P. Penning, *J. Phys. Chem. B* **107** 5357 (2003).

[Bud2003]   A. Buda, D. E. Demco, M. Bertmer, B. Blümich, B. Reining, H. Keul, H. Höcker, *Solid State Nucl. Magn. Reson.* **24**, 39 2003.

[Bud2004]   A. Buda, D. E. Demco, B. Blümich, V. M. Litvinov, J. P. Penning, *ChemPhysChem* **5,** 876-883 (2004).

[Bun1939]   C. W. Bunn, *Trans. Farad. Soc.* **35**, 482, (1954).

[Bus1990]   W. R. Busing, *Macromolecules* **23**, 4608, (1990).

[Cam1993]   R. A. Campbell, P. J. Philips, *Polymer* **34**, 4809, (1939).

[Cla1993]   J. Clauss, K. Schmidt-Rohr, H. W. Spiess, *Acta Polym.* **44**, 1-17 (1993).

[Cha1977]   Y. Chantani, Y. Ueda, H. Tadokoro, *Annual meeting of the Society of Polymer Science, Japan, Tokyo*, Preprint, p 1326, (1977).

[Cha1980]   C. K. Chai, N. G. McCrum, *Polymer* **21**, 706 (1980).

[Cha2002]   A.C. Chang, L. Tau, A. Hiltner and E. Baer. *Polymer* **43,** 4923 (2002).

[Cha2002]   A.C. Chang, S.P. Chum, A. Hiltner and E. Baer. *J Appl Polym Sci* **86,** 3625 (2002).

[Che1994]   J. Cheng, M. Fone, V. N. Reddy, K. B. Schwartz, H. P. Fisher, B. Wunderlich *J.Polym.Sci.: Part B: Polym.Phys.* **32**, 2683 (1994).

[Che2006]   B. R. Cherry, C. H. Fujimoto, C. J. Cornelius, T. M. Alam, *Macromolecules* **38**, 1201-1206 (2005).

References

[Cho1988]   J.C. Chou, K. Vijayan, D. Kirby, A. Hiltner, E. Baer, *J. Mater. Sci.* **23**, 2521 (1988).

[Chi1961]   R. Chiang, P.J. Flory, *J. Am. Chem. Soc.* **83**, 2857 (1961).

[Cop1987]   F. Coppola, R. Greco, E. Martucelli, H.W. Kammer and C. Kummerlowe. *Polymer* **28,** 47 (1987).

[Cru1984]   N. G. McCrum, *Polymer* **25**, 299 (1984).

[Cru2004]   N. G. McCrum, B. E. Read, G. Williams, "Anelastic and Dielectric Effects in Polymeric Solids", *Wiley*, New York, 2004.

[Dad1994]   D. Dadayli, R. K. Harris, A. M. Kenwright, B. J. Say, M. M. Sunnetcioglu, *IRC Polym. and Tech.* **35**, 4083 (1994).

[Dem1995]   D. E. Demco, A. Johansson, J. Tegenfeldt, *Solid State Nucl. Magn. Reson.* **4**, 13-38 (1995).

[Dou1979]   D.C. Douglass.; V.J. McBrierty, Polym. Eng. Sci. **19**, 1054, (1979) and references therein.

[Ear1979]   W. Earl, D. L. VanderHart, *Macromolecules* **12**, 762 (1979).

[Eck1997]   R. R. Eckman, P. M. Henrichs, A. J. Peacock, *Macromolecules* **30**, 2474 (1997).

[Ern1987]   R. R. Ernst, G. Bodenhausen, A. Wokaun "Principles of Nuclear Magnetic Resonance in One and Two Dimensions", *Oxford University Press,* Clarendon, 1987.

[Fed1985]   V. D. Fedotov, N. A. Abdrashitiva. *Polym. Sci. USSR* **27**, 287 (1985).

[Fer1984]   A. Ferrero, E. Ferracini, R. Hosemann, *Polymer* **25**, 1747 (1984).

[Fil1994]   B. Fillon, A. Thierry, B. Lotz, J. Wittman, *J. Therm. Analys.* **42**, 721 (1994)

[Fis1962]   E. W. Fischer, G. F. Z. Schmidt, *Angew. Chem.* **1**, 488 (1962).

[Fis1969]   E. W. Fischer, M. Goddar, *J. Polymer Sci.* **C16**, 4405 (1969).

[Flo1978]   P. J. Flory, D. Y. Yoon, *Nature* **272**, 226-229 (1978).

[Fuj1991]   M. Fujiyama, T. Walino, *J. Appl. Polym. Sci.* **42**, 2739 (1991).

[Gau2000]   S. Gautman, S. Balijepalli, G. C. Rutledge, *Macromolecules* **33**, 9136-9145 (2000).

[Ghe1994]   J. Gheng, M. Fone, N. V. Reddy, B. K. Schwartz, P. H. Fisher, B. Wunderlich, *J. Polym. Sci.: Polym. Phys.* **32**, 2683-2693 (1994).

[Goi1992]   G. Goizueta, T. Chiba and T. Inoue, *Polymer* **33,** 886 (1992).

[Goi1993]   G. Goizueta, T. Chiba and T. Inoue, *Polymer* **34,** 253 (1993).

[Gol1961]   M. Goldman, L. Shen, *Phys. Rev.* **144**, 321 (1961).

References

[Gos1996]   U. Goschel, K. Deutscher, V. Abetz, *Polymer* **37**, 1 (1996).

[Gre2002]   C. Grein, C.J.G. Plummer, H.-H. Kausch, Y. Germain and P. Beguelin. *Polymer* **43,** 3279 (2002).

[Hai1965]   I. L. Hay, A. Keller, *Kolloid-Z. & Z. Polymere* 204, 43 (1965).

[Hal1972]   J. C. Halpin, J. L. Kardos, *J Appl. Phys.* **43**, 2235 (1972).

[Han1974]   J. M. Hannon, *J. Appl. Poly. Sci.* **18**, 3761, (1974).

[Han1998]   E. W. Hansen, P. E. Kristiansen   , B. Pedersen, *J.Phys..Chem. B* **102**, 5444 (1998).

[Hed2007]   C. Hedesiu, D. E. Demco, R. Kleppinger, A. A. Buda, B. Blumich, K. Remerie, V. M. Litvinov, *Polymer* **48**, 763 (2007).

[Hed2007]   C. Hedesiu, D. E. Demco, R. Kleppinger, G. Vanden Poel, W. Gijsbers, B. Blümich, K. Remerie, V. M. Litvinov, *Macromolecules*, **40**, 3977-3989 (2007).

[Hei1959]   W. Heinsen, *Journal of Polymer Science* **38**, 134 1959.

[Hel1997]   S. Hellinckx , *Colloid Polym. Sci.* **275**, 116 (1997)

[Hen1984]   D. Hentschel, H. Sillescu, H. W. Spiess, *Polymer* **25**, 1078 (1984).

[Hik1997]   M. Hikosaka, K. Amano, S. Rastogi, A. Keller, *Macromolecules* **30,** 2067 (1997).

[Hill1998]   L. Hillebrand, A. Schmidt, A. Bolz, M. Hess, W. Veeman, R. J. Meier, G. Van der Velden, *Macromolecules* **31**, 5010 (1998).

[Hir1990]   J. Hirschinger, H. Miura, A. D. English, *Macromolecules* **23**, 2153 (1990).

[His1999]   R. Hiss, S. Hobeika, C. Lynn, G. Strobl, *Macromolecules* **32**, 4390 (1999).

[Hu1999]   W. G. Hu, C. Boeffel, K. Schmidt-Rohr, *Macromolecules* **32**, 1611-1619 (1999).

[Hu2000]   W.-G. Hu, K. Schmidt-Rohr, *Polymer* **41**, 2979 (2000).

[Hu2000]   J. Z. Hu, W. Wang, S. Bai, R. J. Pugmire, G. M..V. Taylor, D. M. Grant, *Macromolecules* **33**, 3359 (2000).

[Ibh1996]   A. O. Ibhadon, *J. Appl. Polym. Sci*. **62**, 1843 (1996).

[Idi1996]   D. S. H. Idiyatullin, E. V. Khozina, V. S. Smirnov, *Solid State Nucl. Magn. Reson.* 7, 17 (1996).

[Iij2000]   M. Iijima, G. Strobl, *Macromolecules* **33**, 5204 (2000).

[Isa1999]   J. R. L. Isasi, M. J. Mandelkern, R. G. Galante Alamo, *J. Polym. Sci., Polym. Phys.* **37**, 323 (1999).

[Ito1981]   M. Ito, T. Kanamoto, K. Tanaka, *Macromolecules* **14**, 1779 (1981).

[Ito1992]   J. Ito, K. Mitani, Y. Mizutani, *J. Appl. Polym. Sci.* **46**, 1221 (1992).

References

[Iwa2002]	Iwata K. *Polymer* **43**, 6609 (2002).
[Jan1993]	J. Jancar, A. T. J. Dibenedetto, J. Kucera, *Polymer* **34**, 1684 (1993).
[Jan1994]	J. Jancar, A. T. J. Dibenedetto, *J.Matter. Sci.* **29**, 4651 (1994).
[Jan1996]	J. Jancar, *J.Matter. Sci.* **31**, 3983 (1996).
[Kak1985]	T. Kakudate, M. Kakizaki , T. Hideshima, *J.Polym.Sci.: Polym.Phys.* **23,** 787 (1985).
[Kar1979]	J. Karger-Kocsis, A. Kallo, A. Szafner, G. Bodar and Z. Senyei. *Polymer* **20,** 37 (1979).
[Kar1995]	J. Karger – Kocsis, *Polypropylene; structure, blends and composites; Vol. 1*, Champman and hall, London, (1995).
[Kar1999]	H. G. Karian, *Handbook of Polypropylene and Polypropylene Composites*; Marcel Dekker: New York, 1999.
[Kav1971]	S. Kavesh, J.M. Schultz, *J. Polym. Sci. Part A-2* **9**, 85 (1971).
[Kha1996]	A. Khare, A. Mitra, *J. Mater. Sci.* **31**, 5691 (1996).
[Kim1996]	G.-M. Kim, G.H. Michler, M. Gahleitner and J. Fiebig. *J Appl Polym Sci* **60,** 1391 (1996).
[Kim1998]	G.-M. Kim and G.-H. Michler. *Polymer* **39,** 5689 (1998).
[Kis1983]	Y. V. Kissin, *J. of Polym. Sci.: Polym. Phys. Edit.* **31**, 2085 (1983).
[Kit1977]	R. Kitamaru, F. Horii, F. Hyon, *J Polym Sci Polym Phys* 15, 821 (1977).
[Kit1978]	R. Kitamaru, F. Horii, *Adv Polym. Sci.* **26**, 139 (1978).
[Kit1986]	R. Kitamaru, F. Horii, K. Murayama, *Macromolecules* **19**, 636 (1986).
[Kit1994]	R. Kitamaru, F. Horii, Q. Zhu, D. C. Bassett, R. H. Olley, *Polymer* **35,** 1171 (1994).
[Kiv1986]	A. Kivinen, M. Ovaska, K. Soljamo, *Chemical Physics Letters* **128**, 4 (1986).
[Kle2002]	P. G. Klein, M. A. N. Driver, *Macromolecules* **35**, 6598 (2002).
[Kri1999]	P. E. Kristiansen, E. W. Hansen, B. Pedersen, *J.Phys..Chem. B:* **103,** 3552 (1999).
[Kri2000]	P. E. Kristiansen, E. W. Hansen, B. Pedersen, *Polymer* **41,** 311 (2000).
[Kuw2000]	K. Kuwabara, H. Kaji, M. Tsuji , F. Horii, *Macromolecules* **33**, 7093 (2000).
[Lab2001]	T. Labour, C. Gauthier, R. Seguela, G. Vigier, Y. Bomal, G. Orange, *Polymer* **42**, 7127 (2001).
[Li1999]	J. X. Li, W. L. Cheung, C. M. Chan, *Polymer* **40**, 2089 (1999).
[Lin1974]	L. Lin, A. S. Argon, *J. Mater. Sci.* **9**, 2034 (1974).
[Lit2002]	V.M. Litvinov, V. B. F. Mathot, *Solid State Nuclear Mag. Res.* **22**, 218

(2002).

[Lit2004]	V.M. Litvinov, J. P. Penning, *Macromol. Chem. Phys.* **205,** 172 (2004).
[Lit2005]	V. M. Litvinov, M. Soliman, *Polymer* **46**, 3077 (2005).
[Lot1991]	B. Lotz, S. Graff, C. Staupe, J. C. Wittman, *Polymer* **32**, 2903, (1991).
[Lot1996]	B. Lotz, J. C. Wittmann, Polymer **37**, 4979, (1996).
[Lov1983]	A. J. Lovinger, *J. Polm. Phys.* **21**, 97, (1983).
[Mag1996]	S. N. Magonov, *Surface analysis with STM and AFM*, VCH Publisher, New York, 1996
[Mai2000]	P. Maiti, M. Hikosaka, K. Yamada, A. Toda, F. Gu, *Macromolecules* **33**, 9069 (2000).
[Man1964]	L. Mandelkern, "Crystallization of polymers*"*, *McGraw-Hill*, New York, 1964.
[Man1968]	L. Mandelkern, A. L. Allou, M. Gopalan, *J. Phys. Chem.* **72**, 309 (1968).
[Man1985]	L. Mandelkern, *Polymer J.* **17**, 337 (1985).
[Man1988]	L. Mandelkern, A. J. Peacock, *Stud. Phys. Theor. Chem.* **54**, 201-217 (1988).
[Man1990]	L. Mandelkeren, R. G. Aloma, M. A. Kennedy, *Macromolecules* **23**, 4721-4723 (1990).
[Man1990]	L. Mandelkern, *Acc. Chem. Res. 23*, 380-394, (1990).
[Mar2000]	H. Marand, A. Alizadeh, R. Farmer, R. Desai, V. Velikov, *Macromolecules* **33**, 3392 (2000).
[Mar1998]	A. Martorana, S. Piccarolo, D. Sapoundjieva, *Macromolec. Chem. Phys.* **3**, 531 (1998).
[Mat1994]	V. B. F. Mathot, "Calorimetry and Thermal Analysis of Polymers" *Hanser Publishers: Munich, Germany, Vienna, and New York*, 1994.
[Mat2000]	H. Matsuda, T. Aoike, H. Uehara, T. Yamanobe, T. Komoto, *Polymer* **42**, 5013-5021 (2000).
[Men2003]	R. Mendoza, G. Regnifer, W. Seiler, J. L. Lebrun, *Polymer* **44**, 3363 (2003).
[Mez1994]	K. Mezghani, R. A. Cambell, P. J. Phillips, *Macromolecules* **27**, 997 (1994).
[Mez1997]	K. Mezghani, P. J. Phillips, *Polymer* **38**, 5725, (1997)
[Mes1995]	P. B. Messersmith, E. P. Giannelis, J. *Polym. Sci. Part A: Polym. Chem.* **33**, 1047 (1995).
[Mun1987]	M. Munowitz, A. Pines, *Adv. Chem. Phys.* **66**, 1-152 (1987).
[Nat1955]	G. Natta, P. Pino, P. Corrandini, F. Danusso, E. Mantica, G. Mazzanti, G. Moragilo, *J. Am. Chem. Soc.* **77**, 1708, (1955).
[Nat1956]	G. Natta, *Angew. Chem.* **68**, 541, (1956).

References

[Nat1964]   G. Natta, *Angew. Chem.* **76**, 553, (1964).

[Neg1992]   M. Negahban, A. S. Wineman, *Int. J. Engng. Sci.* **30**, 819 (1992).

[Nor1995]   T. Normura, T. Nishio, T. Fujii, J. Sakai, M. Yamamoto, A. Uemura, M. Kakugo. *Polym Engng Sci*. **35,** 1261, 1995.

[Nys1995]   B. Nysten, R. Legras and J.-L. Costa. *J. Appl. Phys*. **78,** 5953 (1995).

[Nys1999]   B. Nysten, A. Ghanem, J.-L. Costa and R. Legras. *Polym. Int*. **48,** 334 (1999).

[Oll1989]   R. H. Olley, D. C. Bassett, *Polymer* **30**, 399-409 (1989).

[Ora1982]   L. D'Orazio, N. Greco, C. Mancarella, E. Martuscelli, G. Nagosta and C. Silvereste. *Polym Engng Sci* **22,** 536 (1982).

[Ora2001]   L. D'Orazio and G. Cecchin. *Polymer* **42,** 2675 (2001).

[Pac1984]   K. J. Packer, J. M. Pope, R. R. Yeung, *J. Polym. Sci.: Polym. Phys.* **22**, 589-616 (1984).

[Pau1993]   R. Paukkeri, T. Vaananen, A. Lehtinen, *Polymer* **34**, 2488, (1993).

[Pav2005]   S. Pavel, T. Hashimoto, S. Kenji, G. Arkadiusz, *Polymer* **46**, 513-521, (2005).

[Pea1990]   A. Peacock, L. Mandelkern, *J. Polym. Sci., Polym. Phys.* Ed. **28**, 1917, (1990).

[Per1999]   E. Perez, D. Zucchi, M. C. Sacchi, F. Forlini, A. Bello, *Polymer* **40**, 675, (1999)

[Pet1963]   A. Peterlin, *J. Polym. Sci. B1* **B1**, 279 (1963).

[Pet1967]   A. Peterlin, *Polymer* **6**, 25 (1967).

[Pet1971]   A. Peterlin, *J. Mater. Sci.* **6**, 490 (1971).

[Pet1973]   A. Peterlin, *Appl. Polym. Symp.* **20**, 269 (1973).

[Pet1987]   A. Peterlin, *Colloid&Polymer Sci.* **265,** 357 (1987).

[Pet1996]   F. Coppola, R. Greco, E. Martucelli, H.W. Kammer and C. Kummerlowe. *Polymer* **28,** 47 (1987).

[Poe2003]   P. Poelt, E. Ingolic, M. Gahleitner, K. Bernreitner and W. Geymayer. *J Appl Polym Sci* **78,** 1152 (2000).

[Pop1987]   R. Popli, L. Mandelkern, *J. Polym. Sci. , Polym. Phys.* **25**, 441-449, (1987)**.**

[Pou1998]   L. Poussin, Y. A. Bertin, J. Parisot, C. Brassy, *Polymer* **39**, 4261 (1998).

[Pre2000]   R. Premphet, P. Horanont, *J. Appl. Polym. Sci.* **76**, 1929 (2000).

[Ros1992]   S. Rostami, I. S. Miles, "Multicomponent Polymer Systems" *Wiley: New York,* 1992.

[Ros2002]   C. De Rosa, F. Auriemma, T. Circelli, R. M. Waymouth, *Macromolecules* 35, 3622, **(2002).**

[Rul1961]   W. Ruland, *Acta Crystallogr.* **14**, 1180 (1961).

References

[Rul1964]   W. Ruland, *Polymer* **5**, 89 (1964).

[Sam1981]   R. J. Samuels, *Makromol. Chem.* **4**, 241 (1981).

[San1973]   I. C. Sanchez, J. P. Colson , R. K. Egy, *J. Appl. Phys.* **44**, 4332 (1973).

[San1974]   I. C. Sanchez, A. Peterlin, R. K. Egy, F. L. McCrackin, *J. Appl. Phys.* 45, 4216 (1974).

[San1986]   H. Sano, T. Usami and H. Nakagawa, *Polymer* **27,** 1497 (1986).

[Set1968]   T. Seto, T. Hara, K. Tanaka, *Japanese J. Phys.* **48**, 282, (1968)

[Son1987]   H. H. Song, R. J. Roe, *Macromolecules* **20**, 2723 (1987).

[Sch1994]   K. Schmidt-Rohr, H. W. Spiess, „Multidimensional Solid-State NMR and Polymers" , *Academic Press*, London, 1994.

[Sch1991]   K. Schmidt-Rohr, H. W. Spiess, *Macromolecules* **24**, 5288 (1991).

[Sch1999]   M. Schneider, L. Gasper, D. E. Demco, B. Blümich, J. *Chem. Phys.* **111**, 402 (1999).

[Sch1999]   S. Schreurs, J. P. Francois, P. Adriaenens, J. Gelan, *J.Phys.Chem. B* **103**, 1393 (1999).

[Sil1998]   R. Silvestry, P. Sgarzi, *Polymer* **39**, 5871 (1998).

[Sta1961]   W. C. Statton, *J. Appl. Phys.* **32**, 2332 (1961).

[Sta1998]   J.U. Starke, G.U. Michler, W. Grellmann, S. Seidler, M. Gahleitner, J. Fiebig and E. Nezbedova. *Polymer* **39,** 75 (1998).

[Ste1969]   R. S. Stein, *Polymer Eng. Sci.* **9**, 320 (1969).

[Str1980]   G. R. Strobl, M. J. Schneider, I. G. Voigt-Martin, *J.Polym.Sci.* **18**, 1361 (1980).

[Str1997]   G. R. Strobl, "The Physics of Polymers", *Springer-Verlag*, Berlin 1997.

[Str1987]   L. C. E. Struik, *Polymer* **28**, 1521 (1987).

[Swa1998]   K. Swaminathan and D.W.M. Maw. *J Appl Polym Sci* **78,** 452 (2000).

[Tan1989]   H. Tanaka, F. Kohrogi, K. Suzuki, *Eur. Polym. J.* **25**, 449 (1989).

[Tan1993]   H. Tanaka, Y. Inoue, *Polymer International* **31**, 9 (1993).

[Tea1957]   P. W. Teare, D. R. Holmes, *J. Polym. Sci.* **24**, 496, (1957).

[Tho1996]   R. Thomann, C. Wang, J. Kressler, *Macromolecules* **29**, 8425, (1996).

[Tom1996]   P. E. Tomlins, *Polymer* **37**, 3907 (1996).

[Tom1998]   P. E. Tomlins, B. E. Read, *Polymer* **39**, 355 (1998).

[Tom1998]   E. Tomasetti, B. Nysten and R. Legras. *Nanotechnology* **9,** 305 (1998).

[Tom2000]   E. Tomasetti, R. Legras, B. Henri-Mazeaud and B. Nysten. *Polymer* **41,** 6597 (2000).

References

[Tri1998]   D. Trifonova, J. Varga, G.J. Vancso, *Polm. Bull.* **41**, 341, (1998).

[Ueh2000]   H. Uehara, T. Yamanobe, T. Komoto, *Macromolecules* **33**, 4861-4870 (2000).

[Uzo1997]   T. C. Uzomah, S. C. O Ugbolue, *J Appl Polym. Sci.* **65**, 625 (1997).

[Van1996]   D. L. VanderHart, G. B. McFadden, *Solid State Nucl. Magn. Reson.* 7, 45-66 (1996).

[Van2003]   D.L.VanderHart, C. R. Snyder, *Macrololecules* **36**, 4813-4826 (2003).

[Var1992]   J. Varga, *J. Mat. Sci.* **27**, 2557, (1992).

[Vle1997]   S. Vleeshouwers, *Polymer* **38**, 3213, (1997)

[Vod2006]   A. M. Voda, D. E. Demco, A. Voda, T. M. SchauberAdler, T. Dabisch, A. Adams, M. Baias, B. Blümich, *Macromolecules,* **39**, 4802 (2006).

[Von1971]   C. G. Vonk, *J.Appl.Crystallogr* **4**, 340 (1971).

[Von1973]   C. G. Vonk, *J.Appl.Crystallogr* **6**, 149 (1973).

[Vor1996]   F. J. Wortmann, K.V. Schulz, *Polymer* 37, 819 (1996).

[Wan1996]   J. Wang, *J.Chem.Phys.* **104,** 48 (1996).

[Web1]   www.yellow-design.de

[Web2]   www.imc.cas.cz

[Weg2000]   W. P. Weglarz, H. Peemoeller, A. Rudin, *J Polym Sci, B: Polym Phys.* **38**, 2487 (2000).

[Wen1993]   W. Wenig, F. Herzog, *J. App. Polym. Sci.* **50**, 2163 (1993).

[Woo1993]   R. P. Wool, *Macromolecules* **26**, 1564 (1993).

[Wun2005]   B. Wunderlich, "Thermal analysis of polymeric materials"*, Springer*, 2005.

[Yam1998]   K. Yamada, S. Matsumoto, K. Tagashira, M. Hikosaka *Polymer* **39**, 5327 (1998).

[Yam1999]   M. Yamaguchi and K.H. Nitta. *Polym Engng Sci* **39,** 833 (1999).

[Yam2003]   K. Yamada, M. Hikosaka, A. Toda, S. Yamazaki, K. Tagashira *Macromolecules* 36, 4790 (2003).

[Yok1997]   Y. Yokoyama and T. Ricco. *J Appl Polym Sci* **66,** 1007, (1997).

[Zie1955]   K. Ziegler, E. Holzkamp, H. Briel, H. Martin, Angew. Chem. **67**, 426, (1955).

[Zha2000]   X. C. Zhang, M. F. Butler, R. E. Cameron, *Polymer* **41**, 3797 (2000).

[Zha2002]   M. Zhang, Y. Liu, X. Zhang, J. Gao, F. Huang, Z. Song, G. Wei and J. Qiao. *Polymer* **43,** 5133 (2002).

[Zho2005]   J. J. Zhou, J. G. Liu, S. K. Yan, J. Y. Dong, L. Li, C. M. Chan, J. Schultz, *Polymer* **46**, 4077 (2005).

References

[Zhu2004]   P. Zhu, E. Graham, *Polymer* **45**, 2603 (2004).

[Zhu2005]   P. Zhu, J. Tung, G. Edward, *Polymer* **46**, 10960 (2005).

Acknowledgements

At the end of this thesis I would like to express my gratitude to everyone who directly or indirectly contributed to this work and its completion.

First and foremost I must single out my promoter **Prof. Dr. Dr. h. c. Bernhard Blümich** who gave me the opportunity to perform my PhD in his group. It was a pleasure and a privilege for me to be part of his team.

Many thanks to **Prof. Dan Demco** for his permanent advices and help related to any NMR problem.

I would kindly like to thanks **Dr. Klaas Remerie, Dr. Rieky Steenbakkers, Dr Maria Soliman** from SABIC Europe, for many hours of useful discussions, for the support and understanding during these years. Thank you for being around anytime I needed.

Many thanks are addressed to **Dr. Victor Litvinov**, **Dr. Ralf Kleppinger**, **Dr. Rudy Debliek** from DSM Research Resolve for their support and interesting discussions we had.

I would like to thank my colleagues and friends from RWTH Aachen **Dr. Alina Adams**, **Dr. Adrian Voda, Lavinia Utiu, Maria Baias, Isa Fonseca, Elena Talnishnikh, Claudiu Melian** for good advices and nice time we had together.

I would like to thank my colleagues and friends from DSM Research and SABIC Europe **Dr. Mihai Morariu, Dr. Elena Trezza, Harrie Linssen**, **Gerda Kolfschoten and Dr. Aurora Bastinas** for the nice moments we have shared together during the coffee breaks and for the friendly environment.

For sure I do not forget all my friends from the five stars hotel AMVJ Geleen where I had very nice time during my PhD thesis.

At the end I want to say the biggest thanks for my mother **Valeria** and my father **Virgil** who gave me the power to go on. I am also deeply thankful to my sister **Ioana** and my brother **Nicu**.

Curriculum Vitae

Cristian Eugen Hedesiu

Birth date and place: 08 April 1980, Iclod, Romania

E-mail: cristihed@gmail.com

Nationality: Romanian

Education

2007 December **Thesis:**	Defence for the Doctoral Degree in natural science „Structure – Property Relationship in Semi - Crystalline Polymers (Polyethylene and Polypropylene)"
04. 2004 – 2006	*PhD Student*, RWTH Aachen, Germany and SABIC – Europe B.V., The Netherlands
09.2002 – 08.2003 **Dissertation:**	Master of science (Biophysics and Medical Physics), "Babes-Bolyai" University, Cluj-Napoca, Romania, in collaboration with RWTH, Aachen, Germany "Investigation of Nylon6 fibers by Solid State NMR"
09.1998 – 07.2002 **Dipolma:**	Dip. Phys.**, Faculty of Physics,** Babes-Bolyai University, Cluj-Napoca, Romania "Application of gamma rays in cardiology"

Professional Experience

2004 – 2007	SABIC Research Campus, Geleen, The Netherlands; DSM Resolve Research Campus, Geleen, The Netherlands**;** IIT Research Institute, New Delhi, India. DAAD Program;
2003	Erasmus – Socrates Scholarship at the Institute for Technical and Macromolecular Chemistry, RWTH Aachen, Germany; Lecturer at "Emil Racovita" High-school, Cluj, Romania;
2002	"N.S. Stancioiu" Heart Institute, Cluj-Napoca, Romania Nuclear Cardiology Department;

Publications

1. C. Hedesiu, D. E. Demco, R. Kleppinger, A. A. Buda, B. Blümich, K. Remerie, V. Litvinov, *The effect of temperature and annealing on the phase composition, molecular mobility and the thickness of domains in high-density polyethylene*, Polymer, 48 (2007) 763-777

2. C. Hedesiu, D. E. Demco, R. Kleppinger, G. Vanden Poel, W. Gijsbers, B. Blümich, K. Remerie, V. Litvinov, *The effect of temperature and annealing on the phase composition, molecular mobility and the thickness of domains in isotactic*

polypropylene studied by proton solid-state NMR, SAXS and DSC, Macromolecules, 40 (2007) 3977 – 3989.

3. C. Hedesiu, D. E. Demco, B. Blümich, K. Remerie, V.M Litvinov, *Study of uniaxially deformed isotactic polypropylene by ^{1}H solid state NMR and IR spectroscopy.* Accepted to Macromolecular Chemistry and Physics

4. C. Hedesiu, D. E. Demco, R. Steenbakkers, R. Kleppinger, G. Vanden Poel, B. Blümich, K. Remerie, V.M Litvinov, *Aging Study on Polypropylene by ^{1}H solid state NMR, X-ray, and DSC.* In preparation

5. C. Hedesiu, D. E. Demco, R. Steenbakkers, B. Blümich, K. Remerie, V.M Litvinov, *Study of PP impact polypropylene by ^{1}H solid state NMR, SAXS, TEM and SEM.* In preparation